Dissertations (1934 -)

Dissertations, Theses, and Professional
Projects

Micropollutant-Free Nutrient Recovery: Adsorption of Micropollutants on Ion Exchangers and Biosolids-Derived Biochar

Yiran Tong
Marquette University

Follow this and additional works at: https://epublications.marquette.edu/dissertations_mu

Part of the Environmental Engineering Commons

MICROPOLLUTANT-FREE NUTRIENT RECOVERY: ADSORPTION OF
MICROPOLLUTANTS ON ION EXCHANGERS AND
BIOSOLIDS-DERIVED BIOCHAR

By

Yiran Tong

A Dissertation submitted to the Faculty of the Graduate School,
Marquette University,
in Partial Fulfillment of the Requirements
for the Degree of Doctor of Philosophy

Milwaukee, Wisconsin

May 2018

ABSTRACT
MICROPOLLUTANT-FREE NUTRIENT RECOVERY: ADSORPTION OF
MICROPOLLUTANTS ON ION EXCHANGERS AND
BIOSOLIDS-DERIVED BIOCHAR

Yiran Tong

Marquette University, 2018

The presence of excessive nutrients in treated wastewater effluent is a growing concern in terms of water quality and ecological balance. Thus, removal of nutrients is of great interest. Moreover, the removed nutrients can be recovered in forms amenable for agricultural reuse, which yields a sustainable supply of nonrenewable phosphorus that can be used to support global food production. As nutrient recovery gains interest, it is essential that the products be free of harmful contaminants. One class of contaminants of great concern is organic micropollutants. To help address these issues, this study evaluated the fate and impact of micropollutants during nutrient recovery via an ion exchange-regeneration-precipitation process. The adsorptive behavior of the micropollutants was evaluated for the ion exchangers and for a sustainable biosolids-derived biochar that may be useful for separating micropollutants from nutrients prior to ion exchange. Bench-scale batch reactors were operated for ion exchange-regeneration and adsorption tests. The surface properties of ion exchangers and biochar were characterized to help assess the mechanisms of micropollutant adhesion on solid adsorbents. The presence of micropollutants in water reduced the kinetic rates of nutrient exchange onto ion exchangers. Micropollutants were adsorbed to the phosphate exchangers and were released with phosphate ions during ion exchange regeneration. To remove micropollutants from water prior to ion exchange, biosolids-derived biochar was used since micropollutants were adsorbed to the biochar, but ionic nutrients were not. Biochar produced at higher pyrolysis temperatures increased adsorption capacity, as did higher ambient temperatures for batch sorption experiments. Under multi-solute conditions, not all target micropollutants demonstrated suppressed adsorption. Biochar, ammonium, and phosphate exchangers were accordingly arranged in sequence in a flow-through system. The biochar column removed more than 80% of influent hydrophobic micropollutants and 50% of hydrophilic micropollutants, thereby reducing the presence of micropollutants in the nutrient removal/recovery process. Thermodynamic parameters indicated an endothermic adsorption reaction and heterogeneity in adsorption site distribution on the biochar surface. The binding energy and entropy change of adsorption were not affected by the presence or absence of other solutes in the matrix. The underlying binding mechanism for biosolids-derived biochar adsorption was potentially dominated by non-specific hydrophobic interaction and non-covalent interaction including hydrogen bonding and π-stacking.

ACKNOWLEDGMENTS

Yiran Tong

Erik Anderson, Dylan Friss, Lee Kimbell, Paige Peters, Vinny Martino, Donald Ryan, Will Lynn, John Ross, Tom Hoffman, Carlan Johnson and Nick Benn. They are not only great friends, but also my mentors on techniques to some extent.

Words just can't describe how much thankfulness I have for my beloved mom and dad. They have always been extremely supportive and empathetic to the decisions I made. And my dearest boyfriend, Zhuozhi, I feel blessed to have him for putting our endeavors together to achieve shared life goals.

TABLE OF CONTENTS

LIST OF TABLES

LIST OF FIGURES

1 INTRODUCTION

1.1   The Nutrients-Energy-Water Nexus at Water Resource Reclamation Facilities

Treating polluted water to high standards for the protection of human and environmental health has always been the major focus of water resource reclamation facilities (WRRFs). Today, a paradigm shift is occurring that focuses on solving problems at the nexus of Nutrients, Energy, and Water (NEW). It is imprudent to consider one of these aspects without accounting for their influences on the others.

The water that is produced at WRRFs is not only discharged to the environment, but is also reused in applications such as industry, nuclear power production, and direct and indirect potable reuse. With these uses in mind, treatment technologies must account for removal of traditional pollutants such as oxygen demanding waste (e.g., biochemical oxygen demand [BOD]) as well as emerging pollutants such as pharmaceuticals and personal care products, also known as micropollutants.

Additionally, energy recovery is highly desirable, as is the production of value-added products from waste streams (Liu et al., 2017; McCarty et al., 2011; Mo and Zhang, 2013). Anaerobic treatments such as anaerobic membrane bioreactors (AnMBRs) and anaerobic digestion (AD) produce methane, which can offset some energy requirements for WRRFs. Anaerobic processes also offer an opportunity for downstream nutrient recovery, and thus an option to produce and recover a valuable product instead of using energy to convert nutrients to a wasted product (e.g., as N_2 off-gas). Treatment systems such as these offer an integrated resource-centric approach to remove micropollutant contaminants while recovering resources such as carbon, nitrogen, and phosphorus to produce value-added products in the form of energy (e.g., methane, electricity) and nutrient-enriched fertilizers.

1.2   Anaerobic Treatment and Nutrient Recovery

Due to the nature of anaerobic treatment, non-reactive phosphorous and nitrogen can be transformed biologically to orthophosphate and ammonium, which makes WRRF effluents a potential point source for discharging reactive nutrients into natural waterbodies (Bravo et al., 2017; Seib et al., 2016). Excess concentrations of phosphorus and nitrogen in natural waterways stimulate the overgrowth of algae, or eutrophication. This can result in serious environmental damage, including hypoxic "dead" zones (as in the Gulf of Mexico and about 400 other locations worldwide), toxic cyanobacteria blooms, loss of fish habitat, and deterioration of water quality for human use due to color, taste, and odor (Mayer et al., 2013; Rittmann et al., 2011). To mitigate these issues, wastewater discharges must meet phosphorus and nitrogen discharge limits. Regulations and guidelines defining allowable nutrient concentrations are becoming increasingly more stringent, as evidenced by recent regulations in Wisconsin (Wisconsin DNR, 2010).

Ironically, with the problem of too much nutrients, global food production simultaneously faces the threat of nutrient scarcity. The source of fertilizer phosphorus is currently non-renewable mineral reserves, and Haber-Bosch nitrogen fixation for fertilizer production is energy intensive (Neset and Cordell, 2012), both of which can limit global food production. Wastewater treatment systems need to play a critical role in minimizing the risks to agriculture and water quality by incorporating treatment processes focused on sustainable nutrient management, *i.e.,* remove orthophosphate and ammonium from water and recover them for reuse as fertilizer. One approach is to use ion exchange-regeneration followed with struvite precipitation to concentrate and recover phosphate and ammonium in the form of solid fertilizer (Williams et al., 2015).

1.3   Pyrolysis for Biosolids Treatment

Residual wastewater solids are another by-product of wastewater treatment that can serve as a valuable resource. Pyrolysis offers great potential for WRRFs as a biosolids management strategy. Pyrolysis is a process that involves heating biomass in the absence of oxygen at approximately 500-800°C. The process produces high-energy products in py-gas and py-oil, and a solid product, biochar (Liu et al., 2017). The biochar can serve as a beneficial soil amendment (Lehmann and Joseph, 2009). A WRRF could pyrolyze biosolids to reduce the volume of biosolids produced, which would reduce the costs of transporting biosolids for final disposal, and also produce a marketable beneficial soil amendment, biochar. If a WRRF already dries biosolids, the energy available in py-gas and py-oil can be used to offset drying costs (McNamara et al., 2016). In addition to serving as a valuable soil amendment, biosolids-derived biochar also has potential as a sustainable adsorbent material and could potentially be used to remove micropollutants via adsorption.

1.4   Organic Micropollutants in Wastewater

The occurrence of organic micropollutants in the environment is usually associated with increasing population and anthropogenic activities. Industries and municipalities are the biggest sources of organic micropollutants (Schwarzenbach et al., 2006). It is estimated that 300 million tons per year of synthetic industrial chemicals, consumer products such as pharmaceuticals, flame retardants, artificial sweeteners, and hormones enter natural waters globally, mainly through industrial and municipal wastewater discharges (Blair et al., 2013; Phillips et al., 2010; Schwarzenbach et al.,

2006; Servos et al., 2005). Other sources that contribute to water pollution include agricultural runoff carrying pesticides and herbicides and accidental gasoline spills (Schwarzenbach et al., 2006), which can contaminate surface and groundwater directly. As WRRFs collect the majority of discharges from anthropogenic activities, they are a major collection and release point of organic micropollutants (Servos et al., 2005).

Micropollutants are of concern because they elicit biological and ecological impacts at very low concentrations (ng/L). These compounds do not necessarily result in acute toxicity; instead, they cause long-term effects in organisms chronically exposed to these compounds. For example, in the South Platte River in Boulder, Colorado, minnow populations were sampled upstream and downstream from discharge of a wastewater effluent that contained low concentrations of estrogenic compounds. Upstream of the treatment plant, the minnow population was approximately 50% male, but downstream, males accounted for approximately 20% of the population, and nearly a third of the population was intersex (Vajda et al., 2008). Other impacts of micropollutants include inducing antibiotic resistance in bacteria in natural and engineered environments (Carey et al., 2016).

1.5 Adsorptive Behavior of Micropollutants in WRRFs

Micropollutant's fate in WRRFs can follow one of the following pathways: 1) biodegradation during biological treatments, 2) release in the treated effluent, 3) volatilization into air, or 4) adsorption onto solids. In this dissertation, only the adsorptive behavior of micropollutants onto solid materials will be discussed. The fate of micropollutants due to adsorption during biological treatment has been studied previously on the basis of the adhesive nature of some micropollutants on sludge solids. The amount

adsorbed varies greatly depending on the sludge, as well as the physical and chemical properties (such as K_{ow} and pK_a) of the pollutants. For example, the extent of adsorption of triclosan onto sludge can vary substantially, ranging from 15% to 100%, resulting in sludge concentrations ranging from µg/kg to several mg/kg sludge (Blair et al., 2013; Lozano et al., 2013).

The removal of micropollutants in WRRFs can also be achieved via adsorption onto solid engineered adsorbents such as activated carbon. For example, activated carbon was shown to remove carbamazepine, 17β-estradiol, and sulfamethoxazole removal via adsorption (Snyder et al., 2007). Biochar is also a carbonaceous solid material, the ability of which to adsorb organic micropollutants from wastewater is gaining more attention. For example, endocrine disruption compounds (Jung et al., 2013) and triazine herbicides (Xiao and Pignatello, 2015) were removed via adsorption by plant-derived biochar. Previous research utilizing biochar as an adsorbent have been primarily conducted using biochar derived from plant residuals, whereas very little assessment of biosolids-derived biochar's micropollutant adsorption capacity has been performed.

Nutrient removal and recovery from wastewater, which is an emerging side stream treatment strategy, is gaining more attention, and may also present an adsorptive pathway for micropollutants. The treatment process of ion exchange and regeneration followed with struvite precipitation can effectively concentrate nutrient ions to produce solid fertilizer (Williams et al., 2015). Research has shown that polymeric ion exchange resins and the natural ion exchanger zeolite adsorb pharmaceuticals and pesticides (Humbert et al., 2008; de Ridder et al., 2012). In this dissertation, solid exchangers are used for removing nutrients; however, there is lack of research describing how

micropollutant's adsorptive behavior influences their fate and impact during nutrient ion exchange process. Therefore, more adsorption research on this topic is required. There are very few studies on micropollutant's fate during struvite precipitation. Depending on micropollutant properties and struvite precipitation conditions, different outcomes may be observed. For example, tetracycline in wastewater ended up in struvite crystals (Başakçilardan-Kabakci et al., 2007), while carbamazepine and ethinylestradiol concentrations in urine remained unchanged during struvite precipitation (). The fate of a broader suite of micropollutants during struvite precipitation for nutrient recovery needs to be studied.

Solid adsorbents, including activated carbon or biochar, could be used to remove micropollutants from wastewater as a polishing treatment step. For example, hormonal micropollutants can be removed via powdered activated carbon (Yoon et al., 2003). This removal strategy utilizes the adsorptive behavior of micropollutants. Similarly, biochar can be made from pyrolysis of a variety of carbon based feedstocks, but research on adsorption to biochar is still in its infancy as an adsorbent to remove micropollutants (McLaughlin, 2016). Multiple studies have been conducted to test the feasibility of using biochars that are derived from plant residuals and animal manure to adsorb hormones, pharmaceuticals and pesticides (Jung et al., 2013; Cederlund et al., 2016; Ahmad et al., 2013). Similarly, biochar derived from wastewater treatment biosolids should be able to adsorb some organic micropollutants. With biosolids-derived biochar's easy accessibility and abundancy for those WRRFs that equipped with a pyrolyzer, more research is needed in order to assess removal of micropollutants with biosolids-derived biochar via adsorption. Moreover, biochar could potentially be employed prior to nutrient removal

and recovery strategies to remove micropollutants prior to forming value-added nutrient products such as struvite.

1.6   Research Objectives

The overall objective of this dissertation was to qualitatively and quantitatively evaluate the adsorptive behaviors of a suite of commonly detected organic micropollutants on biochar and ion exchange resins. The compounds were selected due to their detection in anaerobic treatment effluents and differences in their physical-chemical properties (dissociation constants and hydrophobicity). Their adsorptive behaviors were characterized to help determine the impact and fate of micropollutants during nutrient removal/recovery processes using ion exchange resins, and the feasibility of employing biosolids-derived biochar as an adsorbent for removal of micropollutants.

Specifically, the first objective was to determine how micropollutants, triclosan, 17β-estradiol, and sulfamethoxazole impact nutrient removal and recovery using ion exchange-regeneration followed by struvite precipitation. Batch experiments were conducted to determine the aqueous-phase concentrations of the micropollutants were quantified at each stage of the process. The results are presented in **Chapter 3**.

The second objective was to establish the feasibility and mechanisms of micropollutant removal by biosolids-derived biochar via adsorption. Pyrolysis temperature and water quality parameters were varied, and their influences on triclosan were evaluated. Biochar properties including surface charge, functional groups, pore size distribution and specific surface area were analyzed to assess micropollutant-biochar interactions. This study on TCS adsorption is presented in **Chapter 4**.

The third objective was to determine the thermodynamic parameters characterizing micropollutant-biochar adsorption to assist in evaluating the spontaneity of adsorption, the adsorption mechanisms, and the adsorbent's binding affinity for the micropollutants. Batch experiments were performed on benzalkonium chloride, carbamazepine, 17β-estradiol, 17α-ethynylestradiol, and triclosan. These results are presented in **Chapter 5**.

The forth objective was to explore the reusability of biosolids-derived biochar, and its functionality as a pre-polishing step to remove triclosan, 17β-estradiol, and triclosan, for the nutrient ion exchange process. The experiments were operated in flow-through column reactors. The results are presented in **Chapter 6**. Finally, conclusions are presented in **Chapter 7**.

1.7   References

Ahmad, M., Moon, D.H., Vithanage, M., Koutsospyros, A., Lee, S.S., Yang, J.E., Lee, S.E., Jeon, C., Ok, Y.S., 2013. Production and use of biochar from buffalo-weed (Ambrosia trifida L.) for trichloroethylene removal from water. J. Chem. Technol. Biotechnol. 89, 150-157. doi: 10.1002/jctb.4157

Alvarino, T., Suarez, S., Lema, J.M., Omil, F., 2014. Understanding the removal mechanisms of PPCPs and the influence of main technological parameters in anaerobic UASB and aerobic CAS reactors. J. Hazard. Mater. 278, 506–513. doi:10.1016/j.jhazmat.2014.06.031

Blair, B.D., Crago, J.P., Hedman, C.J., Klaper, R.D., 2013. Pharmaceuticals and personal care products found in the Great Lakes above concentrations of environmental concern. Chemosphere 93, 2116–2123. doi:10.1016/j.chemosphere.2013.07.057

Blair, B.D., Crago, J.P., Hedman, C.J., Treguer, R.J.F., Magruder, C., Royer, L.S., Klaper, R.D., 2013. Evaluation of a model for the removal of pharmaceuticals, personal care products, and hormones from wastewater. Sci. Total Environ. 444, 515–21. doi:10.1016/j.scitotenv.2012.11.103

Bravo, H.R., Bootsma, H., Khazaei, B., 2017. Modeling the transport and fate of phosphorus from a point source in the Lake Michigan nearshore zone, in: 37th

International Association of Hydraulic Research World Congress.

Carey, D.E., Zitomer, D.H., Hristova, K.R., Kappell, A.D., McNamara, P.J., 2016. Triclocarban Influences Antibiotic Resistance and Alters Anaerobic Digester Microbial Community Structure. Environ. Sci. Technol. 50, 126–134. doi:10.1021/acs.est.5b03080

Cederlund, H., Borjesson, E., Lundberg, D., Stenstrom, J., 2016. Adsorption of pesticides with different chemical propertis to a wood biochar treated with heat and iron. Water Air Soil Pollut. 227-203. doi: 10.1007/s1127

Humbert, H., Gallard, H., Suty, H., Croue, J., 2008. Natural organic matter (NOM) and pesticides removal using a combination of ion exchange resin and powdered activated carbon (PAC). Water Res. 42, 1635-1643. doi: 10.1016/j.watres.2007.10.012

Joss, A., Andersen, H., Ternes, T., Richle, P.R., Siegrist, H., 2004. Removal of Estrogens in Municipal Wastewater Treatment under Aerobic and Anaerobic Conditions: Consequences for Plant Optimization. Environ. Sci. Technol. 38, 3047–3055. doi:10.1021/es0351488

Jung, C., Park, J., Lim, K.H., Park, S., Heo, J., Her, N., Oh, J., Yun, S., Yoon, Y., 2013. Adsorption of selected endocrine disrupting compounds and pharmaceuticals on activated biochars. J. Hazard. Mater. 263 Pt 2, 702–10. doi:10.1016/j.jhazmat.2013.10.033

Lehmann, J., Joseph, S., 2009. Biochar for Environmental Management, Science And Technology. Earthcan.

Liu, Z., McNamara, P., Zitomer, D., 2017. Autocatalytic Pyrolysis of Wastewater Biosolids for Product Upgrading. Environ. Sci. Technol. 51, 9808–9816. doi:10.1021/acs.est.7b02913

Lozano, N., Rice, C.P., Ramirez, M., Torrents, A., 2013. Fate of Triclocarban, Triclosan and Methyltriclosan during wastewater and biosolids treatment processes. Water Res. 47, 4519–27. doi:10.1016/j.watres.2013.05.015

Mayer, B.K., Gerrity, D., Rittmann, B.E., Reisinger, D., Brandt-Williams, S., 2013. Innovative strategies to achieve low total phosphorus concentrations in high water flows. Crit. Rev. Environ. Sci. Technol. 43, 409–441. doi:http://dx.doi.org/10.1080/10643389.2011.604262

McCarty, P.L., Bae, J., Kim, J., 2011. Domestic wastewater treatment as a net energy producer - can this be achieved? Environ. Sci. Technol. 45, 7100–6. doi:10.1021/es2014264

McLaughlin, H., 2016. An overview of the current biochar and activated carbon markets. http://www.biofuelsdigest.com/bdigest/2016/10/11/an-overview-of-the-current-biochar-and-activated-carbon-markets/

McNamara, P., Koch, J., Liu, Z., Zitomer, D., 2016. Pyrolysis of dried wastewater biosolids can be energy positive. Water Environ. Res. 9, 804-810

Mo, W., Zhang, Q., 2013. Energy-nutrients-water nexus: Integrated resource recovery in municipal wastewater treatment plants. J. Environ. Manage. 127, 255–267. doi:10.1016/j.jenvman.2013.05.007

Monsalvo, V.M., McDonald, J.A., Khan, S.J., Le-Clech, P., 2014. Removal of trace organics by anaerobic membrane bioreactors. Water Res. 49, 103–112. doi:10.1016/j.watres.2013.11.026

Neset, T.S.S., Cordell, D., 2012. Global phosphorus scarcity: Identifying synergies for a sustainable future. J. Sci. Food Agric. 92, 2–6. doi:10.1002/jsfa.4650

Phillips, P.J., Smith, S.G., Kolpin, D.W., Zaugg, S.D., Buxton, H.T., Furlong, E.T., Esposito, K., Stinson, B., 2010. Pharmaceutical formulation facilities as sources of opioids and other pharmaceuticals to wastewater treatment plant effluents. Environ. Sci. Technol. 44, 4910–4916. doi:10.1021/es100356f

Rittmann, B.E., Mayer, B., Westerhoff, P., Edwards, M., 2011. Capturing the lost phosphorus. Chemosphere 84, 846–853. doi:10.1016/j.chemosphere.2011.02.001

Schwarzenbach, R.P., Escher, B.I., Fenner, K., Hofstetter, T.B., Johnson, C.A., von Gunten, U., Wehrli, B., 2006. The challenge of micropollutants in aquatic systems. Science 313, 1072–1077. doi:10.1126/science.1127291

Seib, M.D., Berg, K.J., Zitomer, D.H., 2016. Reduced energy demand for municipal wastewater recovery using an anaerobic floating filter membrane bioreactor. Environ. Sci. Water Res. Technol. 2, 290–297. doi:10.1039/C5EW00244C

Servos, M.R., Bennie, D.T., Burnison, B.K., Jurkovic, A., McInnis, R., Neheli, T., Schnell, A., Seto, P., Smyth, S.A., Ternes, T.A., 2005. Distribution of estrogens, 17β-estradiol and estrone, in Canadian municipal wastewater treatment plants. Sci. Total Environ. 336, 155–170. doi:10.1016/j.scitotenv.2004.05.025

Snyder, S.A., Adham, S., Redding A.M., Cannon, F.S., DeCarolis, J., Oppenheimer, J., Wert, E.C., Yoon, Y., 2007. Role of membranes and activated carbon in the removal of endocrine disruptors and pharmaceuticals. Desalination. 202, 156-181

Vajda, A.M., Barber, L.B., Gray, J.L., Lopez, E.M., Woodling, J.D., Norris, D.O., 2008. Reproductive disruption in fish downstream from an estrogenic wastewater effluent. Environ. Sci. Technol. 42, 3407–14.

Van Der Wal, L., Jager, T., Fleuren, R.H.L.J., Barendregt, A., Sinnige, T.L., Van Gestel,

C.A.M., Hermens, J.L.M., 2004. Solid-phase microextraction to predict bioavailability and accumulation of organic micropollutants in terrestrial organisms after exposure to a field-contaminated soil. Environ. Sci. Technol. 38, 4842–4848. doi:10.1021/es035318g

Williams, A.T., Zitomer, D.H., Mayer, B.K., 2015. Ion exchange-precipitation for nutrient recovery from dilute wastewater. Environ. Sci. Water Res. Technol. 1, 832–838. doi:10.1039/C5EW00142K

Wisconsin DNR, 2010. Effluent Standards And Limitations For Phosphorus. US.

Yoon, Y., Westerhoff, P., Snyder, S.A., Esparza, M., 2003. HPLC-fluorescence detection and adsorption of bisphenol A, 17β-estradiol, and 17α-ethynyl estradiol on powdered activated carbon. Water Res. 37, 3530-3537. doi: 10.1016/S0043-1354(03)00239-2

2 LITERATURE REVIEW: ADSORPTION OF ORGANIC MICROPOLLUTANTS ONTO SOLID ADSORBENTS

Nomenclature

Q	mass loading of adsorbate on solids (mg/g)
Q_e	mass loading of adsorbate at adsorption equilibrium (mg/g)
J	flux of adsorbate (mg/g/min)
k_f	film diffusion coefficient
A	volumetric surface area of adsorbent (m^2/m^3)
C	adsorbate concentration in aqueous phase (mg/L)
C_e	adsorbate concentration in aqueous phase at equilibrium (mg/L)
D_s	effective surface diffusion coefficient (mm^2/s)
k_1, k_2	pseudo first-order (/min) and second-order rate constants (mol/L/s)
K_{ow}	octanol-water distribution coefficient
K	partition/distribution coefficient
K_L	Langmuir constant
K_f	Freundlich constant
K_c	thermodynamic equilibrium constant
ΔH_{st}	isosteric heat of adsorption (kJ/mol)
ΔH^0	standard enthalpy change of adsorption (kJ/mol)
ΔG^0	standard free energy change of adsorption (kJ/mol)
ΔS^0	standard entropy change of adsorption (J/mol/K)

2.1   Introduction

With respect to micropollutant fate during water/wastewater treatment, micropollutants can be discharged with liquid effluent, biodegraded, volatilized, or retained on sludge (wastewater) or filter beds packed with ion exchangers via adsorption (Jung et al., 2013; Neale et al., 2010). Adsorptive behavior of organic micropollutants onto solids in engineered and natural environments substantially affects the fate and removal of pollutants that are not favorable to biodegradation (Blair et al., 2013). From the perspective of removing micropollutants from the aqueous phase in WRRF, commonly used treatment technologies include adsorption filter beds packed with carbonaceous materials such as activated carbon. To design better treatment processes for removal of micropollutants, the fate and removal of micropollutants related to adsorption must be understood. Therefore, deeper insights into the kinetics, equilibrium, and

mechanisms that characterize adsorption behavior are required. For example, analysis of both the molecular structure of micropollutants and surface functional groups of the adsorbent are needed to extrapolate the potential inter-molecular forces that promote adhesion of micropollutants to adsorbents. Additionally, quantifying diffusion or reaction rate coefficients for adsorption is helpful in predicting breakthrough curves for fixed bed reactors (Chatzopoulos and Varma, 1995).

The purpose of this chapter is to provide a theoretical basis for adsorption equilibrium between organic micropollutants and engineered porous media. The discussion draws from contemporary published literature focused on the driving force, kinetics, molecular-scale interaction forces, and quantitative methods within the scope of aqueous-solid adsorption systems. Moreover, this chapter specifically describes how adsorption capacity relates to surface properties of biochar and ion exchange resins. Finally, the key research gaps that are addressed in this dissertation are presented at the end of this chapter.

2.2 Adsorbent surface properties and their adsorption abilities

The adsorption of organic contaminants on solid adsorbents is greatly affected by both the nature of the compounds—polar vs. non-polar and neutral molecules vs. dissociated ions—and the surface properties of the adsorbent. For instance, an adsorbent with smaller sized mesopores can have more steric hindrance effect on molecules diffusing onto adsorption sites deep in the pores (Pignatello et al., 2017). Additionally, an adsorbent that has a high non-polar organic carbon moiety ratio can be attractive to neutral hydrophobic molecules (Meyer et al., 2006). Understanding adsorption kinetics

and mechanisms therefore requires knowledge of the adsorbent itself. In this section, the surface properties of carbonaceous biochar and ion exchangers are discussed.

2.2.1 Biochar surface properties and the adsorption of organic contaminants

Biochar is the carbonaceous residual solid product produced by pyrolysis, which is a process that involves heating biomass feedstock in the absence of oxygen (Liu et al., 2017). Biochar surface properties depend on the characteristics of feedstock biomass, the pyrolysis process, and post-pyrolysis handling/treatment of biochar (Downie et al., 2012).

Structure and pores: Unlike coals and cokes that contain crystalline particles composing graphite-like layers, biochar structure is amorphous in nature (Downie et al., 2012). Therefore, the types of adsorption sites on biochar vary, and the site type distribution is usually not homogeneous. The carbon backbone structure of biochar often features slit-shaped pores or honeycomb structures (Keiluweit et al., 2010; Sun et al., 2012). Biochar pore size can range from sub-nanometer to tens of micrometers (Brewer et al., 2014; Downie et al., 2012), but a large portion of biochar pores are micropores (<2 nm) inside the pore network, while pores connecting to the biochar surface are mostly mesopores (2 nm to 50 nm) (Tseng and Tseng, 2006; Xiao and Pignatello, 2015). Steric hindrance due to pore geometry occurs when the pore aperture is too narrow for adsorbate molecules to quickly diffuse into deeper micropore sites. This effect is important when the ratio of pore aperture to the minimum critical organic molecular diameter is below 10 (Ruthven, 1992). Xiao and Pignatello (2015) studied biochar for adsorption of a series of triazines: pyridine, quinoline and prometon. The diffusion coefficient of these compounds into the biochar pores followed the order of pyridine>quinolone>prometon, which is the reverse order of the critical diameter. This

case showed that steric effect is important for triazines to diffuse into deep tunnels. The free energies of triazines and benzene on the same biochar also suggested that the adsorption of the triazine is suppressed by ~6.2 kJ/mol compared to benzene due to steric effects (Xiao and Pignatello, 2015).

Surface charge: The surface charge of biochar is an important property for adsorbing ionic molecules. Biochar may bear electrical charge deficits due to dissociable functional groups such as –OH, -H and –COOH in the biochar structures (Mukherjee et al., 2011). Surface charge can be measured using ion exchange capacity or zeta potential/iso-electric point. Ion exchange capacity for biochar is a term adapted from soil property (Mehlich, 1948). Cation exchange capacity (CEC) measures the negative charge of biochar for retaining cations, and vice-versa for anion exchange capacity (AEC). Zeta potential is more commonly used to quantify surface charge. Zeta potential is the potential at the hydrodynamic shear surface of a particle and can be used to predict the interaction (repulsion or attraction) between the particle and ions (Zhu and Pignatello, 2005). Zeta potential is impacted by aqueous phase pH and solution ionic strength. The pH at which zeta potential is zero is called the isoelectric point (IEP). The differentiation of the terms IEP and point of zero net charge (PZNC) is not clear. Some researchers pointed that IEP represents the external surface charge, while PZNC is for external and internal surface charges (Mukherjee et al., 2011, Radovic, 2012). However, researchers are in agreement that both of these terms represent a zero-surface charge condition.

The interactions between a charged surface and ions are likely affected by coulombic attraction. Both surface charge of biochar and the extent of dissociation of

organic pollutants as a function of pH should be taken into consideration when probing the role of coulombic interaction.

Organic content: Aromaticity and polarity are the two common indicators of organic content in biochar. Aromaticity is the proportion of aromatic carbon content over total carbon content (IUPAC, 2014). The aromaticity of biochar is influenced by feedstock and pyrolysis conditions. For example, using wood as the pyrolysis feedstock can promote aromaticity because of the high amount of aromatic lignin inherent in wood (Antal and Grønli, 2003). Biosolids derived from ash-rich feedstocks, such as municipal biosolids and manure, tend to have less aromaticity, which is also less impacted by pyrolysis conditions (Wang et al., 2012). As for the impact of pyrolysis conditions, the highest heat treatment temperature is often researched for the development of aromaticity of biochar. The Hydrogen/Carbon (H/C) index is used to indirectly represent the aromaticity—a low value indicates a high organic carbon portion and high aromaticity. As pyrolysis temperature increases, carbon concentration in biochar tends to increase, and aliphatic carbons become incorporated into aromatic rings by losing a hydrogen (Wang et al., 2012). Chen et al. observed that H/C values of pine-needle biochar decreased from 1.44 to 0.18 as pyrolysis temperature increased from 100˚C to 700 ˚C (Chen et al., 2008). Direct detection of aromatic structures in biochar can be conducted through nuclear magnetic resonance (McBeath et al., 2011). Negative correlations between biochar aromaticity and the Freundlich parameter n were observed when using biochar pyrolyzed at 100-700˚C to adsorb organic contaminants (Chen et al., 2008; Sun et al., 2011). High aromaticity (approximately 78% aromatic carbon) and strong nonlinear sorption (low n values, <0.4) observed for plant chars suggested that low-

molecular weight aromatic carbon may play a significant role in the overall sorption of fluorinated herbicides (Sun et al., 2011).

Polarity of carbonaceous adsorbents accounts for the aliphatic portion of the biochar and is also related to the adsorption of organic compounds (Kang and Xing, 2005). The proportion of polar functional groups can be indirectly represented using the Oxygen+Nitrogen/Carbon ((O+N)/C) index (Chen et al., 2008). High amounts of oxygen-containing functional groups, such as carboxyl groups, may increase the overall polarity of biochar. In general, high polarity biochar has stronger adsorption affinity and higher capacity for polar and ionic organic compounds, and a lower affinity for hydrophobic compounds (Grathwohl, 1990; Kang and Xing, 2005). For instance, the adsorption capacity parameter, K, of hydrophobic phenanthrene was inversely correlated with the polarity index (Kang and Xing, 2005). Increasing pyrolysis temperature can also substantially decrease biosolids-biochar polarity (Yuan et al., 2013).

Other dissociable functional groups: Other groups such as –COOH, -OH, and –NH$_2$, can serve as hydrogen donors to form H-bonds with organic compounds. The increase of these functional groups on biochar often relates to post-treatment steps used to condition biochar after pyrolysis. Treatment using oxidizers such as H$_2$SO$_4$ and HNO$_3$ increased the content of –COOH for cotton seed hull-biochar (Uchimiya et al., 2012). Due to the complexity of biosolids, it is also possible for the biochar to retain organic hydroxyl groups such as alcohol or phenolic hydroxyl groups (Lu et al., 2012).

2.2.2   Surface properties of non-carbonaceous adsorbents

Non-carbonaceous adsorbents such as natural and artificial ion exchangers are often employed for adsorbing inorganic and ionic contaminants for water/wastewater

treatment. The interactions between organic micropollutants and ion exchangers were less well known previously, but the structural properties of ion exchangers allow for adsorption of organic micropollutants. Since the backbone structures of artificial ion exchange resins are more well ordered than amorphous biochar, resin surface properties can be more easily elucidated in order to unveil their interactions with organic compounds. Widely used DOWEX-M4195 base resins consist of styrene, and to confer specificity, functional groups such as bispicolylamine can be permanently attached to this matrix (Sengupta and Pandit, 2011). The styrene matrix and the neutral functional groups of resins can be attractive to neutral organic compounds. Potential interactions can include weak intermolecular forces such as H-bonds and π-interactions. Exchangeable sites such as metallic groups on ion exchangers are responsible for the surface charge of ion exchangers and their ion exchange potential for ionic compounds via coulombic attraction. Ion exchangers can be used to remove and recover ionic orthophosphate and ammonium from wastewater. Due to micropollutants presence in wastewater and their potential interactions with ion exchange resins, the fate and impact of micropollutants during ion exchange for nutrient recovery needs to be addressed.

2.3   The kinetics of adsorption of aqueous-phase organic compounds onto porous media

Adsorption of dissolved molecules or ions onto porous adsorbents is typically described as a mass transfer process (diffusion) followed by adsorbate-adsorbent surface interactions. On this basis, several mathematical kinetic models have been developed. Based on incorporation of consecutive diffusion-adsorption steps (or not), the proposed

kinetic models can be categorized into two types: diffusion-controlled kinetics and reaction-controlled kinetics.

2.3.1 Diffusion-controlled kinetics

For molecules or ions in water, diffusion into the pores of porous adsorbents includes the following steps (Pignatello and Xing, 1996; Qiu et al., 2009): 1) diffusion in bulk liquid, 2) diffusion in the water film surrounding the porous adsorbent, and 3) diffusion in the liquid contained in the pores, in most cases called intraparticle diffusion.

The first step of mass transfer is diffusion of the adsorbate through the bulk liquid. This occurs nearly instantaneously after adding the adsorbent into the liquid. Its contribution to controlling the diffusion rate is negligible (Pignatello and Xing, 1996; Tran et al., 2017). Therefore, diffusion-controlled kinetic models are always controlled by film or intraparticle diffusion in batch adsorption systems (Xu et al., 2013).

The second step of mass transfer is film diffusion. Extending from the surface of the adsorbent, liquid forms a relatively stagnant thin film layer that the adsorbate must traverse before reaching the solid surface. In the case of liquid/solid adsorption, this thin film layer is sometimes called the hydraulic boundary layer (Benjamin and Lawler, 2013). If film diffusion is the rate-limiting step, the rate of adsorbate accumulation onto solids over time can generally be expressed using the simplified linear driving force model (LDF) (Britain, 1992; Qiu et al., 2009). In this model, the rate of accumulation of adsorbate on an adsorbent is proportional to the concentration gradient between bulk solution and the particle-liquid interface; this concentration gradient is the driving force for film diffusion. This rate model is derived from a mass balance setting the rate of

change of mass of adsorbate on solid equal to the net transport flux of adsorbate into bulk

solution from the boundary layer (eq. 2.1) (Benjamin and Lawler, 2013; Cooney, 1998):

$$\frac{dQ}{dt} = J_{BL} = k_f A(C - C_s) \quad \text{eq. 2.1}$$

where Q is the mass load of adsorbate on solids, J_{BL} is the flux at boundary layer

(mg/g/min), k_f is the film diffusion coefficient, A is the volumetric surface area of

adsorbent (m^2/m^3), C is the adsorbate concentration at the boundary layer and C_s is the

adsorbate concentration at the exterior surface of the adsorbent.

In a well-mixed batch reactor, the concentration gradient in the liquid film is

negligible; therefore, film diffusion is usually not rate limiting. In column systems,

however, the concentration gradient could be significant (Pignatello and Xing, 1996).

Sircar and Hufton (2000) compared the simplified LDF model with other more rigorous

models such as Fickian Diffusion and Quadratic Driving Force for analysis of adsorption

column data. They concluded that LDF was comparable with other models. Therefore,

LDF can be applied to describe kinetics for column adsorption, in which film diffusion is

the rate-limiting process. Furthermore, LDF can be applied to predict breakthrough

curves of fixed bed operation.

The third step of diffusion includes *pore diffusion*, which is when the adsorbate

penetrates to the center of the adsorbent particle, or *surface diffusion*, which is when the

adsorbate flux diffuses along the interior surface of the pores. These two types of

diffusion are difficult to distinguish in practice (Benjamin and Lawler, 2013). If the

adsorbate molecules encounter the greatest resistance during the third step, pore/surface

diffusion will be the rate-limiting step. Therefore, the mass balance will only characterize

the adsorbate in the solid phase, since changes of adsorbate concentration in bulk liquid

and film are negligible. In this case, a control volume is modeled as a thin, annular layer of adsorbent bounded by concentric spheres at radii of r and r+dr, and the basic mass balance relationship is written as (Benjamin and Lawler, 2013):

Rate of change of mass of adsorbate stored in the annulus between the two concentric spheres=flux of adsorbate diffusing into the annulus at r+dr – flux of adsorbate diffusing out of the annulus at r.

By substituting flux (J) in the mass balance equation with its pseudo-Fick's law expression (Collins and Kimball, 1949), the homogenous diffusion model can provide insight into changes in Q in time and space, as shown in eq. 2.2 (Cooney, 1998):

$$\frac{\partial Q}{\partial t} = \frac{D_s}{r^2}\frac{\partial}{\partial r}\left(r^2\frac{\partial Q}{\partial r}\right) \quad \text{eq. 2.2}$$

where D_s refers to the effective surface diffusion coefficient and is assumed to be constant for the particle, and r is the distance to the center of the adsorbent particle. Many special-case rate models have been developed, including the homogenous surface diffusion model (HSDM) (Tien, 1994), which considers only surface diffusion, whereas the pore diffusion model (PDM) only accounts for pore diffusion (Brauch and Schlünder, 1975; McKay, 1991; Merk et al., 1981). Since it is difficult to distinguish between pore diffusion and surface diffusion, the intraparticle model, a general homogenous diffusion model(Cooney, 1998), is commonly used to group pore/surface diffusion together.

Initial and boundary conditions need to be considered to solve the intraparticle diffusion rate equations as Q varies over time (Benjamin and Lawler, 2013; Xu et al., 2013). For example, the initial condition for the entire adsorbent particle at time 0 is Q=0 (zero uptake of adsorbate). The boundary conditions can include 1) no gradient of Q at the center of the particle and 2) equilibrium conditions between solid and solution phases, i.e., equilibrium isotherm ($Q_e=f(C_e)$) (Benjamin and Lawler, 2013). However, numerical

solutions to intraparticle diffusion rate equations are complicated even with proper assumptions (Cooney, 1998; Westwater and Drickamer, 1957). Therefore, the LDF model for intraparticle diffusion is derived as an approximated expression (Alpay and Scott, 1992). This linear driving force model for intraparticle diffusion assumes that the concentration in solid phase decreases linearly toward the center of the particle (Xu et al., 2013). Notably, the actual concentration gradient is not linear due to tortuosity in the interior of porous adsorbent particles. Therefore, the linear driving force model for intraparticle diffusion is a simplified approach of limited validity (Nakao and Suzuki, 1983).

2.3.2 Reaction-controlled kinetics

Another case to consider is the "adsorption reaction", when adhesion of the adsorbate onto the solid surface's adsorption sites is rate limiting, thereby controlling the overall adsorption rate. Therefore, reaction-controlled kinetic models characterize only the last step of adsorption, treating the rate of diffusion as negligible. The reaction rate-limiting kinetic approach is more appropriate for binding with adsorption sites via ion exchange or sharing electron pairs via covalent or ionic bond (Y.S. Ho and McKay, 1998).

The mathematical expressions of pseudo first-order (PFO) (Lagergren, 1898) and pseudo second-order (PSO) rates (Blanchard et al., 1984; Ho and McKay, 1999) are illustrated in eq. 2.3 and 2.4, respectively:

$$\frac{dQ}{dt} = k_1(Q_e - Q) \quad \text{eq. 2.3}$$

$$\frac{dQ}{dt} = k_2(Q_e - Q)^2 \quad \text{eq. 2.4}$$

where Q (mass adsorbate/mass adsorbent) is the mass adsorption capacity at time t, Q_e is the capacity at equilibrium, and k_1 and k_2 are the pseudo first-order and second-order rate constants, respectively. The kinetic order of the reactions is related to the stoichiometry of adsorption site and adsorbate molecule (Plazinski et al., 2009).

These two adsorption reaction models are used when adsorption itself is the rate-limiting step during the entire transport-adsorption process. For example, formation of a covalent bond between adsorbate and adsorbent or strong physical adsorption, such as ion exchange processes, are usually considered rate limiting. Proper applications of PFO and PSO kinetic models include adsorption of acidic pharmaceuticals on magnetic nanoparticles coated with zeolite (Salem Attia et al., 2013), and adsorption of divalent metal ions onto peat (Y. S. Ho and McKay, 1998), all of which were ion exchange processes.

Kinetic models provide direct information on the rate of diffusion or reaction. A higher diffusion or reaction rate constant indicates faster uptake of the adsorbate. Besides providing straightforward information, adsorption kinetics derived from batch tests are important in modeling the fate and transport of adsorbates through porous media such as soil, subsurface aquifer and other engineering environments because dynamic fate and transport models all include terms for adsorption (Pignatello and Xing, 1996; Xu et al., 2013). From the perspective of water treatment engineering, kinetic models are a prerequisite for predicting fixed bed adsorption performance. While fitting experimental data to kinetic models is necessary, it is not sufficient to extrapolate mechanism information. To achieve deeper comprehension of adsorptive behavior, batch kinetic studies combined with other approaches may be necessary to elucidate the underlying

mechanism of sorption (e.g., covalent binding or other physical adsorptions) (Simonin, 2016; Xu et al., 2013). Complimentary studies on adsorption kinetics, isotherms, thermodynamics, characterization of surface properties and adequate numerical analysis are needed to elucidate adsorption mechanisms.

2.4   Adsorption mechanisms of organic micropollutants binding to porous sorbents

In this literature review, the "mechanism of adsorption" refers to the mechanism of actual attachment, regardless of molecule/ion diffusion. Therefore, "pore filling", which is mentioned in some articles as an adsorption mechanism (Inyang and Dickenson, 2015), is excluded from this discussion because it does not characterize attachment. Attachment via adsorption is a process that takes place spontaneously since the associated free energy is negative. The driving force of attachment is the sum of a number of forces contributing to the total free energy of adsorption (Zhang and Somasundaran, 2006). Driving forces include intra- and inter-molecular interactions due to electrostatic attractions such as covalent bonding, coulombic attraction and dipole interactions. Dipole interactions can include hydrogen bonding (H-bonding), π-interaction, dipole-dipole interaction (Keesom interactions), dipole induced dipole interaction (Debye interactions), charge-dipole interactions, and fluctuating dipoles (dispersive forces/London Forces). For adsorption of organic molecules onto carbonaceous materials, van der Waals forces have been included as one type of non-coulombic interaction, in addition to H-bonding, and π/dipole interactions (Moreno-Castilla, 2004; Ni et al., 2011). However, this classification is problematic because the term van der Waals forces is used by some to describe the totality of all intermolecular non-covalent forces, while others use it to describe subsets of intermolecular forces ("Get your force right," n.d.; Williams, 2017).

Since this term is lacking in physical meaning and is not sufficiently descriptive, the use of "van der Waals force" to describe adsorption mechanisms should be avoided. Hydrophobic interactions between non-polar moieties has also been considered a mechanism for adsorption attachment (Inyang and Dickenson, 2015). However, hydrophobic interaction is not an intermolecular force. It is a non-specific interaction that has more to do with decreasing entropy related to chemicals leaving water as opposed to being attracted to adsorbents (Williams, 2017).

Covalent bonding is irreversible chemisorption through sharing electron pairs and is stronger than any form of non-covalent intermolecular forces. Conversely, adsorption involving non-covalent interactions is usually considered to be physical adsorption. Chemisorption is widely utilized to modify adsorbent surfaces with functional group additions. Preparation of hybrid ion exchangers with selectivity for certain ions is usually done by chelating functional groups onto polymeric backbone matrices (Blaney et al., 2007; Zhao and Sengupta, 1998). Functionalization of carbon nanoparticles with covalent modification is also widely achieved via reactions such as carboxylation, amidation, fluorination, and free radical chemistry (Kanagaraj and Rao, 1992; Yang and Xing, 2010).

Coulombic interaction is the interaction between two charged moieties. In the case of adsorption of organic compounds from aqueous solution, coulombic interaction relates to the dissociation of the organic adsorbate and dissociable functional groups on the adsorbent surface. Opposite charges on the adsorbate and adsorbent induce coulombic attraction. Ion exchanger functionality relies on different strengths of coulombic attraction. In the case of water/solid adsorption, pH and ionic strength is critical to the

dissociation of functional groups of organic adsorbates. This is reflected in their pKa (acid dissociation constant) values. Also, pH can contribute to adsorbent surface charge. In some reports, coulombic interactions are referred to as "Electrostatic interactions" (Hu et al., 2013; Hyung et al., 2007), which is inaccurate because electrostatic interaction is the fundamental basis for all non-covalent intermolecular forces (Hardinger, 2015)

Hydrogen bonding (H-bonding) is a special case of strong dipole interaction occurring between hydrogen donor and acceptor. The hydrogen donor is usually bonded to nitrogen (N), oxygen (O) or fluorine (F) within a functional group, such as –COOH, -OH, –NH$_2$, and electron-rich π-systems. Atoms such as N, O, and F act as hydrogen acceptors (IUPAC, 2014; Kah et al., 2017; Yang and Xing, 2010). These hydrogen donor/acceptor functional groups on either adsorbent surface or organic molecules can form H-bonds. For example, wood-derived biochar rich in oxygen-containing groups anchoring on its aromatic and hydrophobic surfaces resulted in high affinity for the electronegative ClO_4^- group in perchlorate via H-bonding (Fang et al., 2014).

Charge-assisted H-bonding (CAHB) is stronger than regular H-bonding. CAHB includes three categories: double charge-assisted (($\pm$)CAHB), positive charge-assisted ((+)CAHB), and negative charge-assisted ((-)CAHB) H-bonding (Gilli et al., 2009). Among these categories, (-)CAHB is often found in dissociable organic compound adsorption onto adsorbent functional groups (Lian et al., 2014; Teixidó et al., 2011). Gilli et al. defined (-)CAHB as strong H-bonding between proton donor/acceptor pairs (base as donor and acid as acceptor), e.g., between carboxyl group and its conjugate acid ([R-COO $\cdots$ H $\cdots$ OOC-R]$^-$) or different acid/base pairs (Gilli et al., 2009). The more similar the pKa values of the groups at either end of the hydrogen bond, the stronger the

(-)CAHB. Therefore, the strongest (-)CAHB occurs between an acid and its conjugated

base. Teixido et al. (2011) postulated formation of (-)CAHB between sulfmethoxazole

and the carboxylate group on biochar's surface at pH 3-7, where sulfmethoxazole

molecules dominate (Figure 2.1). The small pKa difference between sulfmethoxazole and

HOOC-surface values allows close sharing of the proton and confers covalent character

on this type of H-bond (Teixidó et al., 2011).
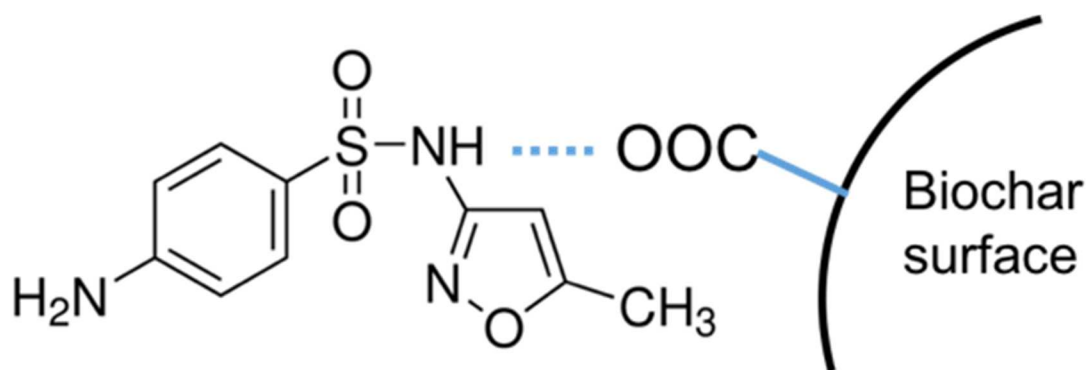
Figure 2.1 Sulfamethoxazole interaction with a COO- group on biochar's surface via negative charge-assisted hydrogen bonding ((-)CAHB). The dashed line denotes H-bonding.

π-interaction is another type of dipole interaction that is weaker than H-bonding.

This term is used to interpret attractions between neutral organic molecules and electron

rich π-systems, A π-system is usually a functional group that has π-bonds, which result

from overlap of diffusive electron orbitals. π-systems such as C=C double bonds or

aromatic rings can be attractive to polar molecules and other π-systems. For example,

biomass-derived carbon black has high aromatic content, facilitating π-interactions. The

aromaticity of biochar usually increases with pyrolysis temperature, since most of the

aliphatic structures are destroyed (Domingues et al., 2017; Fang et al., 2014). Polymeric

hybrid adsorbents such as ion exchange resins also contain aromatic rings (Blaney et al.,

2007). An aromatic π-system is electron rich and can either enhance existing H-bonds or

behave as proton acceptors. Mahmudov et al. (2010) found that a graphite-like activated carbon with aromatic sheet structure favored perchlorate adsorption due to π-system facilitation (Fang et al., 2014; Mahmudov and Huang, 2010). Due to the highly electronegative nature of π-systems, the attraction to cations is also favorable.

Intermolecular attractions between π-systems, known as π-π interactions, occur as well. π-π interactions occur between oppositely polarized quadrapoles of arene systems oriented in a parallel-planar fashion ("stacking") (Teixidó et al., 2011). Opposite polarization of aromatic systems induced their opposite preference to electrons. Therefore, the most widely adopted conceptual model to describe π-π interaction is the π-electron donor-acceptor model (EDA) (Hunter and Sanders, 1990; Kah et al., 2017). For instance, nitroaromatic moieties as π-electron acceptors can attach to the aromatic sheet structures (π-electron donor) of graphite and charcoal (Zhu and Pignatello, 2005). Using charge-transfer absorbance in the UV-visible absorption spectrum, π-π EDA interactions can be characterized as (Hunter and Sanders, 1990; Wijnja et al., 2004). Raman, NMR and fluorescence techniques are also applied to characterize other π interactions (Yang and Xing, 2010).

Other dipole interactions include permanent dipole interactions (also known as Keesom interactions), dipole-induced dipole interaction (Debye interactions) and fluctuating dipoles (dispersive forces or London Forces). These intermolecular forces may be applicable for adsorbents and adsorbates containing polar functional groups such as alkyl halide, ether and nitrile, etc. (Kah et al., 2017; Yang and Xing, 2010).

Hydrophobic interaction is a type of non-specific interaction that is primarily driven by entropy. While its underlying basis is not fully known, it is widely accepted

that hydrophobic interactions occur due to the tendency of non-polar groups to aggregate in water to minimize their contact with water molecules. Since this non-specific interaction is not driven by intermolecular forces with adsorbents, it is inappropriate to use the term "bond" for hydrophobic interaction (Meyer et al., 2006; Wijnja et al., 2004; Williams, 2017). The octanol-water distribution coefficient (K_{ow}) is an indicator of hydrophobicity of organic chemicals. If hydrophobic interaction is the dominant mechanism, adsorption of non-polar chemicals on porous materials would be proportional to K_{ow} values (Kah et al., 2017); however, this correlation is generally not observed, implying that hydrophobic interactions are not the dominant mechanism of attraction (Pan and Xing, 2008). Pan and Xing analyzed literature for adsorption coefficient of organics on carbon nanomaterials and compounds' K_{ow}, and failed to establish an explicit relationship (Pan and Xing, 2008).

Table 2.1 summarizes potential mechanisms for aqueous-phase organic compound adhesion onto solid adsorbents.

Table 2.1 Adsorption mechanisms. For intermolecular forces, the strength increases from bottom to top.

physical adsorption	non-specific intermolecular interaction	hydrophobic interaction
	intermolecular force	dipole interactions
		π-interaction
		H-bonding
		coulombic attraction
chemisorption	**intermolecular force**	covalent bond

2.5 Quantitative methods for characterizing adsorption of organic micropollutants on porous media from water

2.5.1 Isotherms

An adsorption isotherm is a quantitative method to characterize adsorbate equilibrium between aqueous and solid phase at a constant ambient temperature. Typical isotherm models used for organic contaminants include Langmuir, Freundlich, Toth (Tóth, 1971), Tempkin (Temkin and Pyzhev, 1940) and Dubinin–Radushkevich (Dubinin, M.M., Radushkevich, 1947), and other empirical models. The derivations of isotherm models for certain chemicals are based on the binding affinity/strength distribution on the adsorbent surface (Benjamin and Lawler, 2013). Assuming one adsorbate molecule binds with a single site on the adsorbent, and the total number of adsorption sites on the surface is limited, binding affinity of the chemical to the adsorption site is usually indicated by a partition or distribution coefficient, K, which is expressed as shown in eqs. 2.5 and 2.6:

$$\equiv S + A(aq) \leftrightarrow \equiv SA \quad \text{eq. 2.5}$$
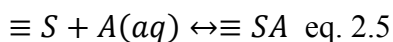
$$K = \frac{C_{\equiv SA}}{C_{\equiv SA}C_{A(aq)}} \quad \text{eq. 2.6}$$

Where $\equiv S$ is the adsorption site on the surface, A (aq) is the adsorbate molecule in aqueous phase, $\equiv SA$ is adsorbate-adsorption site complex, K is the distribution coefficient, and C represents the concentration of the respective species.

The derivation of the Langmuir isotherm assumes that a surface has a uniform K value, i.e., all adsorption sites are identical and have the same affinity for a certain adsorbate. Also, the binding of a single adsorbate does not interfere with the binding of other molecules. The sites on the adsorbent can be classified as $Q_{\equiv SA}$, or the occupied

sites per unit mass of adsorbent (adsorption capacity), or $Q_{\equiv S}$, the unoccupied sites. The

total adsorption sites per unit mass of adsorbent is Q_{max}. By substituting these values into

the expression for K, the Langmuir isotherm model is generated (eq. 2.8):

$$Q_{\equiv SA} = \frac{Q_{max}KC_A}{KC_A+1} \text{ eq. 2.8}$$

The term $\frac{KC_A}{KC_A+1}$ is also called the fractional coverage of the sites with a

distribution value of K (Benjamin and Lawler, 2013) because it equals $\frac{Q_{\equiv SA}}{Q_{max}}$. Artificial

polymeric adsorbents, such as ion exchangers are considered to have adsorption sites

with a single binding affinity K (Xing et al., 1996), which is usually denoted as K_L in the

case of the Langmuir isotherm. Therefore, Langmuir isotherm are often good choices for

modeling removal of inorganic ions (Rengaraj et al., 2003; Rengaraj and Moon, 2002).

However, equilibrium data for adsorption of organic compounds on carbonaceous

materials such as activated carbon, biochar and carbon nanotubes is rarely fit to the

conventional Langmuir isotherm.

In the case that multiple types of sites have different K values, the Langmuir

isotherm model for each type of adsorption site can be summed to obtain the multi-site

Langmuir isotherm (eq. 2.9):

$$Q_{total} = \sum_{j=1}^{n} \frac{Q_{max,j}K_jC}{1+K_jC} \text{ eq. 2.9}$$

where K_j is the binding affinity of each type of adsorption site (j). The multi-site

Langmuir isotherm has been applied, e.g., in the adsorption of phosphate onto soil via ion

exchange, where the soil samples may have two to three types of adsorption sites

(Holford et al., 1974; Syers et al., 1973).

In many adsorbents, the distribution of site types is variable and sites with single-value or multiple-value K are hard to find. This leads to the extrapolation of the Freundlich isotherm, where site distribution is described as semi-continuous. The adsorbent comprises a small number of sites with high affinities (larger K values) and an exponentially increasing number of sites with steadily decreasing K values. A small group of sites is considered to have nearly uniform K value (between K and K+dK). In this differential area, it is assumed that the concentration of total adsorption sites can be described as a distribution (eq. 2.10) associated with K (Benjamin and Lawler, 2013; Halsey and Taylor, 1947):

$$\Phi_{diff} = \alpha K^{-n} \quad \text{eq. 2.10}$$

where α and n are constants and $0 \leq n \leq 1$. The differential adsorption capacity, Q_{diff}, for this area can be characterized by the Langmuir isotherm, modified as shown in eq. 2.11:

$$Q_{diff} = \Phi_{diff} \frac{KC_A}{KC_A+1} \quad \text{eq. 2.11}$$

By substituting eq. 2.10 into eq. 2.11, and integrating the adsorption capacity over all sites (K from 0 to ∞), eq. 2.12 is obtained to describe adsorption capacity:

$$Q = \int_0^\infty \frac{\alpha K^{1-n} C_A}{KC_A} dK \quad \text{eq. 2.12}$$

Halsay and Taylor (Halsey and Taylor, 1947) developed the solution for eq. 13, yielding the Freundlich isotherm (eq. 2.13):

$$Q = K_f C_A^n \quad \text{eq. 2.13}$$

Where K is the Freundlich parameter, which is usually denoted as K_f in this case, reflecting adsorption capacity. The n term ranges from 0 to 1, and is an indicator of distribution of binding affinity or binding energy on adsorbent surface—the more

drastically the binding affinity changes (indicating the existence of remarkably strong affinity sites) across the adsorbent surface, the smaller the n value. For carbonaceous materials such as activated carbon and biochar, the adsorption of organic contaminants from dilute solution (C <500 µg/L) is often characterized by an n value between 0.2 to 0.7 (Benjamin and Lawler, 2013). Compared to the Langmuir isotherm, the Freundlich isotherm often fits better in the case of adsorption of organic chemicals onto carbonaceous materials, possibly because of the uneven distribution of adsorption sites. For example, in a study adsorbing the acidic herbicides dicamba and 2,4,5-T on carbon nanotubes, Pyrzynska et al. (2007) found that the Freundlich isotherm provided a better fit than Langmuir for describing their adsorption equilibrium.

The Freundlich isotherm is described as an empirical model in some literature (Ho, 2006; Matsumoto, 1993). However, as shown previously, the Freundlich isotherm has a theoretical basis and is related to the Langmuir model, i.e., integration of the Langmuir isotherm yields the Freundlich equation (Xing et al., 1996). A few studies found that the adsorption/exchange of fluoride and cobalt onto ion exchange resins can fit both Langmuir and Freundlich at certain C_{aq} ranges (Meenakshi and Viswanathan, 2007; Rengaraj and Moon, 2002), which supports the inherent relationship between these two isotherm models.

In many cases where organic compounds are present at more than trace amounts (mg/L) in water, more complicated models are needed (Limousin et al., 2007). Foo and Hameed's (2010) review summarized a collection of isotherms including Toth (Tóth, 1971), Tempkin (Temkin and Pyzhev, 1940), Dubinin–Radushkevich (Dubinin, M.M., Radushkevich, 1947), empirical isotherms, etc., which are used to characterize organic

compound adsorption (Gholizadeh et al., 2013; Lee et al., 2004; Nastaj et al., 2016). Regardless of the form of the isotherm, Limousin et al. (2007) stated that treating the model as an integral of the Langmuir isotherm is reasonable. The generalized isotherm can be generated by integrating eq. 12 over all available K values, with the site distribution equation Φ_{diff} determined in each case.

An isotherm is a useful tool to aid in numeric characterization of adsorption behavior. The expression of isotherm equations can predict adsorption capacities on solid phases at different equilibrium aqueous-phase concentrations. The Langmuir constant Q_{max} is the measurement of a monolayer's maximum adsorption capacity, and the Freundlich parameter K_f can also roughly reflect adsorption capacity when comparing multiple adsorbent-adsorbate systems. Besides providing straightforward information, such as illustrating the equilibrium status of adsorbate molecules between aqueous and solid phases, isotherm equations are also an important boundary condition to solve transport equations for an adsorbate in fixed bed reactors (Benjamin and Lawler, 2013; Chatzopoulos and Varma, 1995). Chern and Chien (2002) studied nitrophenol adsorption onto a fixed bed of activated carbon. They used kinetics and transport equations, in combination with Langmuir or Freundlich isotherms, to extrapolate breakthrough curves describing the relationship between time and effluent concentration.

The distribution coefficient K used in derivation of isotherms is related to the thermodynamic equilibrium constant (K_c=exp (-ΔG^0/RT)), and the surface site distribution function Φ_{diff} is related to K. These underlying thermodynamic bases of isotherms can provide insight into adsorption mechanisms, adsorbent surface properties, and the degree of affinity of the adsorbents (Foo and Hameed, 2010).

2.5.2 Thermodynamics of adsorption

Thermodynamics, like isotherms, plays an essential role in characterizing adsorption equilibrium and mechanisms. Important thermodynamic parameters for adsorption include the change of enthalpy/heat (ΔH^0), the change of entropy (ΔS^0) and the change of standard free energy (ΔG^0), which are related as shown in eq. 2.14:

$$\Delta G^0 = \Delta H^0 - T\Delta S^0 \quad \text{eq. 2.14}$$

The dimensionless equilibrium constant of adsorption, K_c, is related to ΔG^0 (eq. 2.15):

$$\Delta G^0 = -RTlnK_C \quad \text{eq. 2.15}$$

where R is the gas constant, T is the ambient temperature (K), and K_c is the thermodynamic equilibrium constant. The equilibrium constant can be derived from the constants in Langmuir, Freundlich and other isotherm models (Tran et al., 2017). Therefore, the two-phase equilibrium of adsorption, i.e., an isotherm, is related to the thermodynamic properties of the adsorption system (both adsorbate and adsorbent). In this section, the thermodynamics of adsorption is discussed to provide additional quantitative insights into the equilibrium of organic micropollutant adsorption and the related binding mechanisms.

2.5.2.1 Isosteric heat of adsorption

Isosteric heat of adsorption is the differential heat of adsorption at a fixed surface (or adsorption capacity, Q_e) at equilibrium. This term was originally introduced for quantifying gaseous-phase adsorption (Do et al., 2011; Myers, 2002; Myers and Monson, 2014), and was adapted for adsorption from aqueous solution (Builes et al., 2013;

Srivastava et al., 2006). It is defined according to the Clausius-Clapeyron equation (eq. 2.16):

$$q_{st} = \Delta H_{st} = R \frac{dlnC_e}{d1/T}\bigg|_{Q_e} \quad \text{eq. 2.16}$$

where ΔH_{st} is the isosteric heat of adsorption (kJ/mol), R is the gas constant (J/mol·K), C_e is the aqueous phase concentration at equilibrium (mol/L) and T is temperature (K). On the basis of this relationship, isosteric heat of adsorption at certain adsorbent coverages can be experimentally determined by obtaining C_e values using isotherm curves at multiple ambient temperatures, and calculating the slope of the lnC_e versus 1/T curve. Figure 2.2A and 2.2B are typical profiles of isosteric heat changing with adsorbent surface coverage.
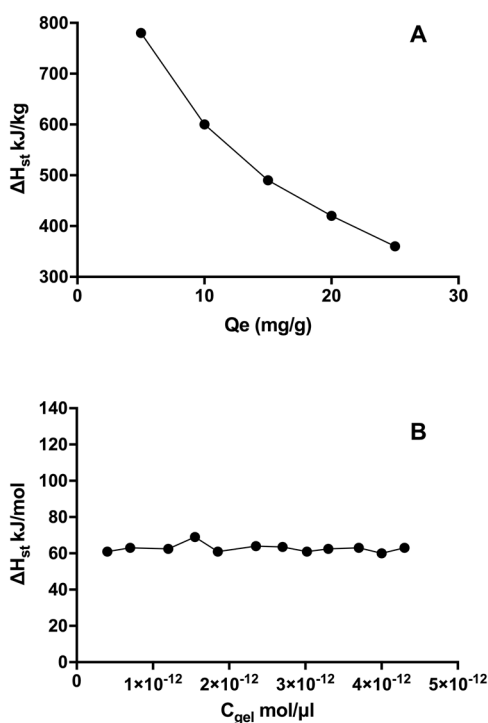
Figure 2.2: A) isosteric heat of phenol adsorption by bagasse fly ash varying with surface loading, adapted from Srivastava et.al (2006), and B) isosteric heat change of protein adsorption on ion exchange resin gel, adapted from Chen et al. (2007).

The different trends in isosteric heat change over surface loading stem from different adsorption site properties. Since isosteric heat is a widely used term that is indicative of the energy and strength of binding interactions (Murialdo et al., 2015; Weber and Talapatra, 2000), the adsorption site distribution of an adsorbent can be postulated from the q_{st} versus Q_e profile. For phenol adsorption on bagasse fly ash, Figure 2.2a shows isosteric heat decreasing with surface coverage. Figure 2.2b is the isosteric heat of lysozyme binding with different ion exchange resins; some curves stayed quite flat over the range of surface coverage tested. The ion exchange resin's binding with lysozyme can be well characterized by the Langmuir model, which assumes adsorption sites have a fixed binding affinity and no interaction among adsorbed molecules. The isosteric heat of adsorption should therefore not change with surface adsorbate loading (Benjamin and Lawler, 2013; Yoo, 2013). Since bagasse fly ash has highly heterogeneous adsorption sites, phenol binding is highest with high-strength sites at low surface coverage, because high-energy binding sites are more favorable (Srivastava et al., 2006). Thus, the isosteric heat of adsorption is higher at the left part of the curve. As high-energy sites are gradually occupied, low-energy sites bind with phenol molecules, absorbing less heat at high surface coverage (Srivastava et al., 2006). This type of isosteric heat distribution aligns with equilibrium isotherm models describing multi-type site distribution, such as the Freundlich isotherm (Benjamin and Lawler, 2013).

Weber et al. proposed a relationship between isosteric heat (q_{st}) and binding energy (E_b), as shown in eq. 2.17:

$$q_{st} = E_b + 2kT \text{ eq. 2.17}$$

where E_b is the binding energy of the adsorbate molecule adsorbing on a certain type of adsorption site, k is the Boltzmann constant, and T is the temperature. This equation shows that the binding energy can be extracted from adsorption isotherm measurements (Weber and Talapatra, 2000; Yoo, 2013).

2.5.2.2   Enthalpy change of adsorption

The enthalpy change of adsorption is different from isosteric heat of adsorption, but the two terms are related. However, use of the two terms is often confusing and, in many cases, the isosteric heat of adsorption is described as heat/enthalpy of adsorption (Srivastava et al., 2007, 2006). Ideally, the enthalpy change of adsorption can be obtained by integrating the isosteric heat from zero to the maximum surface coverage, and averaged by the maximum surface coverage (Everett et al., 1972). and the integral of enthalpy should be used to estimate free energy change of adsorption (Inglezakis and Zorpas, 2012; Tarasevich and Polyakov, 1999). However, there are obstacles for this method as well: isosteric heat values can be unpredictable (as shown in the case of the 1.5 SP line in Figure 2.2b) and it is difficult to determine the value of the maximum coverage (Q_e).

Another approach to estimating the enthalpy change of adsorption is based on the Van't Hoff equation at a constant pressure:

$$\Delta H^0 = -R\frac{d ln K_C}{d(1/T)} \quad \text{eq. 2.18}$$

which can also be written in the form of eq. 2.19:

$$ln K_c = -\frac{\Delta H^0}{RT} + \frac{\Delta S^0}{R} \quad \text{eq. 2.19}$$

This equation is derived from eqs. 2.14 and 2.15. By plotting $\ln K_c$ versus $1/T$, ΔH is obtained from the slope (noting that enthalpy change of a certain system is not impacted by ambient temperature), and ΔS can be generated from the intercept. Therefore, knowing K_c, the thermodynamic equilibrium constant, is critical for the estimation of enthalpy and free energy change of adsorption. According to the expression, K_c is a dimensionless constant. There are a number of studies simply using the partitioning coefficient $K_p = C_s/C_e$, as the thermodynamic equilibrium constant, where C_s is the adsorbate concentration on the solid (mg/g) and C_e is that in liquid (mg/L) (Feng et al., 2013; Shahwan et al., 2005; Srivastava et al., 2006). However, in this relationship, K_p is apparently not dimensionless based on the units of C_s and C_e. Additionally, at a fixed temperature, the partitioning coefficient is not constant for an adsorption system that behaves as a non-linear isotherm. Therefore, K_p cannot be directly used for estimating the enthalpy of adsorption. Senthil Kumar et al. (2014) incorrectly applied partitioning coefficients, which varied with equilibrium aqueous phase concentration as adsorption thermodynamic equilibrium constants. Tran et al. (2017) corrected the mistake and generated a single Kc value at a fixed temperature. Adsorption equilibrium constants can be derived from parameters of isotherms, such as the Langmuir constant (K_L) (Liu, 2009; Milonjić, 2007) and the Freundlich constant (K_f) (Ghosal and Gupta, 2015; Tran et al., 2017).

The sign of the enthalpy change indicates whether the reaction is endothermic (positive) or exothermic (negative). Vithanage et al. (2016) used van't Hoff's equation for estimating enthalpy of tea waste-derived biochar adsorbing carbofuran from the aqueous phase. The ΔH^0 was approximately -46 KJ/mol. The negative magnitude

indicates that adsorption was an exothermic process. However, endothermic adsorption of organic pollutants from the aqueous phase onto carbonaceous materials has also been observed (Chen et al., 2012; Fontecha-Cámara et al., 2006; Srivastava et al., 2006). For example, Chen et al. (2012) estimated the change of enthalpy for 1,3-dinitrobenzene adsorption on biomass-derived biochar to be 14 kJ/mol, and the value for naphthalene adsorption was 16 kJ/mol. The endothermic nature of these reactions can be attributed to the formation of covalent bonds during adsorption or the roles of adsorbate-solution or adsorbent-solution interactions. An absolute value of change of enthalpy greater than hundred kJ/mol can indicate the realm of chemisorption via forming of covalent bonds (Chowdhury, 2003; Thomas, 1961). Alternatively, in the case of aqueous-phase adsorption, endothermic adsorption occurs when adsorbate-water or adsorbent-water interactions are overcome before the adsorbate adheres onto the adsorbent. The heat-consuming steps include:

1) adsorbate diffusion in the water matrix, which has to break hydrogen bonds formed among water molecules (Fontecha-Cámara et al., 2006),

2) adsorbate diffusion in adsorbent pores (Anirudhan and Radhakrishnan, 2008; García-Araya et al., 2003), and

3) adsorbate replacing pre-adsorbed water molecules, which also needs heat to break hydrogen bonds between water molecules and adsorbent.
Increasing adsorption temperature promotes external heat input and therefore has a positive impact on endothermic adsorption capacity.

2.5.2.3 Free energy change of adsorption

The ability of an adsorption interaction to proceed spontaneously is energetically described by the change in Gibbs free energy of the process, ΔG^0. When diffusion-adsorption can be driven or hindered by a collection of factors such as concentration gradient, coulombic forces, or other non-coulombic interactions, ΔG^0 reflects the balance between these driving/hindrance forces. The absolute value of ΔG^0 reflects the degree of spontaneity, where a more energetically favorable adsorption usually has a higher absolute value (Liu, 2009). A negative ΔG^0 value indicates that the driving forces promote adsorption rather than hinder adsorption. Usually physical adsorption is spontaneous with an overall negative ΔG^0 value (Tran et al., 2017).

Similar to the standard enthalpy change, ΔG^0 is also related to K_c (eq. 16). Therefore, the estimation of ΔG^0 depends heavily on correct understanding of K_c, which has to be a strictly dimensionless value, as mentioned earlier. Experimentally determined $|\Delta G^0|$ of spontaneous organic micropollutant adsorption can be on the order of 10 kJ/mol or less, and the value is rarely above 50 kJ/mol. (Chen et al., 2012; Wu et al., 2014; Zhao et al., 2013). It is relatively straightforward to experimentally derive the overall free energy change of adsorption from adsorption isotherms. However, partitioning overall free energy change into multiple contributions stemming from different mechanisms (coulombic and non-coulombic driving forces) requires molecular dynamic simulation (Samaraweera et al., 2014) or thermodynamic models derived from experimental approaches (Lattao et al., 2014; Zhu and Pignatello, 2005).

2.6   Conclusions and Research Gaps

The adsorptive behavior of organic micropollutants is closely associated to their fate and removal in natural and engineered environments. Specifically, for engineered processes used at WRRFs, insight into the driving force, molecular-scale interactions and adsorption equilibrium is helpful for resolving engineering aims including prediction, validation and improvement of removal performance via adsorption. Determining adsorption isotherms is of essential importance for research on adsorptive behavior, as it builds bridges between qualitative and quantitative interpretation of adsorption equilibrium, between molecular interaction and pilot scale operation, and between batch and continuous reactor performance.

Within the scope of this dissertation, biochar and ion exchangers are studied due to their potential role in the NEW paradigm of wastewater treatment. Specifically, four research questions will be addressed, as outlined below:

1) *What is the adsorptive behavior of micropollutants on ion exchangers used for nutrient removal and recovery and do micropollutants hinder nutrient recovery?* The ion exchange-regeneration process for removing and recovering nutrients from wastewater plays an essential role in the NEW nexus. One goal for nutrient recovery is to generate nutrient-rich products, such as struvite, as value-added products derived from wastewater. Due to the presence of micropollutants in wastewater, the fate and impact of micropollutants on this engineering process needs to be addressed. Specifically, how do ion exchangers' surface properties, including surface charge, functional groups and pore size, along with physicochemical properties of micropollutants, affect the fate of micropollutants through nutrient removal and recovery processes?

2) *Is biosolids-derived biochar able to remove micropollutants via adsorption from aqueous phase?* Using wastewater biosolids as the pyrolysis feedstock has inherent advantages for WRRFs because of on-site accessibility and the necessity of wastewater solids handling. Adsorption of micropollutants onto biosolids-derived biochar has been much less studied in comparison to studies on biochar derived from other plant wastes. Biosolids-derived biochar surface properties, including surface charge, functional groups and surface area need to be characterized. Fundamental knowledge generated on biosolids-derived biochar properties and their impact on sorption capacity for micropollutants in Milli-Q water and wastewater is necessary to frame the potential of using biosolids-derived biochar as a useful adsorbent.

3) *What are the thermodynamic profiles for biosolids-derived biochars with various micropollutants?* It is important to generate a thermodynamic profile for a suite of micropollutants (cationic, neutral, anionic) adsorbing onto biosolids-derived biochar due to better understand the feasibility of employing biosolids-derived biochar for a range of micropollutants. The number of different micropollutants in wastewater is too high to conduct experiments on every micropollutant. Thus, experiments that can provide fundamental knowledge on how classes of micropollutants sorb to biosolids-derived biochar could help inform best practices for biosolids-derived biochar. The change of adsorption enthalpy, entropy and free energy needs to be estimated to generate the knowledge on binding affinity distribution on biosolids-derived biochar surface and to infer dominant adsorption mechanisms. Establishing relationships between these thermodynamic parameters and micropollutant's physicochemical properties can be

beneficial for future research to develop models that can guide effective engineering design.

    4) *Can biosolids-derived biochar serve as a pre-polishing step, which separates organic micropollutants from the nutrient-rich stream that undergoes nutrient removal and recovery via ion exchange in a flow-through column system?* With the fundamental knowledge generated on micropollutants' fate during nutrient ion exchange and the potential of biosolids-derived biochar as a useful adsorbent to remove micropollutants, it is necessary to further address how nutrients in turn affect micropollutant removal by biochar. Biochar's pre-polishing functionality should be tested prior to ion exchange process. The mass distribution of micropollutants and nutrients in the biochar-ion exchange integrated system should be established to determine how well the separation of micropollutants from nutrient stream can be. A flow-through column reactor need to be conducted to better understand scale-up issues from batch to column operations for real world applications.

2.7   References

Alpay, E., Scott, D.M., 1992. The linear driving force model for fast-cycle adsorption and desorption in a spherical particle. Chem. Eng. Sci. 47, 499–502. doi:10.1016/0009-2509(92)80041-A

Anirudhan, T.S., Radhakrishnan, P.G., 2008. Thermodynamics and kinetics of adsorption of Cu(II) from aqueous solutions onto a new cation exchanger derived from tamarind fruit shell. J. Chem. Thermodyn. 40, 702–709. doi:10.1016/j.jct.2007.10.005

Antal, M.J., Grønli, M., 2003. The Art, Science, and Technology of Charcoal Production. Ind. Eng. Chem. Res. 42, 1619–1640. doi:10.1021/ie0207919

Benjamin, M.M., Lawler, D.F., 2013. Water Quality Engineering: Physical / Chemical Treatment Processes. Wiley.

Blair, B.D., Crago, J.P., Hedman, C.J., Treguer, R.J.F., Magruder, C., Royer, L.S., Klaper, R.D., 2013. Evaluation of a model for the removal of pharmaceuticals, personal care products, and hormones from wastewater. Sci. Total Environ. 444, 515–21. doi:10.1016/j.scitotenv.2012.11.103

Blanchard, G., Maunaye, M., Martin, G., 1984. Removal of heavy metals from waters by means of natural zeolites. Water Res. 18, 1501–1507. doi:10.1016/0043-1354(84)90124-6

Blaney, L.M., Cinar, S., SenGupta, A.K., 2007. Hybrid anion exchanger for trace phosphate removal from water and wastewater. Water Res. 41, 1603–1613. doi:10.1016/j.watres.2007.01.008

Brauch, V., Schlünder, E.U., 1975. The scale-up of activated carbon columns for water purification, based on results from batch tests-II. Theoretical and experimental determination of breakthrough curves in activated carbon columns. Chem. Eng. Sci. 30, 539–548. doi:10.1016/0009-2509(75)80024-8

Brewer, C.E., Chuang, V.J., Masiello, C.A., Gonnermann, H., Gao, X., Dugan, B., Driver, L.E., Panzacchi, P., Zygourakis, K., Davies, C.A., 2014. New approaches to measuring biochar density and porosity. Biomass and Bioenergy 66, 176–185. doi:10.1016/j.biombioe.2014.03.059

Britain, G., 1992. the linear driving force model for fast cycle adsorption and desorption in a spherical particles 499, 4111.

Builes, S., Sandler, S.I., Xiong, R., 2013. Isosteric heats of gas and liquid adsorption. Langmuir 29, 10416–10422. doi:10.1021/la401035p

Chatzopoulos, D., Varma, A., 1995. Aqueous-phase adsorption and desorption of toluene in activated carbon fixed beds: Experiments and model. Chem. Eng. Sci. 50, 127–141. doi:10.1016/0009-2509(94)00195-W

Chen, B., Zhou, D., Zhu, L., 2008. Transitional adsorption and partition of nonpolar and polar aromatic contaminants by biochars of pine needles with different pyrolytic temperatures. Environ. Sci. Technol. 42, 5137–5143. doi:10.1021/es8002684

Chen, W.-Y., Liu, Z.-C., Lin, P.-H., Fang, C.-I., Yamamoto, S., 2007. The hydrophobic interactions of the ion-exchanger resin ligands with proteins at high salt concentrations by adsorption isotherms and isothermal titration calorimetry. Sep. Purif. Technol. 54, 212–219. doi:https://doi.org/10.1016/j.seppur.2006.09.008

Chen, Z., Chen, B., Zhou, D., Chen, W., 2012. Bisolute sorption and thermodynamic behavior of organic pollutants to biomass-derived biochars at two pyrolytic temperatures. Environ. Sci. Technol. 46, 12476–12483. doi:10.1021/es303351e

Chern, J.M., Chien, Y.W., 2002. Adsorption of nitrophenol onto activated carbon: Isotherms and breakthrough curves. Water Res. 36, 647–655. doi:10.1016/S0043-

1354(01)00258-5

Chowdhury, P.S. and S., 2003. Insight Into Adsorption Thermodynamics. J. Hazard. Mater. 162, 440. doi:10.1007/978-3-642-30391-3

Collins, F.C., Kimball, G.E., 1949. Diffusion-controlled reaction rates. J. Colloid Sci. 4, 425–437. doi:10.1016/0095-8522(49)90023-9

Cooney, D.O., 1998. Adsorption Design for Wastewater Treatment. CRC Press.

Del Bubba, M., Arias, C.A., Brix, H., 2003. Phosphorus adsorption maximum of sands for use as media in subsurface flow constructed reed beds as measured by the Langmuir isotherm. Water Res. 37, 3390–3400. doi:10.1016/S0043-1354(03)00231-8

Do, D.D., Nicholson, D., Fan, C., 2011. Development of equations for differential and integral enthalpy change of adsorption for simulation studies. Langmuir 27, 14290–14299. doi:10.1021/la203531j

Domingues, R.R., Trugilho, P.F., Silva, C.A., De Melo, I.C.N.A., Melo, L.C.A., Magriotis, Z.M., Sánchez-Monedero, M.A., 2017. Properties of biochar derived from wood and high-nutrient biomasses with the aim of agronomic and environmental benefits. PLoS One 12. doi:10.1371/journal.pone.0176884

Downie, A., Crosky, A., Munroe, P., 2012. Physical properties of biochar, in: Biochar for Environmental Management: Science and Technology. pp. 13–32. doi:10.4324/9781849770552

Dubinin, M.M., Radushkevich, L.V., 1947. Equation of the characteristic curve of activated charcoal. Proc. Acad. Sci. Phys. Chem. Sec. USSR 55, 331–333. doi:10.1016/j.clay.2009.07.022

Everett, D. H. Manual of Symbols and Terminology for Physicochemical Quantities and Units, Appendix II: Definitions, Terminology and Symbols in Colloid and Surface Chemistry. Pure Appl. Chem. 1972, 31, 577−638

Fang, Q., Chen, B., Lin, Y., Guan, Y., 2014. Aromatic and hydrophobic surfaces of wood-derived biochar enhance perchlorate adsorption via hydrogen bonding to oxygen-containing organic groups. Environ. Sci. Technol. 48, 279–288. doi:10.1021/es403711y

Feng, Y., Dionysiou, D.D., Wu, Y., Zhou, H., Xue, L., He, S., Yang, L., 2013. Adsorption of dyestuff from aqueous solutions through oxalic acid-modified swede rape straw: Adsorption process and disposal methodology of depleted bioadsorbents. Bioresour. Technol. 138, 191–197. doi:10.1016/j.biortech.2013.03.146

Fontecha-Cámara, M.A., López-Ramón, M. V., Álvarez-Merino, M.A., Moreno-Castilla, C., 2006. About the endothermic nature of the adsorption of the herbicide diuron

from aqueous solutions on activated carbon fiber. Carbon N. Y. doi:10.1016/j.carbon.2006.05.031

Foo, K.Y., Hameed, B.H., 2010. Insights into the modeling of adsorption isotherm systems. Chem. Eng. J. doi:10.1016/j.cej.2009.09.013

García-Araya, J.F., Beltrán, F.J., Álvarez, P., Masa, F.J., 2003. Activated carbon adsorption of some phenolic compounds present in agroindustrial wastewater. Adsorption 9, 107–115. doi:10.1023/A:1024228708675

Hardinger, S., 2015. Chemistry 14C thinkbook twelfth edition. Hayden-Mcneil Publishing. ISBN: 978-0738068107

Gholizadeh, A., Kermani, M., Gholami, M., Farzadkia, M., 2013. Kinetic and isotherm studies of adsorption and biosorption processes in the removal of phenolic compounds from aqueous solutions: Comparative study. J. Environ. Heal. Sci. Eng. 11. doi:10.1186/2052-336X-11-29

Ghosal, P.S., Gupta, A.K., 2015. An insight into thermodynamics of adsorptive removal of fluoride by calcined Ca–Al–(NO$_3$) layered double hydroxide. RSC Adv. 5, 105889–105900. doi:10.1039/C5RA20538G

Gilli, P., Pretto, L., Bertolasi, V., Gilli, G., 2009. Predicting Hydrogen-Bond strengths from Acid-Base molecular properties. the pKa slide rule: Toward the solution of a Long-Lasting problem. Acc. Chem. Res. 42, 33–44. doi:10.1021/ar800001k

Grathwohl, P., 1990. Influence of Organic Matter from Soils and Sediments from Various Origins on the Sorption of Some Chlorinated Aliphatic Hydrocarbons: Implications on KocCorrelations. Environ. Sci. Technol. 24, 1687–1693. doi:10.1021/es00081a010

Halsey, G., Taylor, H.S., 1947. The Adsorption of Hydrogen on Tungsten Powders. J. Chem. Phys. 15, 624–630. doi:10.1063/1.1746618

Ho, Y.S., 2006. Second-order kinetic model for the sorption of cadmium onto tree fern: A comparison of linear and non-linear methods. Water Res. doi:10.1016/j.watres.2005.10.040

Ho, Y.S., McKay, G., 1999. Pseudo-second order model for sorption processes. Process Biochem. 34, 451–465. doi:10.1016/S0032-9592(98)00112-5

Ho, Y.S., McKay, G., 1998. A Comparison of Chemisorption Kinetic Models Applied to Pollutant Removal on Various Sorbents. Process Saf. Environ. Prot. doi:10.1205/095758298529696

Ho, Y.S., McKay, G., 1998. Sorption of dye from aqueous solution by peat. Chem. Eng. J. 70, 115–124. doi:10.1016/S1385-8947(98)00076-X

Holford, I.C.R., Wedderburn, R.W.M., Mattingly, G.E.G., 1974. A Langmuir two-surface equation as a model for phosphate adsorption by soils. J. Soil Sci. 25, 242–255. doi:10.1111/j.1365-2389.1974.tb01121.x

Hu, Y., Guo, T., Ye, X., Li, Q., Guo, M., Liu, H., Wu, Z., 2013. Dye adsorption by resins: Effect of ionic strength on hydrophobic and electrostatic interactions. Chem. Eng. J. 228, 392–397. doi:10.1016/j.cej.2013.04.116

Hunter, C.A., Sanders, J.K.M., 1990. The Nature of π-π Interactions. J. Am. Chem. Soc. 112, 5525–5534. doi:10.1021/ja00170a016

Hyung, H., Fortner, J.D., Hughes, J.B., Kim, J.-H., 2007. Natural Organic Matter Stabilizes Carbon Nanotubes in the Aqueous Phase. Environ. Sci. Technol. 41, 179–184. doi:10.1021/es061817g

Inglezakis, V.J., Zorpas, A.A., 2012. Heat of adsorption, adsorption energy and activation energy in adsorption and ion exchange systems. Desalin. Water Treat. 39, 149–157. doi:10.1080/19443994.2012.669169

Inyang, M., Dickenson, E., 2015. The potential role of biochar in the removal of organic and microbial contaminants from potable and reuse water: a review. Chemosphere 134, 232–240.

IUPAC, 2014. Compendium of Chemical Terminology: Gold Book. IUPAC Compend. Chem. Terminol. 1670. doi:10.1351/goldbook.I03352

Jung, C., Park, J., Lim, K.H., Park, S., Heo, J., Her, N., Oh, J., Yun, S., Yoon, Y., 2013. Adsorption of selected endocrine disrupting compounds and pharmaceuticals on activated biochars. J. Hazard. Mater. 263 Pt 2, 702–10. doi:10.1016/j.jhazmat.2013.10.033

Kah, M., Sigmund, G., Xiao, F., Hofmann, T., 2017. Sorption of ionizable and ionic organic compounds to biochar, activated carbon and other carbonaceous materials. Water Res. doi:10.1016/j.watres.2017.07.070

Kanagaraj, G., Rao, G.N., 1992. Synthesis and characterization of some first row transition metal complexes of 4-amino-N-(5-methyl-3-isoxazolyl-benzenesulfonamide (sulfamethoxazole). Synth. React. Inorganic, Met. Nano-Metal Chem. 22, 559–574.

Kang, S., Xing, B., 2005. Phenanthrene sorption to sequentially extracted soil humic acids and humins. Environ. Sci. Technol. 39, 134–140. doi:10.1021/es0490828

Keiluweit, M., Nico, P.S., Johnson, M.G., Kleber, M., 2010. Dynamic Molecular Structure of Plant Biomass-Derived Black Carbon (Biochar). Environ. Sci. Technol. 44, 1247–1253. doi:10.1021/es9031419

Lattao, C., Cao, X., Mao, J., Schmidt-Rohr, K., Pignatello, J.J., 2014. Influence of

molecular structure and adsorbent properties on sorption of organic compounds to a temperature series of wood chars. Environ. Sci. Technol. 48, 4790–4798. doi:10.1021/es405096q

Lee, J.W., Shim, W.G., Yang, M.S., Moon, H., 2004. Adsorption isotherms of polar and nonpolar organic compounds on MCM-48 at (303.15, 313.15, and 323.15) K. J. Chem. Eng. Data 49, 502–509. doi:10.1021/je030208a

Lian, F., Sun, B., Song, Z., Zhu, L., Qi, X., Xing, B., 2014. Physicochemical properties of herb-residue biochar and its sorption to ionizable antibiotic sulfamethoxazole. Chem. Eng. J. 248, 128–134. doi:10.1016/j.cej.2014.03.021

Limousin, G., Gaudet, J.-P., Charlet, L., Szenknect, S., Barthès, V., Krimissa, M., 2007. Sorption isotherms: A review on physical bases, modeling and measurement. Appl. Geochemistry 22, 249–275. doi:10.1016/j.apgeochem.2006.09.010

Liu, Y., 2009. Is the free energy change of adsorption correctly calculated? J. Chem. Eng. Data 54, 1981–1985. doi:10.1021/je800661q

Liu, Z., McNamara, P., Zitomer, D., 2017. Autocatalytic Pyrolysis of Wastewater Biosolids for Product Upgrading. Environ. Sci. Technol. 51, 9808–9816. doi:10.1021/acs.est.7b02913

Lu, H., Zhang, W., Yang, Y., Huang, X., Wang, S., Qiu, R., 2012. Relative distribution of Pb 2+ sorption mechanisms by sludge-derived biochar. Water Res. 46, 854–862. doi:10.1016/j.watres.2011.11.058

Mahmudov, R., Huang, C.P., 2010. Perchlorate removal by activated carbon adsorption. Sep. Purif. Technol. 70, 329–337. doi:10.1016/j.seppur.2009.10.016

Matsumoto, M.R., 1993. Modeling cadmium adsorption by activated carbon using the langmuir and freundlich isotherm expressions. Sep. Sci. Technol. 28, 2179–2195. doi:10.1080/01496399308016742

McBeath, A. V., Smernik, R.J., Schneider, M.P.W., Schmidt, M.W.I., Plant, E.L., 2011. Determination of the aromaticity and the degree of aromatic condensation of a thermosequence of wood charcoal using NMR. Org. Geochem. 42, 1194–1202. doi:10.1016/j.orggeochem.2011.08.008

McKay, G., 1991. Two solutions to adsorption equations for pore diffusion. Water. Air. Soil Pollut. 60, 117–133. doi:10.1007/BF00293970

Meenakshi, S., Viswanathan, N., 2007. Identification of selective ion-exchange resin for fluoride sorption. J. Colloid Interface Sci. 308, 438–450. doi:10.1016/j.jcis.2006.12.032

Mehlich, A., 1948. Determination of cation- and anion-exchange properties of soils. Soil Sci. 66, 429-446

Merk, W., Fritz, W., Schlünder, E.U., 1981. Competitive adsorption of two dissolved organics onto activated carbon-III. Adsorption kinetics in fixed beds. Chem. Eng. Sci. 36, 759–764. doi:10.1016/0009-2509(81)85090-7

Meyer, E.E., Rosenberg, K.J., Israelachvili, J., 2006. Recent progress in understanding hydrophobic interactions. Proc. Natl. Acad. Sci. U. S. A. 103, 15739–46. doi:10.1073/pnas.0606422103

Milonjić, S.K., 2007. A consideration of the correct calculation of thermodynamic parameters of adsorption. J. Serbian Chem. Soc. 72, 1363–1367. doi:10.2298/JSC0712363M

Moreno-Castilla, C., 2004. Adsorption of organic molecules from aqueous solutions on carbon materials. Carbon N. Y. 42, 83–94. doi:10.1016/j.carbon.2003.09.022

Mukherjee, A., Zimmerman, A.R., Harris, W., 2011. Surface chemistry variations among a series of laboratory-produced biochars. Geoderma 163, 247–255. doi:10.1016/j.geoderma.2011.04.021

Murialdo, M., Stadie, N.P., Ahn, C.C., Fultz, B., 2015. Observation and Investigation of Increasing Isosteric Heat of Adsorption of Ethane on Zeolite-Templated Carbon. doi:10.1021/jp510991y

Myers, A.L., 2002. Thermodynamics of adsorption in porous materials. AIChE J. 48, 145–160. doi:10.1002/aic.690480115

Myers, A.L., Monson, P.A., 2014. Physical adsorption of gases: The case for absolute adsorption as the basis for thermodynamic analysis. Adsorption 20, 591–622. doi:10.1007/s10450-014-9604-1

Nakao, S., Suzuki, M., 1983. Mass transfer coefficient in cyclic adsorption and desorption. J. Chem. Eng. Japan 16, 114–119. doi:10.1252/jcej.16.114

Nastaj, J., Witkiewicz, K., Chybowska, M., 2016. Modeling of multicomponent and multitemperature adsorption equilibria of water vapor and organic compounds on activated carbons. Adsorpt. Sci. Technol. 34, 144–175. doi:10.1177/0263617415623423

Neale, P.A., Mastrup, M., Borgmann, T., Schäfer, A.I., 2010. Sorption of micropollutant estrone to a water treatment ion exchange resin. J. Environ. Monit. 12, 311–317.

Ni, J., Pignatello, J.J., Xing, B., 2011. Adsorption of aromatic carboxylate ions to black carbon (Biochar) is accompanied by proton exchange with water. Environ. Sci. Technol. 45, 9240–9248. doi:10.1021/es201859j

Pan, B., Xing, B., 2008. Adsorption Mechanisms of Organic Chemicals on Carbon Nanotubes. Environ. Sci. Technol. 42, 9005–9013. doi:10.1021/es801777n

Pignatello, J.J., Mitch, W.A., Xu, W., 2017. Activity and Reactivity of Pyrogenic Carbonaceous Matter toward Organic Compounds. Environ. Sci. Technol. 51, 8893–8908. doi:10.1021/acs.est.7b01088

Pignatello, J.J., Xing, B., 1996. Mechanisms of Slow Sorption of Organic Chemicals to Natural Particles. Environ. Sci. Technol. 30, 1–11. doi:10.1021/es940683g

Plazinski, W., Rudzinski, W., Plazinska, A., 2009. Theoretical models of sorption kinetics including a surface reaction mechanism: A review. Adv. Colloid Interface Sci. doi:10.1016/j.cis.2009.07.009

Pyrzynska, K., Stafiej, A., Biesaga, M., 2007. Sorption behavior of acidic herbicides on carbon nanotubes. Microchim. Acta 159, 293–298. doi:10.1007/s00604-007-0739-6

Qiu, H., Lv, L., Pan, B., Zhang, Q., Zhang, W., Zhang, Q., 2009. Critical review in adsorption kinetic models. J. Zhejiang Univ. A 10, 716–724. doi:10.1631/jzus.A0820524

Radovic, L.R., 2012. Chemistry and physics of carbon: volume 31. CRC Press

Rengaraj, S., Joo, C.K., Kim, Y., Yi, J., 2003. Kinetics of removal of chromium from water and electronic process wastewater by ion exchange resins: 1200H, 1500H and IRN97H. J. Hazard. Mater. 102, 257–275. doi:10.1016/S0304-3894(03)00209-7

Rengaraj, S., Moon, S.-H., 2002. Kinetics of adsorption of Co(II) removal from water and wastewater by ion exchange resins. Water Res. 36, 1783–1793. doi:10.1016/S0043-1354(01)00380-3

Ruthven, J.K.D.M., 1992. Diffusion in Zeolites and Other Microporous Solids. John Wiley 1. doi:10.1002/apj.5500040311

Salem Attia, T.M., Hu, X.L., Yin, D.Q., 2013. Synthesized magnetic nanoparticles coated zeolite for the adsorption of pharmaceutical compounds from aqueous solution using batch and column studies. Chemosphere 93, 2076–85. doi:10.1016/j.chemosphere.2013.07.046

Samaraweera, M., Jolin, W., Vasudevan, D., Mackay, A.A., Gascón, J.A., 2014. Atomistic Prediction of Sorption Free Energies of Cationic Aromatic Amines on Montmorillonite: A Linear Interaction Energy Method. Environ. Sci. Technol. Lett. 1, 284–289. doi:10.1021/ez500136g

Schwarzenbach, R.P., Escher, B.I., Fenner, K., Hofstetter, T.B., Johnson, C.A., von Gunten, U., Wehrli, B., 2006. The challenge of micropollutants in aquatic systems. Science 313, 1072–1077. doi:10.1126/science.1127291

Sengupta, S., Pandit, A., 2011. Selective removal of phosphorus from wastewater combined with its recovery as a solid-phase fertilizer. Water Res. 45, 3318–3330. doi:10.1016/j.watres.2011.03.044

Senthil Kumar, P., Fernando, P.S.A., Ahmed, R.T., Srinath, R., Priyadharshini, M., Vignesh, A.M., Thanjiappan, A., 2014. Effect of temperature on the adsorption of methylene blue dye onto sulfuric acid-treated orange peel. Chem. Eng. Commun. 201, 1526–1547. doi:10.1080/00986445.2013.819352

Shahwan, T., Akar, D., Eroğlu, A.E., 2005. Physicochemical characterization of the retardation of aqueous Cs + ions by natural kaolinite and clinoptilolite minerals. J. Colloid Interface Sci. 285, 9–17. doi:10.1016/j.jcis.2004.11.016

Simonin, J.P., 2016. On the comparison of pseudo-first order and pseudo-second order rate laws in the modeling of adsorption kinetics. Chem. Eng. J. 300, 254–263. doi:10.1016/j.cej.2016.04.079

Sircar, S., Hufton, J.R., 2000. Why does the linear driving force model for adsorption kinetics work? Adsorption 6, 137–147. doi:10.1023/A:1008965317983

Srivastava, V.C., Mall, I.D., Mishra, I.M., 2007. Adsorption thermodynamics and isosteric heat of adsorption of toxic metal ions onto bagasse fly ash (BFA) and rice husk ash (RHA). Chem. Eng. J. 132, 267–278. doi:10.1016/j.cej.2007.01.007

Srivastava, V.C., Swamy, M.M., Mall, I.D., Prasad, B., Mishra, I.M., 2006. Adsorptive removal of phenol by bagasse fly ash and activated carbon: Equilibrium, kinetics and thermodynamics. Colloids Surfaces A Physicochem. Eng. Asp. 272, 89–104. doi:10.1016/j.colsurfa.2005.07.016

Sun, H., Hockaday, W.C., Masiello, C.A., Zygourakis, K., 2012. Multiple controls on the chemical and physical structure of biochars. Ind. Eng. Chem. Res. 51, 3587–3597. doi:10.1021/ie201309r

Sun, K., Keiluweit, M., Kleber, M., Pan, Z., Xing, B., 2011. Sorption of fluorinated herbicides to plant biomass-derived biochars as a function of molecular structure. Bioresour. Technol. 102, 9897–9903. doi:10.1016/j.biortech.2011.08.036

Syers, J.K., Browman, M.G., Smillie, G.W., Corey, R.B., 1973. Phosphate sorption by soils evaluated by the Langmuir adsorption equation. Soil Sci Soc Am Proc 37, 358–363. doi:10.2136/sssaj1973.03615995003700030015x

Tarasevich, Y.I., Polyakov, V.E., 1999. Calorimetric studies of ion-exchange equilibria on clinoptilolite involving uncharged cations, in: Kiricsi, I., Pál-Borbély, G., Nagy, J.B., Karge, H.G.B.T.-S. in S.S. and C. (Eds.), Porous Materials in Environmentally Friendly Pocesses. Elsevier, pp. 315–320. doi:https://doi.org/10.1016/S0167-2991(99)80229-8

Teixidó, M., Pignatello, J.J., Beltrán, J.L., Granados, M., Peccia, J., 2011. Speciation of the ionizable antibiotic sulfamethazine on black carbon (Biochar). Environ. Sci. Technol. 45, 10020–10027. doi:10.1021/es202487h

Temkin, M., Pyzhev, V., 1940. Kinetics of ammonia synthesis on promoted Iron catalysts. Acta Physicochim. URSS 12, 217–222.

Thomas, J.M., 1961. The existence of endothermic adsorption. J. Chem. Educ. 38, 138. doi:10.1021/ed038p138

Tien, C., 1994. Adsorption Calculations and Modeling. Butterworth-Heinemann.

Tran, H.N., You, S.J., Hosseini-Bandegharaei, A., Chao, H.P., 2017. Mistakes and inconsistencies regarding adsorption of contaminants from aqueous solutions: A critical review. Water Res. 120, 88–116. doi:10.1016/j.watres.2017.04.014

Tseng, R.-L., Tseng, S.-K., 2006. Characterization and use of high surface area activated carbons prepared from cane pith for liquid-phase adsorption. J. Hazard. Mater. 136, 671–680. doi:10.1016/j.jhazmat.2005.12.048

Tóth, J., 1971. State Equations of the Solid-Gas Interface Layers. Acta Chim. Acad. Sci. Hungaricae 69, 311–328.

Uchimiya, M., Bannon, D.I., Wartelle, L.H., 2012. Retention of heavy metals by carboxyl functional groups of biochars in small arms range soil. J. Agric. Food Chem. 60, 1798–1809. doi:10.1021/jf2047898

Van Der Wal, L., Jager, T., Fleuren, R.H.L.J., Barendregt, A., Sinnige, T.L., Van Gestel, C.A.M., Hermens, J.L.M., 2004. Solid-phase microextraction to predict bioavailability and accumulation of organic micropollutants in terrestrial organisms after exposure to a field-contaminated soil. Environ. Sci. Technol. 38, 4842–4848. doi:10.1021/es035318g

Vithanage, M., Mayakaduwa, S.S., Herath, I., Ok, Y.S., Mohan, D., 2016. Kinetics, thermodynamics and mechanistic studies of carbofuran removal using biochars from tea waste and rice husks. Chemosphere 150, 781–789. doi:10.1016/j.chemosphere.2015.11.002

Wang, T., Camps Arbestain, M., Hedley, M., Bishop, P., 2012. Chemical and bioassay characterisation of nitrogen availability in biochar produced from dairy manure and biosolids. Org. Geochem. 51, 45–54. doi:10.1016/j.orggeochem.2012.07.009

Weber, S.E., Talapatra, S., 2000. Determination of the binding energy of methane on single-walled carbon nanotube bundles 61, 150–154.

Westwater, J.W., Drickamer, H.G., 1957. The Mathematics of Diffusion. J. Am. Chem. Soc. 79, 1267–1268. doi:10.1021/ja01562a072

Wijnja, H., Pignatello, J.J., Malekani, K., 2004. Formation of p-p complexes between phenanthrene and model p-acceptor humic subunits. J. Environ. Qual. 33, 265–275. doi:10.2134/jeq2004.2650

Williams, L.D., 2017. Molecular Interactions (Noncovalent Interactions) illustrated by biochemical systems [WWW Document]. URL https://ww2.chemistry.gatech.edu/~lw26/structure/molecular_interactions/mol_int.html

Wu, Z., Zhong, H., Yuan, X., Wang, H., Wang, L., Chen, X., Zeng, G., Wu, Y., 2014. Adsorptive removal of methylene blue by rhamnolipid-functionalized graphene oxide from wastewater. Water Res. doi:10.1016/j.watres.2014.09.026

Xiao, F., Pignatello, J.J., 2015. Interactions of triazine herbicides with biochar: Steric and electronic effects. Water Res. 80, 179–188. doi:10.1016/j.watres.2015.04.040

Xing, B., Pignatello, J.J., Gigliotti, B., 1996. Competitive sorption between atrazine and other organic compounds in soils and model sorbents. Environ. Sci. Technol. 30, 2432–2440. doi:10.1021/es950350z

Xu, Z., Cai, J., Pan, B., 2013. Mathematically modeling fixed-bed adsorption in aqueous systems. J. Zhejiang Univ. Sci. A 14, 155–176. doi:10.1631/jzus.A1300029

Yang, K., Xing, B., 2010. Adsorption of organic compounds by carbon nanomaterials in aqueous phase: Polanyi theory and its application. Chem. Rev. 110, 5989–6008. doi:10.1021/cr100059s

Yoo, J.S.D., 2013. Binding Energy of Oxygen and Methane Adsorbed on Bundles of Open-ended Single-wall Carbon Nanotubes 63, 88–92. doi:10.3938/NPSM.63.88

Yuan, H., Lu, T., Zhao, D., Huang, H., Noriyuki, K., Chen, Y., 2013. Influence of temperature on product distribution and biochar properties by municipal sludge pyrolysis. J. Mater. Cycles Waste Manag. 15, 357–361. doi:10.1007/s10163-013-0126-9

Zhang, R., Somasundaran, P., 2006. Advances in adsorption of surfactants and their mixtures at solid/solution interfaces. Adv. Colloid Interface Sci. 123–126, 213–229. doi:10.1016/j.cis.2006.07.004

Zhao, D., Sengupta, A.K., 1998. Ultimate removal of phosphate from wastewater using a new class of polymeric ion exchangers. Water Res. 32, 1613–1625. doi:10.1016/S0043-1354(97)00371-0

Zhao, X., Ouyang, W., Hao, F., Lin, C., Wang, F., Han, S., Geng, X., 2013. Properties comparison of biochars from corn straw with different pretreatment and sorption behaviour of atrazine. Bioresour. Technol. 147, 338–344. doi:10.1016/j.biortech.2013.08.042

Zhu, D., Pignatello, J.J., 2005. Characterization of aromatic compound sorptive interactions with black carbon (charcoal) assisted by graphite as a model. Environ. Sci. Technol. 39, 2033–2041. doi:10.1021/es0491376

3   THE FATE AND IMPACT OF ORGANIC MICROPOLLUTANTS DURING NUTRIENT REMOVAL AND RECOVERY VIA ION EXCHANGE AND STRUVITE PRECIPITATION

This chapter was published as:

Tong, Y., Mayer, B.K, McNamara, P.J., 2017. Fate and impacts of triclosan, sulfamethoxazole, and 17β-estradiol during nutrient recovery via ion exchange and struvite precipitation. *Environmental Science: Water Research & Technology*. 3 (6), 1109-1119. doi: 10.1039/C7EW00280G

It is republished here, with minor adjustments, with permission from the journal.

3.1   Introduction

Water resource recovery facilities (WRRFs) are inextricably linked to the nutrient, energy, and water nexus as they provide a centralized opportunity to recover energy, e.g., as methane; produce high-quality treated water; and recover valuable products, e.g., for use as agricultural fertilizers or soil amendments (Carey et al., 2016a). Anaerobic treatments, such as anaerobic membrane bioreactors (AnMBRs), produce methane, which can offset some energy requirements for WRRFs. Furthermore, AnMBRs do not require aeration and could be a more sustainable alternative to conventional activated sludge processes (Jimenez et al., 2015; McCarty et al., 2011; Seib et al., 2016; Smith et al., 2014). Additionally, anaerobic processes offer an opportunity for downstream nutrient recovery, and thus an option to produce and recover a valuable product instead of using energy to convert nutrients to a wasted product (e.g., as an off-gas).

The effluent from anaerobic processes usually contains high ammonia nitrogen (NH_4-N) and inorganic phosphate (PO_4-P) (Seib et al., 2016; Smith et al., 2014). Accordingly, additional nutrient removal technologies may be needed to treat anaerobic effluent to meet increasingly stringent nutrient discharge regulations (Wisconsin DNR, 2010). While excess phosphorus and nitrogen in environmental waters causes eutrophication (Mayer et al., 2013), insufficient nutrient availability is also a concern for agriculture (Rittmann et al., 2011). Depleting reserves of mined phosphate, together with the energy-intensive nature of Haber-Bosch nitrogen fixation, could limit global food production (Neset and Cordell, 2012; Smill and Streatfeild, 2002). Anaerobic effluent, as a reservoir of nutrients, is a resource from which to recover nitrogen and phosphorus in the form of a solid fertilizer product that can help to close anthropogenic nutrient loops

by supplementing nonrenewable phosphate mining and energy-intensive atmospheric nitrogen fixation (Mayer et al., 2016).

Wastewater contains a host of inherently valuable constituents including energy and nutrients, but it also contains a mixture of micropollutants that pose potential adverse ecological health impacts (Blair et al., 2013). For example, triclosan (TCS) is an antimicrobial agent used in a variety of consumer products, and can select for antibiotic resistance in engineered and natural systems (Carey et al., 2016b; Carey and Mcnamara, 2015; Carey and McNamara, 2016; McNamara et al., 2014). 17β-estradiol (E2) is a natural hormone that is linked to fish feminization near treatment plant outfalls (Vajda et al., 2008). Sulfamethoxazole (SMX) is one of the most popularly prescribed sulfonamide antibiotics and can affect nutrient cycling in microbial communities (Hruska and Franek, 2012; Underwood et al., 2011). WRRFs were not specifically designed to remove micropollutants, and anaerobic processes are often worse at removing micropollutants compared to aerobic processes. For instance, Chen et al. (2011) achieved 75% removal of TCS in a lab-scale activated sludge reactor, while no removal was observed under anaerobic conditions (Chen et al., 2011). Studies on endocrine disruptors such as estrone (E1), E2, and 17α-ethynylestradiol (EE2) revealed that anaerobic treatments, e.g. AnMBRs, poorly biotransformed these compounds (Monsalvo et al., 2014). Additionally, E1 can convert to E2 under anaerobic conditions (Joss et al., 2004), thereby increasing concentrations of E2. SMX had variable biological transformation in AnMBR systems, ranging from 60% to 99% (Alvarino et al., 2014; Monsalvo et al., 2014). If valuable products such as treated water and nutrients are to be recovered from anaerobic effluents, it is important to understand the fate of micropollutants to minimize their presence in

WRRF products and effluent. This study focused on the impact and fate of TCS, E2, and SMX during nutrient recovery because of the potential presence of these micropollutants in anaerobic effluent and their different physicochemical properties (molecular details of which are included in the Appendix 3A).

One option for removing and recovering nutrients is ion exchange-precipitation. In this process, nutrient-selective materials are used to extract and concentrate nitrogen and phosphorus via ion exchange and subsequent regeneration followed by precipitation of nutrient-rich solid fertilizer products, e.g., struvite ($MgNH_4PO_4$). Clinoptilolite is a natural zeolite that effectively exchanges ammonium ions (Hedström, 2001). In wastewater, phosphorus is most commonly present in the HPO_4^{2-} and $H_2PO_4^{-}$ forms (Razali et al., 2007). These orthophosphate species can exhibit strong ligand sorption to polyvalent metals such as Fe(III) and Cu(II) by forming inner-sphere complexes (Sengupta and Pandit, 2011a; Zhao and Sengupta, 1998). Therefore, polymeric anion exchangers are usually impregnated with metal salts to selectively exchange orthophosphate. After removal, nutrients are concentrated during ion exchange regeneration, thereby facilitating precipitation of nutrient-rich solids that can be used as fertilizer. Controlled struvite precipitation has been studied in mainstream and side-stream wastewater (direct precipitation) (Laridi et al., 2005; Münch and Barr, 2001; O'Neal and Boyer, 2015) and in membrane-concentrated streams and ion exchange regeneration brines (indirect precipitation) (O'Neal and Boyer, 2015; Williams et al., 2015). Compared to direct precipitation, indirect precipitation is more favorable for producing a high purity mineral and easier operational control (O'Neal and Boyer, 2015). However, organic micropollutants such as tetracycline and quinolones have been detected

in struvite produced from digester filtrate and urine (Antakyal et al., 2011; Başakçilardan-Kabakci et al., 2007). Thus, if valuable fertilizer is recovered from anaerobic effluents, it is essential to thoroughly assess the potential for co-concentration of residual micropollutants along with nutrients.

The objective of this work was to evaluate the fate of the micropollutants TCS, E2, and SMX during ammonium and phosphate ion exchange-regeneration and struvite precipitation. Batch experiments were conducted to specifically determine: a) the impact of micropollutants on nutrient exchange reaction rates, capacities, and desorption in Milli-Q water and anaerobically-treated wastewater; b) the fate of the micropollutants during ion exchange-regeneration in both water matrices; and c) micropollutants' fate during struvite precipitation. It was hypothesized that a) micropollutants co-existing in nutrient-rich stream could decrease nutrient exchange rate and nutrient exchange capacities; b) micropollutants could adsorb on ion exchangers and desorb in regeneration brine during ion exchanger regeneration; c) micropollutants in regeneration brine, which was used for struvite precipitation, was able to precipitate out together with struvite.

3.2   Materials and Methods

3.2.1   Ion exchangers

LayneRT and DOW-HFO-Cu were evaluated as phosphate-selective ion exchangers (Blaney et al., 2007; Sengupta and Pandit, 2011a). LayneRT (Layne Christensen, The Woodlands, TX) is a 300 - 1200 μm particle size ready-to-purchase hybrid anion exchange resin consisting of hydrated ferric oxide (HFO) nanoparticles impregnated in a strong base anion exchange polymer (Sengupta and Pandit, 2011a). In

accordance with Sengupta and Pandit 's protocol (Sengupta and Pandit, 2011a), DOWEX M4195 (DOW Chemical Company, Midland, MI, 300 - 850 μm particle size) was used as the base resin for producing functional DOW-HFO-Cu resin by immobilizing Cu(II) and HFO, which provide ligand bonding with HPO_4^{2-} and $H_2PO_4^-$, onto the polymer. Clinoptilolite, a natural zeolite, was used as a selective ammonium exchanger. The clinoptilolite (St. Cloud Mining, Winston, NM, 14X40 mesh, 420 – 1410 μm particle size) was pre-conditioned with 1% NaCl solution and rinsed with de-ionized water.

3.2.2   Ion exchanger characterization

Characterization of ion exchangers was performed to better elucidate the interactions between the dissolved chemicals and the ion exchangers. Ion exchanger surface area and pore size were measured using a Brunauer–Emmett–Teller (BET) surface analysis instrument (NOVA 4200e, Quantachrome Instruments, Boynton Beach, FL). The surface charge of the materials was determined using a Malvern Zetasizer Nano S (Malvern Instruments Ltd, Malvern, UK). The ion exchangers' surface element composition was observed via JEOL JSM-6510LV SEM (JEOL USA, Inc., Peabody, MA) with an energy-dispersive X-ray (EDX) detector at an accelerating voltage of 10 kV.

3.2.3   Ion exchange and regeneration batch experiments

Batch ion exchange tests were conducted to determine if micropollutants would be co-captured with nutrient ions and potential adsorption/desorption mechanisms. These tests were performed in feed Milli-Q water with 40 mg-N/L as NH_4Cl and 5 mg-P/L as K_2HPO_4 (Williams et al., 2015) to mimic plausible nutrient levels in mainstream anaerobic treatment effluents (Seib et al., 2016). The feed water was prepared by

dissolving 300±50 µg/L each of TCS, E2 and SMX in HPLC-grade methanol. The volumetric ratio of methanol stock to water was below 0.5% to negate co-solvent effects (Schwarzenbach et al., 2005). The spiked micropollutant concentrations were higher than in actual anaerobic effluents (Alvarino et al., 2014; Monsalvo et al., 2014) so that reaction rates and adsorption capacities could be determined via liquid chromatography-mass spectrometry (LC-MS; detection limits were in the low µg/L range). The pH of feed water was adjusted to 7 with NaOH.

For ion exchange tests, 50 mL feed water was added to 60 mL serum bottles. Each bottle contained 0.25 g clinoptilolite, 0.05 g LayneRT, or 0.05 g DOW-HFO-Cu resin (higher levels of clinoptilolite were added based on higher ammonium concentrations). The bottles were mixed on a rotating tumbler for 4 days as preliminary tests demonstrated this time was sufficient to achieve equilibrium. For kinetic tests, periodic samples were collected, as shown in Figures 3.1 and 3.2. Nutrient exchange typically achieved equilibrium in less than 1 day and micropollutant adsorption typically achieved equilibrium within 2 days (equilibrium was signified by <5% change in concentrations).

Ion exchange isotherm tests were conducted to assess potential interference with nutrient capture caused by micropollutants. For these tests, 50 mL of feed water were added to 60 mL serum bottles. The amount of ion exchanger in each bottle varied: 0.01, 0.02, 0.03, 0.04, or 0.05 g DOW-HFO-Cu or LayneRT; 0.01, 0.05, 0.1, 0.2, or 0.5 g clinoptilolite. Samples were analyzed at time zero and after 4 days.

Ion exchange regeneration tests were conducted to determine if the micropollutants that were adsorbed on the ion exchangers would be released during subsequent regeneration. All ion exchangers were regenerated using brine solutions with

high levels of Na^+, Cl^- and OH^- (Lunn et al., 2014; Williams et al., 2015). For clinoptilolite, the regeneration brine was fixed at 8% NaCl (Williams et al., 2015). The concentrations of NaCl and NaOH in phosphate exchanger regeneration brine were varied to study their impact on phosphate and micropollutant recovery (Appendix 3B, Tables 3B.1- 3B.4). Differences in recoveries as a function of regeneration solution could enable process optimization to elicit greater desorption of nutrients and less desorption of micropollutants. The regeneration brine for LayneRT ranged from 0 to 2% NaCl and 0 to 2% NaOH. The regeneration brine for DOW-HFO-Cu ranged from 0 to 5% NaCl and 0 to 2% NaOH (Sengupta and Pandit, 2011b). The pH of all regeneration brines was 12 to 14. Ion exchange tests were initially performed in 250 mL water in 500 mL Erlenmeyer flasks. The amount of ion exchanger added to each flask was fixed at 1.25 g clinoptilolite or 0.25 g DOW or LayneRT resin. After completing the 4-day ion exchange period, the flasks were decanted and 150 mL NaCl+NaOH regeneration solution was added. Regeneration lasted for 4 hours, which was sufficient to achieve equilibrium, in accordance with previous tests (Williams et al., 2015). Samples were collected for nutrient and micropollutant analysis from the feed water, after ion exchange, and after regeneration.

3.2.4 Tests in actual anaerobic wastewater filtrate

A filtrate sample from a belt filter press used to dewater anaerobically digested sludge from Jones Island Water Reclamation Facility, Milwaukee, WI, was acquired to test the impact of a complex anaerobic wastewater matrix on the fate and impact of TCS, E2, and SMX during ion exchange-regeneration. Water quality parameters including pH, chemical oxygen demand (COD), total organic carbon (TOC), and total suspended solids

(TSS) were measured in accordance with standard methods (APHA et al., 1998), results of which are provided in Appendix 3M. Ammonium-N content in the filtrate was approximately 110 mg/L; no additional N was added. Phosphate-P content in the filtrate was approximately 1.4 mg/L; additional P was added for a final concentration of 8 mg/L. Approximately 300 μg/L each of TCS, E2 and SMX was added to the anaerobic effluent (background concentrations were below detection). Each bottle was dosed with 5 g/L of clinoptilolite, 1 g/L of LayneRT, or 1 g/L of DOW-HFO-Cu, as described for the batch experiments. Regeneration brine containing 2% NaCl and 2% NaOH was used to regenerate LayneRT, 2% NaOH and 5% NaCl was used to regenerate DOW-HFO-Cu, and 8% NaCl was used to regenerate clinoptilolite. Controls were performed using no ion exchangers to investigate the adsorption of micropollutants to the organic carbon in the wastewater matrix. Samples were analyzed after 4 days to determine the extent of removal and desorption from the ion exchangers.

3.2.5 Struvite precipitation in the presence of micropollutants

Batch tests were conducted to determine the fate of micropollutants during struvite precipitation in Milli-Q water. A molar ratio of P:N:Mg=1:1:1 was targeted by mixing $Na_2HPO_4 \bullet 7H_2O$ (165 mL, 4.26 g/L), NH_4Cl (15 mL, 9.33 g/L), and $MgCl_2 \bullet 6 H_2O$ (20 mL, 26.65 g/L). Approximately 300 μg/L each of TCS, E2, and SMX was added. To mimic the regeneration brine, the pH was adjusted to 9 using NaOH and 2% NaCl was added. The solution was mixed on a shaker table at 180 rpm for 40 min and allowed to settle for 10 min (Williams et al., 2015). Supernatant was collected before and after the precipitation reaction for quantification of micropollutants and nutrients.

3.2.6 Analytical methods

The standard phenate and ascorbic acid methods were used to quantify NH_4-N and PO_4-P, respectively (APHA et al., 1998). To eliminate interferences with micropollutant detection from background ions, micropollutants were quantified via online solid-phase extraction (SPE) with single quadrupole liquid chromatograph-mass spectrometry (LC-MS). An online SPE cartridge (Phenomenex, Torrance, CA, USA) was incorporated in the LC-MS system (LC-MS 2020, Shimadzu, Columbia, MD, USA). All samples were filtered through 0.45 µm PTFE filters. 13C-TCS, estrone (E1), and 13C-SMX were added as internal standards before SPE. Details of the SPE-LC-MS method are provided in the Appendix 3C. Method detection limits were 8 µg/L TCS, 8 µg/L E2, and 9 µg/L SMX. Recovery of TCS, E2, and SMX was 70 – 130% to meet the quality control criteria (Smith et al., 2010).

3.2.7 Data analysis

Adsorption capacity from batch ion exchange tests and percent recovery from exchange-regeneration tests were calculated as described in the Appendix 3D. Nutrient removal kinetics were modelled as pseudo-second order reactions (which demonstrated the best fit for the data), as described in the Appendix 3E.

Isotherm modeling and statistical analysis (t-test, α level = 5%) were conducted using GraphPad Prism 6 (Graphpad Software, Inc., La Jolla, CA). To determine the relative influence of NaOH and NaCl on the recovery of NH_4-N, PO_4-P, or micropollutants during regeneration, response surface methodology (RSM) was used in R (Appendix 3F) (Montgomery, 2003).

3.3   Results and Discussion

3.3.1   The impact of micropollutants on nutrient ion exchange reaction kinetics

The reaction rate of nutrient ion exchange with and without micropollutants was determined in batch studies. The nutrient ion exchange kinetics in Milli-Q water (Figure 3.1) were modeled as pseudo-second order reactions (Ho, 2006; Ho and McKay, 1999), which provided the best fit (equilibrium curves are shown in Appendix Figure 3G and average fitting parameters of linearized nutrient exchange kinetic curves are shown in Appendix 3G, Table 3G). The presence of micropollutants significantly decreased ammonium and phosphate exchange reaction rate constants (Table 3.1, calculated using Appendix 3E, Eq. 5). When micropollutants were present in the water, the reaction rate constants for clinoptilolite, LayneRT, and DOW-HFO-Cu decreased by 32%, 85%, and 80%, respectively (Appendix 3G, Figure 3G).
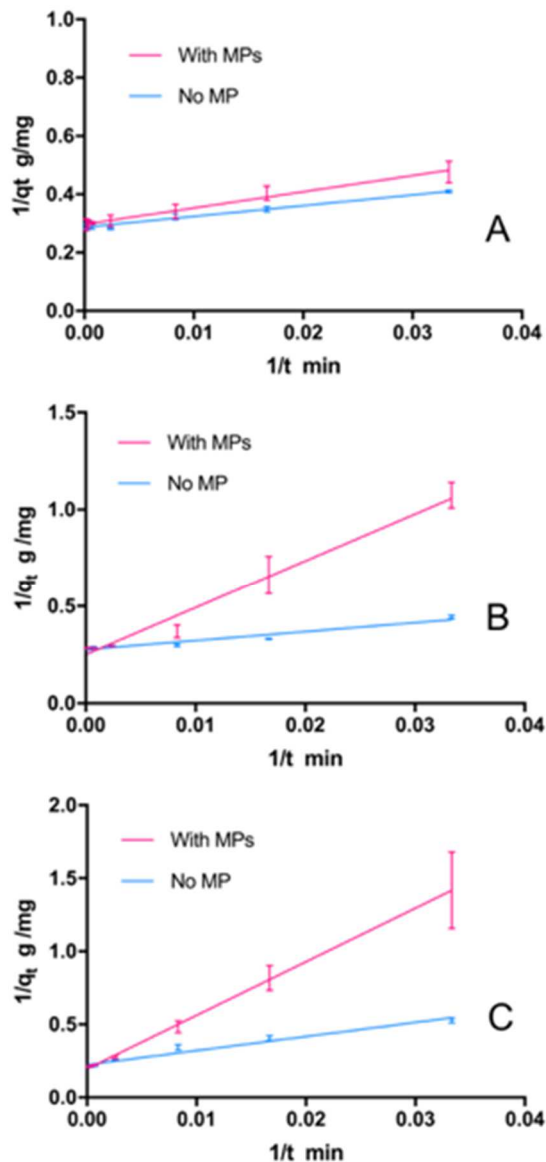
Figure 3.1 Linearized second order nutrient removal kinetics curves, plotted as the reciprocal of total adsorbed amount per unit mass of exchanger ($1/q_t$, g/mg) versus the reciprocal of time ($1/t$, 1/min). The plots show nutrient removal kinetics with and without micropollutants (MPs) in Milli-Q water for: A) NH_4-N removal by clinoptilolite, B) PO_4-P removal by LayneRT, and C) PO_4-P removal by DOW-HFO-Cu. The data points represent averages and error bars represent ± 1 standard deviation of triplicate experiments.

Table 3.1 Pseudo-second order reaction rate constants for nutrient ion exchange reactions with and without micropollutants

Nutrient	Ion Exchanger	Rate Constant (L/mg/min)		p-value
		With Micropollutants	**Without Micropollutants**	
Ammonium	Clinoptilolite	0.015	0.022	0.0002
Phosphate	LayneRT	0.003	0.020	<0.0001
Phosphate	DOW-HFO-Cu	0.001	0.005	<0.0001

According to Planzinski et al. (2013), the pseudo-second order reaction model for spherical sorbent particles can be well interpreted in terms of an intraparticle diffusion model. This model assumes that the overall sorption reaction rate is controlled by the rate of sorbate diffusion across the sorbate/solution interface within pores (Plazinski et al., 2013). In terms of nutrient exchange in this study, reductions in reaction rates in the presence of micropollutants may have been caused by the micropollutants interfering with nutrient diffusion from the aqueous phase to the solid surface of the adsorbent (Klaewkla et al., 2011; Sawyer et al., 2003). Although micropollutants significantly decreased nutrient ion exchange reaction rates, their presence did not impact the total amount of nutrients adsorbed at equilibrium (Appendix 3G, Figure 3G).

3.3.2 Adsorption of micropollutants onto nutrient ion exchangers

Batch studies were conducted to track the fate of micropollutants during nutrient removal via ion exchange in Milli-Q water. The three micropollutants were adsorbed to varying extents, as shown in Figure 3.2. LayneRT adsorbed 85.6±4.5% TCS, 64.4±4.1% E2, and 51.6±8.0% SMX. DOW-HFO-Cu adsorbed 86.2±2.3% TCS, 88.2±4.6% E2, and 65.1±5.1% SMX. Using clinoptilolite to capture ammonium, TCS and E2 were not readily adsorbed (p=0.314 for TCS and p=0.067 for E2), and the SMX concentration at

the end of the equilibrium period did not differ significantly from the initial concentration

(p=0.154), signifying that these micropollutants were not readily removed using

clinoptilolite.
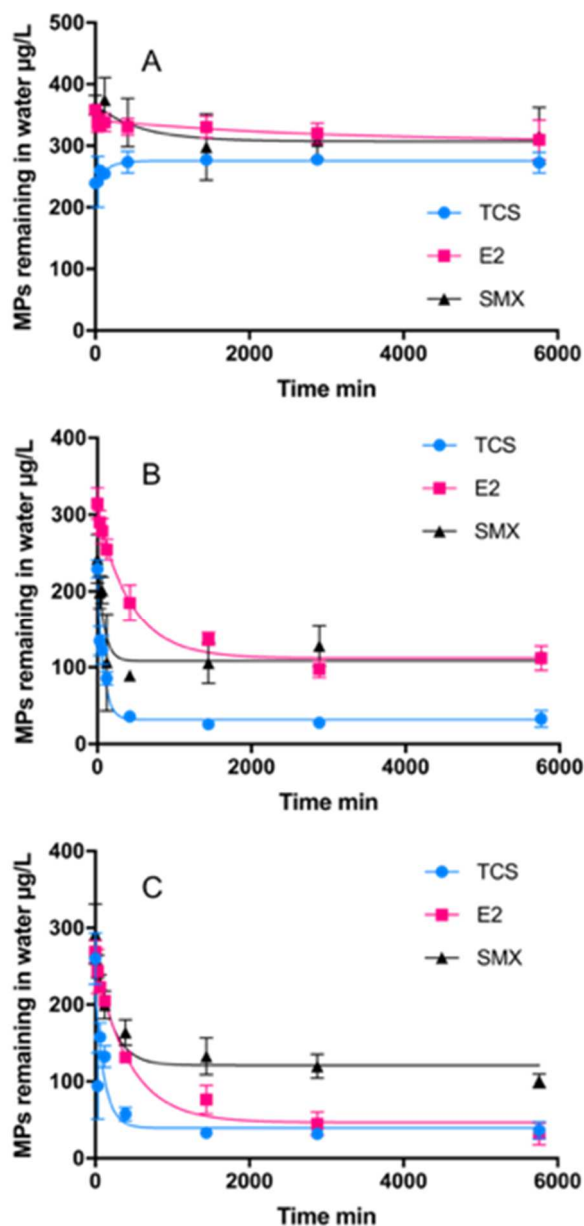
Figure 3.2 Micropollutant (MP) removal by three ion exchangers in Milli-Q water, A) clinoptilolite, B) LayneRT, and C) DOW-HFO-Cu, over time during batch tests. Feed water concentrations were ~300±50 µg/L each for TCS, E2, and SMX. Initial nutrient concentrations were 40 mg-N/L and 5 mg-P/L, with pH=7. The data points represent average results and error bars show ± 1 standard deviation of triplicate experiments.

Clinoptilolite has a negative surface charge (Appendix 3H, Figure 3H), making it unlikely to adsorb the negatively charged dissociated fractions of TCS, E2, or SMX through coulombic attraction. Furthermore, according to pore size analysis, the mode pore width of clinoptilolite is 10.2 Å (Appendix 3I, Figure 3I). According to 3D-structure measurements in ChemDraw®, TCS has a minor dimension of 7.9 Å and a major dimension of 13.7 Å. The minor and major dimensions of E2 are 8.5 Å and 18 Å, respectively, while the minor and major dimensions of SMX are 14 Å and 15 Å, respectively. As the molecular size of the micropollutants is near or larger than clinoptilolite's pores, the likelihood for adsorption of micropollutants is low (Faust and Aly, 1998). Poor adsorption of SMX on clinoptilolite was also demonstrated previously (Farí et al., 2003).

On the other hand, the phosphate-selective exchange resins, LayneRT and DOW-HFO-Cu, readily sorbed TCS, E2, and SMX at neutral pH (Figures 3.2B and 3.2C, respectively). Gas sorption tests indicated that LayneRT has a mode pore size of 20.2 Å, and DOW-HFO-Cu has a mode pore size of 23.4 Å (Appendix 3I, Figure 3I). Thus, the phosphate resins' pores are larger (in comparison to clinoptilolite's mode pore size of 10.2 Å) and more accessible for micropollutant adsorption.

3.3.3 The impact of micropollutants on nutrient ion exchange capacity

Nutrient ion exchange isotherm modeling was performed using data from batch tests conducted with and without micropollutants in the Milli-Q feed water to assess micropollutants' influence on nutrient exchange capacity and mechanisms. Exchange of

ammonium using clinoptilolite fit the Langmuir isotherm model (Appendix 3J, Figure 3A), which assumes one solute ion per adsorption site, forming a single layer on the sorbate surface (Halim et al., 2010). The ammonium exchange isotherms with and without micropollutants were not significantly different (p=0.756).

An empirical isotherm (Butt et al., 2006; Limousin et al., 2007a), provided the best fit for modeling exchange of phosphate via LayneRT and DOW-HFO-Cu resins with and without micropollutants in the feed water (Appendix 3J, Figures 5JB and 4JC). A sigmoidal isotherm often occurs when using a homogenous adsorbent (Butt et al., 2006), such as LayneRT and DOW-HFO-Cu resins, which are manufactured under controlled conditions. Observation using a scanning electron microscope (Appendix 3K, Figure 3K) together with surface pore analysis indicated that these phosphate ion exchangers were more homogeneous than clinoptilolite, reaffirming the underlying basis for the best fit isotherm model behaviors. At near-neutral pH, the predominant orthophosphate species, $H_2PO_4^-$ and HPO_4^{2-}, are Lewis bases (electron pair donors) that can exhibit strong ligand adsorption on the HFO in LayneRT resin, as well as on both HFO and Cu^{2+} in the DOW-HFO-Cu resin, by forming inner-sphere complexes through coordinate bonding. Sigmoidal isotherms provide good representations of this type of phosphate exchange, according to previous reports (Blaney et al., 2007; Cumbal and Sengupta, 2005; Hinz, 2001; Limousin et al., 2007b; Sengupta and Pandit, 2011a). The inflection expected for a Type D isotherm was not observed, likely due to the small phosphorus range tested (less than 5 mg/L).

Similar to the case for clinoptilolite, there was no significant difference in exchange capacity with and without micropollutants for the phosphate-selective resins

(LayneRT p=0.768 and DOW-HFO-Cu p=0.796, Appendix 3J, Figure 3J). Although the presence of micropollutants slowed the reaction rates of nutrient ion exchange, as described previously, the amount (Q_e) of phosphate or ammonium exchanged at equilibrium remained similar with or without micropollutants, as did the shape of the isotherm. For clinoptilolite, the ammonium isotherm was not expected to change since TCS, E2 and SMX did not adsorb effectively (Figure 3.2A). For LayneRT and DOW-HFO-Cu, it is possible that the low initial concentrations of micropollutants relative to nutrients and different adsorption/exchange mechanisms contributed to the lack of observed change in the nutrient exchange isotherms with and without micropollutants.

3.3.4 Potential mechanisms of micropollutant-ion exchanger interaction

There are two plausible means by which micropollutants could bind with phosphate-selective ion exchange resins: A) coulombic attraction due to opposite charges, and B) non-coulombic attractions such as hydrophobic interactions, hydrogen bonding, and aromatic system π stacking (Carmona et al., 2006; Inyang and Dickenson, 2015).

In near-neutral pH feed water, TCS and E2 are predominantly in the neutral form (88.8% neutral for TCS and 99.9% for E2, Appendix 3A, Figure 3A). Therefore, the non-coulombic mechanisms for TCS and E2 adsorption by LayneRT and DOW-HFO-Cu differ from the electrostatic mechanism that controls phosphate exchange. The aromatic pyridyl group in the bis-picolylamine attached to the DOWEX M4195 polymer matrix, and the benzene ring of LayneRT's backbone structure, are able to form π stacking with the benzene rings on TCS and E2 molecules (Janiak, 2000; Sengupta and Pandit, 2011b). Moreover, with high log D_{ow} values, the extent of TCS and E2 adsorption onto phosphate exchangers was relatively high.

Negatively charged dissociated SMX is more likely to adsorb to LayneRT and DOW-HFO-Cu via coulombic attraction with positively charged moieties that are dissociated while in water (Appendix 3H, Figure 3H). At pH 7, the majority of SMX molecules are anionic (98.0%) (Appendix 3A, Figure 3A), and have a low log D_{ow} value that tends to keep SMX in water. On the other hand, ionic SMX may also be adsorbed to the quaternary ammonium groups (R_4N^+) on LayneRT's surface via coulombic attraction. The removal of ionic SMX by DOW-HFO-Cu may be attributed to the coulombic attraction between the ions and chelated HFO or Cu^{2+} that forms outer sphere complexes (Blaney et al., 2007). Therefore, the relatively low extent of adsorption for SMX can be a combined effect of hydrophilicity and columbic attraction. Additionally, the π-electron rich moiety in SMX's structure may form π stacking with the ion exchanger surface, which may play a minor role. Alternately, phosphate prefers ligand adsorption by forming inner sphere complexes via both coulombic and Lewis acid-base attraction with HFO (Blaney et al., 2007; Landry and Boyer, 2013). In accordance with these potentially different adsorption mechanisms and low micropollutant loadings, ionic SMX is unlikely to compete with phosphate for exchange sites on LayneRT and DOW-HFO-Cu resins. However, the absence of an inflection point in the phosphate exchange isotherm indicates that the functional HFO and Cu^{2+} sites are far from saturation. Considering the initial concentrations of TCS, E2 and SMX (approximately 0.0012 mM, whereas phosphate was 0.16 mM), the availability of binding sites on the resins was sufficient for phosphate adsorption.

3.3.5   The impact and fate of micropollutants during ion exchange regeneration

Ion exchange regeneration was performed to investigate the fate of the micropollutants adsorbed on the ion exchangers, and their potential effect on nutrient desorption during regeneration. Following ion exchange in Milli-Q water, regeneration brine containing varying concentrations of NaCl and NaOH was used to increase adsorption capacity of exhausted clinoptilolite, LayneRT, and DOW-HFO-Cu (Crittenden et al., 2012). Micropollutants that were adsorbed onto phosphate exchangers did not impact nutrient desorption, as shown in Figure 3.3 (p=0.058 for LayneRT and p=0.699 for DOW-HFO-Cu). Since micropollutants were not adsorbed by clinoptilolite during the ion exchange stage, micropollutants did not have a significant impact on the desorption of ammonium (p=0.57). Therefore, clinoptilolite was not considered in further studies of micropollutant desorption during regeneration.
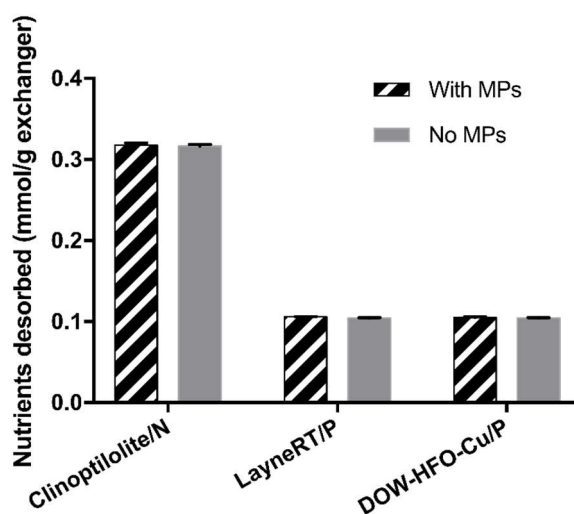
Figure 3.3 Nutrient desorption per mass of ion exchanger during ion exchange-regeneration batch tests, with and without micropollutants (MPs, ~300 µg/L each TCS, E2, and SMX, in the pH=7 ion exchange feed waters). The regeneration brine for phosphate exchangers was 2% NaOH + 2% NaCl, while 8% NaCl was used for clinoptilolite. The data represent average results and error bars show ± 1 standard deviation of triplicate experiments.

To explore the impact of NaCl and NaOH on micropollutant desorption from LayneRT and DOW-HFO-Cu resins, concentrations of NaCl and NaOH in the regenerant were varied, as listed in Appendix 3B, Tables 3B.1—3B.4. There was no significant correlation between regeneration brine constituents and micropollutant desorption (Appendix 3L, Table 3L). Under the tested conditions, micropollutant desorption from LayneRT or DOW-HFO-Cu cannot be accurately predicted using the concentration of constituents in the regeneration brine, nor is it easy to control desorption by varying brine concentration, possibly due to the complexity of micropollutants' binding with ion exchangers. Therefore, the potential desorption of micropollutants is unlikely to influence the selection of regeneration brine in real-life operations. Instead, impacts on nutrient ion exchange capacity and operation costs will be the most important criteria when selecting a regenerant (Cheremisinoff, 2002).

Although there was no significant correlation between regeneration brine concentration and micropollutant desorption, the extent of desorption (based on percent mass desorbed relative to initial mass sorbed) varied among the micropollutants (Figure 3.4). Comparing Figures 3.2 and 3.4, micropollutant desorption was inversely related with the degree of adsorption, where compounds that adsorbed poorly were more easily desorbed (i.e., SMX). For TCS, the extent of adsorption (Figure 3.2) and desorption (Figure 3.4) onto the two phosphate exchangers was similar. For E2, adsorption using LayneRT was lower than for DOW-HFO-Cu (Figure 3.2), and desorption was generally higher for LayneRT than DOW-HFO-Cu (Figure 3.4), which indicates that E2 has stronger binding with LayneRT than DOW-HFO-Cu.
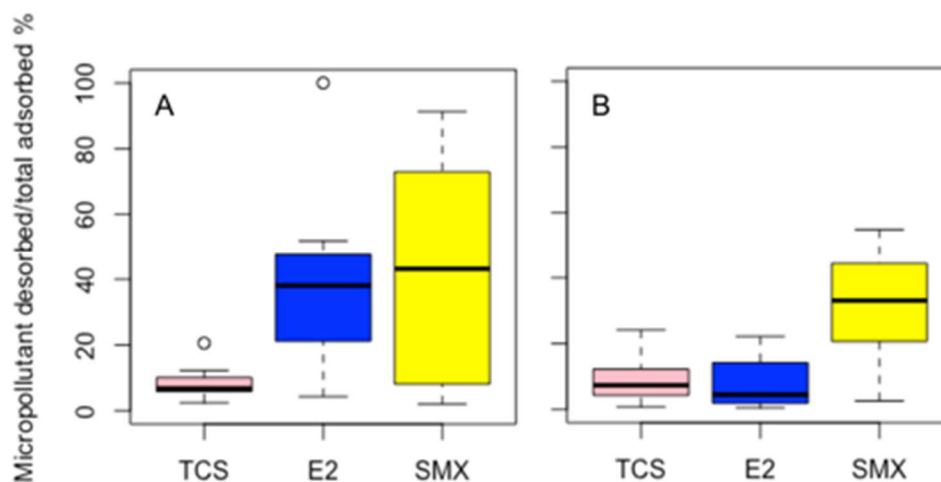
Figure 3.4 Summary of results for micropollutant desorption relative to total adsorption for batch ion exchange-regeneration tests in Milli-Q water using A) LayneRT and B) DOW-HFO-Cu resin (n = 11). Results include triplicate tests of 11 different NaCl and NaOH regenerant brine compositions, as detailed in supplemental information Appendix 5B. Clinoptilolite is not shown because no significant micropollutant adsorption was observed. The horizontal bold line indicates the median. The boxes represent the first and third quartile of the data set. The whiskers above and below the boxes show the locations of the minimum and maximum. The hollow circles signify outliers.

Phosphate readily desorbed from each phosphate exchanger under the regeneration conditions tested, but desorption did not correlate to NaCl or NaOH concentration (p=0.791 for LayneRT and p=0.380 for DOW-HFO-Cu, first order linear regression model; Appendix 3B, Tables 3B.1 and 3B.3). Phosphate desorption was 3.50±0.19 mg-P/g LayneRT (94.5±5.54% of the portion captured was released) and 3.69±0.30 mg-P/g DOW-HFO-Cu (74.35±5.31%). The mass of phosphate desorbed from LayneRT was not significantly different from that desorbed from DOW-HFO-Cu (p=0.12). However, DOW-HFO-Cu resin generally demonstrated greater total mass removal of phosphate and lower desorption, possibly indicating stronger binding.

Phosphate ions are exchanged by forming inner-sphere complexes with HFO and

Cu^{2+} on the exchangers via coulombic interactions, while adsorption of SMX in pH 7

feed water was possibly due to non-selective coulombic attraction forming outer sphere

complexes (Blaney et al., 2007). Thus, the attachment of both phosphate and SMX to

phosphate exchange resins was likely due to electrostatic attractions, which would be

easily disrupted by the concentrated Cl^- and OH^- in the regeneration brine (Landry and

Boyer, 2013). As noted previously, adsorption of TCS and E2 to the two phosphate

exchange resins was not likely due to coulombic attraction, indicating that the presence of

strong counter ions would not significantly affect desorption (Landry and Boyer, 2013).

Desorption of TCS and E2 from both phosphate ion exchangers, and SMX from

DOW-HFO-Cu (medians<50%) were much lower than phosphorus desorption (>90%).

These results indicate that the majority of the micropollutants tended to irreversibly

adsorb to the ion exchangers, regardless of the interactions between micropollutants and

exchangers (e.g., coulombic or non-coulombic). Landry and Boyer (Landry and Boyer,

2013) also reported low desorption of diclofenac sorbed on polymeric strong-base anion

exchange resins (24% using 4% NaCl brine). Even though coulombic forces played a

major role for diclofenac (pKa= 4.7) attaching to the polystyrene resin in fresh urine (pH

= 6), high strength regeneration brine could not disrupt the interaction between the

dissociated diclofenac and the resin (Landry and Boyer, 2013). Previous studies have also

shown favorable adsorption of chlorinated phenols and aromatic micropollutant anions on

polymeric exchangers, with a preference for these contaminants over inorganic chloride

ions present in either feed water or regeneration solutions (Hinrichs and Snoeyink, 1976;

Lee and Ku, 1996). This was attributed to the non-polar moiety of the aromatic ions

leading to simultaneous hydrophobic interactions and coulombic attractions (Li and

SenGupta, 1998).

The low desorption to adsorption ratio of hydrophobic micropollutants from ion

exchangers potentially introduces additional concerns for flow-through reactor operation.

Based on the lack of effective micropollutant desorption during regeneration, over time,

ion exchangers may become saturated with adsorbed micropollutants. Consequently,

micropollutants in the influent may eventually bypass the ion exchange bed, and be

carried into the ion exchange effluent, which would be discharged to receiving waters.

3.3.6 The impact and fate of TCS, E2 and SMX during nutrient ion exchange-regeneration in actual anaerobic filtrate

Ion exchangers were tested in anaerobic filtrate supplemented with 300 µg/L each

TCS, E2, and SMX to investigate the impact of micropollutants on nutrient exchange in a

real anaerobic effluent matrix containing organic carbon (water quality parameters are

listed in Appendix 3M, Table 3M). The presence of micropollutants in actual anaerobic

wastewater did not impact nutrient removal or regeneration (all t-test p-values were

greater than 0.05, as shown in Table 3.2). This finding was similar to the results in the

Milli-Q water tests.

Table 3.2 Nutrient removal and regeneration by ion exchangers in anaerobic filtrate, with and without the presence of micropollutants (MPs). All tests were conducted in triplicate, and values shown are means ± 1 standard deviation.

Ion exchanger	Unit		No MP	With MPs	p-value
Clinoptilolite	NH_4-N mmol/g exchanger	removed	0.69±0.07	0.58±0.15	0.31
		regenerated	0.69±0.07	0.48±0.08	0.31
LayneRT	PO_4-P mmol/g exchanger	removed	0.13±0.00	0.13±0.00	0.97
		regenerated	0.11±0.00	0.10±0.00	0.10
DOW-HFO-Cu		removed	0.13±0.00	0.12±0.00	0.09
		regenerated	0.11±0.01	0.11±0.00	0.09

The extent of micropollutant adsorption and desorption during nutrient ion exchange-regeneration in the complex wastewater matrix differed compared to Milli-Q tests. As shown in Table 3.3, TCS adsorption on the phosphate ion exchangers in the anaerobic filtrate significantly decreased compared with previous Milli-Q tests. Adsorption of E2 using DOW-HFO-Cu in anaerobic filtrate also decreased significantly compared to Milli-Q tests, whereas no difference was observed between the two water matrices using LayneRT. Both TCS and E2 desorption were greater in anaerobic filtrate tests. These results indicate that constituents in the complex wastewater matrix can possibly hinder TCS and E2 adsorption with phosphate exchangers. For these neutral molecules, this could be attributed to competition from suspended solids and organic carbon. The phosphate exchangers removed 57% of the SMX from the anaerobic filtrate, which was similar to results from Milli-Q water tests, indicating suspended solids and organic matter did not hinder SMX adsorption. However, desorption of SMX decreased in the anaerobic filtrate tests compared to Milli-Q, possibly due interactions between SMX and the co-adsorbed wastewater constituents.

Table 3.3 Micropollutant (MP), TCS, E2 and SMX, removal and regeneration by ion exchangers in anaerobic filtrate compared to Milli-Q water. All tests were conducted in triplicate, and values shown are means ± 1 standard deviation. t-tests (p-values shown) were used to compare performance in the two water matrices. Clinoptilolite was also tested, but did not adsorb micropollutants.

Ion Exchanger	MP	% Removal			% Regeneration		
		Anaerobic effluent	Milli-Q water	p-value	Anaerobic effluent	Milli-Q water	p-value
LayneRT	TCS	50.4±1.4	85.6±4.5	0.0002	74.3±10.8	21.5±11.1	0.004
	E2	59.7±1.9	64.4±4.1	0.09	54.8±3.5	36.3±5.2	0.007
	SMX	56.7±6.9	51.6±8.0	0.48	3.3±0.6	83.1±8.1	<0.0001
DOW-HFO-Cu	TCS	53.8±1.2	86.2±2.3	<0.0001	68.4±2.3	20.3±2.5	0.003
	E2	66.7±1.5	88.2±4.6	0.002	68.3±0.5	5.2±3.3	0.0003
	SMX	71.4±7.1	65.1±5.1	0.26	3.6±1.0	31.7±15.3	0.003

In control experiments without ion-exchangers, approximately 44% of TCS (the most hydrophobic compound) was removed by the wastewater matrix, and approximately 26% of E2 was removed. The most hydrophilic compound tested, SMX, was not removed by the wastewater matrix.

3.3.7   The fate of micropollutants during struvite precipitation

The concentrations of TCS, E2 and SMX in the aqueous solution did not decrease during struvite precipitation (Table 3.4), indicating that these micropollutants were not able to adsorb on, or assimilate into, struvite crystals. The distribution coefficient D_{ow} (Appendix 3A, Table 3A) shows that at pH 9, which was used for struvite precipitation, the majority of TCS and E2 molecules were still hydrophobic, whereas SMX was mostly dissociated and hydrophilic. Previous reports suggested that the accumulation of micropollutants in struvite cannot be fully explained by hydrophobicity since the relatively hydrophilic compounds tetracycline (log K_{ow} = -1.37) and quinolones (log K_{ow}

= 0.89) were observed in struvite crystals (Antakyal et al., 2011; Başakçilardan-Kabakci et al., 2007).

Table 3.4 Average ± 1 standard deviation concentrations of TCS, E2 and SMX in the supernatant before and after struvite precipitation (n=3)

Micropollutant	Before precipitation (µg/L)	After precipitation (µg/L)	p-value
TCS	275 ± 31.5	275 ± 18.3	0.98
E2	266 ± 30.7	282 ± 12.6	0.29
SMX	234 ± 1.29	251 ± 34.6	0.49

In previous studies, the majority of tetracycline accumulation in struvite was considered to be due to spontaneous assimilation into struvite's structure during formation, rather than being adsorbed onto the surface of pre-formed struvite (Antakyal et al., 2011; Başakçilardan-Kabakci et al., 2007). This finding was explained by tetracycline's potential as a ligand, wherein the molecule's β-hydroxyl ketone moiety can donate electron pairs to form stable complexes with Mg^{2+} or Ca^{2+} (Başakçilardan-Kabakci et al., 2007; Schmitt and Schneider, 2000; Tolls, 2001; Turel, 2002). Thus, the partitioning of E2, TCS, and SMX to the aqueous phase observed in this study may be explained by the compounds' inability to form coordination complexes with Mg^{2+} in struvite.

According to the pKa value, more than 98% of E2 was in neutral form at pH 9, clearly preventing it from participating in Lewis acid-base reactions with metal ions. For TCS, the charged fractions dominate at pH 9. The dissociated phenolic group on TCS (Appendix 3A, Table 3A) is affected by resonance due to the presence of benzene. The resonance phenomenon makes non-bonded electron pairs of oxygen form double bonds with benzene carbon, turning the dissociated phenolic group into more acidic forms, which can result in difficulty forming a coordinate bond between TCS and Mg^{2+} (DeRuiter, n.d.; Schwarzenbach et al., 2005).

Dissociated SMX also dominates at pH 9. The charged fraction of SMX can form coordinate complexes with first and second row transition metals such as Cr, Mn(II), Zn(II), Cd(II), and Co(II) (Kanagaraj and Rao, 1992; Kesimli and Topacli, 2001). However, as negligible removal of SMX was observed during struvite precipitation, SMX may not be able to form complexes with metals such as Mg(II). According to hard and soft acids and bases rules (Pearson, 1963), Mg is a hard acid that is relatively nonpolarizable; therefore, it is easier for Mg to form stable complexes with hard bases such as OH^-, which is present in tetracyclines. However, it is more difficult for Mg to form stable complexes with the soft base functional groups in SMX such as sulfonamide nitrogen, amino nitrogen, and sulfonyl oxygen. Micropollutants that cannot form coordinate complexes with the metals in struvite are unlikely to be present in precipitated struvite.

3.4   Conclusions

This research demonstrated that ion exchange-precipitation can effectively recover nutrients from nutrient-rich waters (both Milli-Q and actual anaerobically-treated wastewater), regardless of the presence of TCS, E2, and SMX. The result matched the hypothesis that the reaction rate of nutrient exchange decreased in the presence of micropollutants. However, the extent of nutrient adsorption and desorption was not influenced by the presence of these micropollutants, due to low micropollutants concentrations and different adsorption mechanisms. The ammonium-selective clinoptilolite ion exchanger did not adsorb TCS, E2, or SMX. However, these neutral and anionic micropollutants were able to co-adsorb to phosphate exchangers during exchange of orthophosphate and were desorbed during ion exchanger regeneration. The hypothesis

of micropollutants precipitate out with struvite was rejected, since micropollutants did not partition to precipitated struvite, so they do not pose risks in the final solid fertilizer product.

The findings from this research have direct real-world implications. Specifically, the adsorption/desorption behaviors indicated that micropollutants could accumulate on ion exchangers, which may eventually lead to saturation of the ion exchangers, causing bypass of micropollutants into the ion exchange effluent. That would put additional stress on receiving natural waters, once treated AnMBR effluent was discharged to the environment. When the micropollutants were present in actual anaerobic wastewater, they did not interfere with nutrient removal and recovery; however, the complex matrix of anaerobic wastewater tended to decrease co-adsorption and increase desorption of TCS and E2 from phosphate-specific exchangers. To avoid co-adsorption of nutrients and MPs as well as the discharge of micropollutants with the ion exchange effluent, other non-selective adsorbents, such as biosolids-derived biochar, should be employed prior to ion exchange to remove micropollutants before recovering nutrients, which will be studied in **Chapter 4-6**.

The fate of micropollutants through the ion exchange-precipitation process is closely related to the physical and chemical properties of micropollutants, ion exchangers, and struvite. For example, clinoptilolite did not sorb the selected micropollutants, likely on the basis of surface charge and molecular size disparities. Likewise, the inability of the investigated micropollutants to form coordinate complexes with the metal ions in struvite crystals appears to be the key factor determining partitioning of micropollutants between the aqueous phase and the precipitated struvite

product. Future research extending these results to cationic and zwitterionic

micropollutants can help to derive more universal conclusions related to the impact and

fate of micropollutants during nutrient ion exchange.

3.5   References

Alvarino, T., Suarez, S., Lema, J.M., Omil, F., 2014. Understanding the removal mechanisms of PPCPs and the influence of main technological parameters in anaerobic UASB and aerobic CAS reactors. J. Hazard. Mater. 278, 506–513. doi:10.1016/j.jhazmat.2014.06.031

Antakyal, D., Kuch, B., Preyl, V., Steinmetz, H., 2011. Effect of micropollutants in wastewater on recovered struvite. Proc. Water Environ. Fed. 2011, 575–582.

APHA, AWWA, WEF, 1998. Standard methods for the examination of water and wastewater, Standard Methods for the Examination of Water and Wastewater.

Başakçilardan-Kabakci, S., Thompson, A., Cartmell, E., Le Corre, K., 2007. Adsorption and precipitation of tetracycline with struvite. Water Environ. Res. 79, 2551–2556. doi:10.2175/106143007X184618

Blair, B.D., Crago, J.P., Hedman, C.J., Treguer, R.J.F., Magruder, C., Royer, L.S., Klaper, R.D., 2013. Evaluation of a model for the removal of pharmaceuticals, personal care products, and hormones from wastewater. Sci. Total Environ. 444, 515–21. doi:10.1016/j.scitotenv.2012.11.103

Blaney, L.M., Cinar, S., SenGupta, A.K., 2007. Hybrid anion exchanger for trace phosphate removal from water and wastewater. Water Res. 41, 1603–1613. doi:10.1016/j.watres.2007.01.008

Butt, H.-J., Graf, K., Kappl, M., 2006. Physics and chemistry of interfaces. John Wiley & Sons.

Carey, D.E., Mcnamara, P.J., 2015. The impact of triclosan on the spread of antibiotic resistance in the environment   . Front. Microbiol.   .

Carey, D.E., McNamara, P.J., 2016. Altered antibiotic tolerance in anaerobic digesters acclimated to triclosan or triclocarban. Chemosphere 163, 22–26. doi:10.1016/j.chemosphere.2016.07.097

Carey, D.E., Yang, Y., McNamara, P.J., Mayer, B.K., 2016a. Recovery of agricultural nutrients from biorefineries. Bioresour. Technol. 215, 186–198.

Carey, D.E., Zitomer, D.H., Kappell, A.D., Choi, M.J., Hristova, K.R., McNamara, P.J.,

2016b. Chronic exposure to triclosan sustains microbial community shifts and alters antibiotic resistance gene levels in anaerobic digesters. Environ. Sci. Process. Impacts 18, 1060–1067. doi:10.1039/C6EM00282J

Carmona, M., De Lucas, A., Valverde, J.L., Velasco, B., Rodríguez, J.F., 2006. Combined adsorption and ion exchange equilibrium of phenol on Amberlite IRA-420. Chem. Eng. J. 117, 155–160.

Chen, X., Nielsen, J.L., Furgal, K., Liu, Y., Lolas, I.B., Bester, K., 2011. Biodegradation of triclosan and formation of methyl-triclosan in activated sludge under aerobic conditions. Chemosphere 84, 452–456. doi:http://dx.doi.org/10.1016/j.chemosphere.2011.03.042

Cheremisinoff, N.P., 2002. Handbook of water and wastewater treatment technologies, Handbook of Water and Wastewater Treatment Technologies. doi:10.1016/B978-075067498-0/50000-0

Crittenden, J.C., Trussell, R.R., Hand, D.W., Howe, K.J., Tchobanoglous, G., 2012. MWH's water treatment: principles and design. John Wiley & Sons.

Cumbal, L., Sengupta, A.K., 2005. Arsenic removal using polymer-supported hydrated iron(III) oxide nanoparticles: Role of Donnan membrane effect. Environ. Sci. Technol. 39, 6508–6515. doi:10.1021/es050175e

DeRuiter, J., n.d. Resonance and induction tutorial [WWW Document]. URL https://www.auburn.edu/~deruija/pdareson.pdf

Farí, T., Ruiz-Salvador, A.R., Rivera, A., 2003. Interaction studies between drugs and a purified natural clinoptilolite. Microporous Mesoporous Mater. 61, 117–125.

Faust, S.D., Aly, O.M., 1998. Chemistry of water treatment. CRC Press.

Halim, A.A., Aziz, H.A., Johari, M.A.M., Ariffin, K.S., 2010. Comparison study of ammonia and COD adsorption on zeolite, activated carbon and composite materials in landfill leachate treatment. Desalination 262, 31–35. doi:10.1016/j.desal.2010.05.036

Hedström, A., 2001. Ion exchange of ammonium in zeolites: a literature review. J. Environ. Eng. 127, 673–681.

Hinrichs, R.L., Snoeyink, V.L., 1976. Sorption of benzenesulfonates by weak base anion exchange resins. Water Res. 10, 79–87.

Hinz, C., 2001. Description of sorption data with isotherm equations. Geoderma 99, 225–243. doi:10.1016/S0016-7061(00)00071-9

Ho, Y.S., 2006. Second-order kinetic model for the sorption of cadmium onto tree fern: A comparison of linear and non-linear methods. Water Res.

doi:10.1016/j.watres.2005.10.040

Ho, Y.S., McKay, G., 1999. Pseudo-second order model for sorption processes. Process Biochem. 34, 451–465. doi:10.1016/S0032-9592(98)00112-5

Hruska, K., Franek, M., 2012. Sulfonamides in the environment: a review and a case report. Vet Med 57, 1–35.

Inyang, M., Dickenson, E., 2015. The potential role of biochar in the removal of organic and microbial contaminants from potable and reuse water: a review. Chemosphere 134, 232–240.

Janiak, C., 2000. A critical account on π–π stacking in metal complexes with aromatic nitrogen-containing ligands. J. Chem. Soc. Dalt. Trans. 3885–3896.

Jimenez, J., Latrille, E., Harmand, J., Robles, A., Ferrer, J., Gaida, D., Wolf, C., Mairet, F., Bernard, O., Alcaraz-Gonzalez, V., Mendez-Acosta, H., Zitomer, D., Totzke, D., Spanjers, H., Jacobi, F., Guwy, A., Dinsdale, R., Premier, G., Mazhegrane, S., Ruiz-Filippi, G., Seco, A., Ribeiro, T., Pauss, A., Steyer, J.-P., 2015. Instrumentation and control of anaerobic digestion processes: a review and some research challenges. Rev. Environ. Sci. Bio/Technology 14, 615–648. doi:10.1007/s11157-015-9382-6

Joss, A., Andersen, H., Ternes, T., Richle, P.R., Siegrist, H., 2004. Removal of Estrogens in Municipal Wastewater Treatment under Aerobic and Anaerobic Conditions: Consequences for Plant Optimization. Environ. Sci. Technol. 38, 3047–3055. doi:10.1021/es0351488

Kanagaraj, G., Rao, G.N., 1992. Synthesis and characterization of some first row transition metal complexes of 4-amino-N-(5-methyl-3-isoxazolyl-benzenesulfonamide (sulfamethoxazole). Synth. React. Inorganic, Met. Nano-Metal Chem. 22, 559–574.

Kesimli, B., Topacli, A., 2001. Infrared studies on Co and Cd complexes of sulfamethoxazole. Spectrochim. Acta Part A Mol. Biomol. Spectrosc. 57, 1031–1036. doi:10.1016/S1386-1425(00)00419-4

Klaewkla, R., Arend, M., Hoelderich, W.F., 2011. A Review of Mass Transfer Controlling the Reaction Rate in Heterogeneous Catalytic Systems, in: Mass Transfer - Advanced Aspects. pp. 667–684. doi:10.5772/22962

Landry, K.A., Boyer, T.H., 2013. Diclofenac removal in urine using strong-base anion exchange polymer resins. Water Res. 47, 6432–6444. doi:10.1016/j.watres.2013.08.015

Laridi, R., Auclair, J.C., Benmoussa, H., 2005. Laboratory and pilot-scale phosphate and ammonium removal by controlled struvite precipitation following coagulation and flocculation of swine wastewater. Environ. Technol. 26, 525–536.

Lee, K.-C., Ku, Y., 1996. Removal of chlorophenols from aqueous solution by anion-exchange resins. Sep. Sci. Technol. 31, 2557–2577.

Li, P., SenGupta, A.K., 1998. Genesis of selectivity and reversibility for sorption of synthetic aromatic anions onto polymeric sorbents. Environ. Sci. Technol. 32, 3756–3766. doi:10.1021/es980628y

Limousin, G., Gaudet, J.-P., Charlet, L., Szenknect, S., Barthès, V., Krimissa, M., 2007a. Sorption isotherms: A review on physical bases, modeling and measurement. Appl. Geochemistry 22, 249–275. doi:10.1016/j.apgeochem.2006.09.010

Limousin, G., Gaudet, J.P., Charlet, L., Szenknect, S., Barthès, V., Krimissa, M., 2007b. Sorption isotherms: A review on physical bases, modeling and measurement. Appl. Geochemistry 22, 249–275. doi:10.1016/j.apgeochem.2006.09.010

Lunn, G.M., Spencer, L.E., Ruby, A.M.J., McCaskill, A., 2014. A novel ion exchange system to purify mixed ISS waste water brines for chemical production and enhanced water recovery. 44th International Conference on Environmental Systems.

Mayer, B.K., Baker, L.A., Boyer, T.H., Drechsel, P., Gifford, M., Hanjra, M.A., Parameswaran, P., Stoltzfus, J., Westerhoff, P., Rittmann, B.E., 2016. Total value of phosphorus recovery. Environ. Sci. Technol. 50, 6606–6620.

Mayer, B.K., Gerrity, D., Rittmann, B.E., Reisinger, D., Brandt-Williams, S., 2013. Innovative strategies to achieve low total phosphorus concentrations in high water flows. Crit. Rev. Environ. Sci. Technol. 43, 409–441. doi:http://dx.doi.org/10.1080/10643389.2011.604262

McCarty, P.L., Bae, J., Kim, J., 2011. Domestic wastewater treatment as a net energy producer - can this be achieved? Environ. Sci. Technol. 45, 7100–6. doi:10.1021/es2014264

McNamara, P.J., Lapara, T.M., Novak, P.J., 2014. The impacts of triclosan on anaerobic community structures, function, and antimicrobial resistance. Environ. Sci. Technol. 48, 7393–7400. doi:10.1021/es501388v

Monsalvo, V.M., McDonald, J.A., Khan, S.J., Le-Clech, P., 2014. Removal of trace organics by anaerobic membrane bioreactors. Water Res. 49, 103–112. doi:10.1016/j.watres.2013.11.026

Montgomery, D.C., 2003. Applied statistics and probability for engineers third edition, Phoenix Usa. doi:10.2307/1269738

Münch, E. V, Barr, K., 2001. Controlled struvite crystallisation for removing phosphorus from anaerobic digester sidestreams. Water Res. 35, 151–159. doi:10.1016/S0043-1354(00)00236-0

Neset, T.S.S., Cordell, D., 2012. Global phosphorus scarcity: Identifying synergies for a

sustainable future. J. Sci. Food Agric. 92, 2–6. doi:10.1002/jsfa.4650

O'Neal, J.A., Boyer, T.H., 2015. Phosphorus recovery from urine and anaerobic digester filtrate: comparison of adsorption–precipitation with direct precipitation. Environ. Sci. Water Res. Technol. 1, 481–492.

Pearson, R.G., 1963. Hard and soft acids and bases. J. Am. Chem. Soc. 85, 3533–3539.

Plazinski, W., Dziuba, J., Rudzinski, W., 2013. Modeling of sorption kinetics: The pseudo-second order equation and the sorbate intraparticle diffusivity. Adsorption 19, 1055–1064. doi:10.1007/s10450-013-9529-0

Razali, M., Zhao, Y., Bruen, M., 2007. Effectiveness of a drinking-water treatment sludge in removing different phosphorus species from aqueous solution. Sep. Purif. Technol. 55, 300–306. doi:10.1016/j.seppur.2006.12.004

Rittmann, B.E., Mayer, B., Westerhoff, P., Edwards, M., 2011. Capturing the lost phosphorus. Chemosphere 84, 846–853. doi:10.1016/j.chemosphere.2011.02.001

Samaras, V.G., Stasinakis, A.S., Mamais, D., Thomaidis, N.S., Lekkas, T.D., 2013. Fate of selected pharmaceuticals and synthetic endocrine disrupting compounds during wastewater treatment and sludge anaerobic digestion. J. Hazard. Mater. 244, 259–267. doi:10.1016/j.jhazmat.2012.11.039

Sawyer, C.N., McCarty, P.L., Parkin, G.F., 2003. Chemistry for environmental engineering and science.

Schmitt, M.O., Schneider, S., 2000. Spectroscopic investigation of complexation between various tetracyclines and Mg 2+ or Ca 2+. PhysChemComm 3, 42–55.

Schwarzenbach, R.P., Gschwend, P.M., Imboden, D.M., 2005. Environmental organic chemistry. John Wiley & Sons.

Seib, M.D., Berg, K.J., Zitomer, D.H., 2016. Reduced energy demand for municipal wastewater recovery using an anaerobic floating filter membrane bioreactor. Environ. Sci. Water Res. Technol. 2, 290–297. doi:10.1039/C5EW00244C

Sengupta, S., Pandit, A., 2011a. Selective removal of phosphorus from wastewater combined with its recovery as a solid-phase fertilizer. Water Res. 45, 3318–30. doi:10.1016/j.watres.2011.03.044

Sengupta, S., Pandit, A., 2011b. Selective removal of phosphorus from wastewater combined with its recovery as a solid-phase fertilizer. Water Res. 45, 3318–3330. doi:10.1016/j.watres.2011.03.044

Smill, V., Streatfeild, R.A., 2002. Enriching the earth: Fritz Haber, Carl Bosch, and the transformation of world food production. Electron. Green J. doi:10.1353/tech.2002.0114

Smith, A.L., Stadler, L.B., Cao, L., Love, N.G., Raskin, L., Skerlos, S.J., 2014. Navigating Wastewater Energy Recovery Strategies: A Life Cycle Comparison of Anaerobic Membrane Bioreactor and Conventional Treatment Systems with Anaerobic Digestion. Environ. Sci. Technol. 48, 5972–5981. doi:10.1021/es5006169

Smith, G.A., Zaffurio, A.D., Zimmerman, M.L., Munch, D.J., 2010. Determination of Hormones in Drinking Water by Solids Phase Extraction (SPE)and Liquid Chromatography Electrospray Ionization Tandem Mass Spectrometry (LC-ESI-MS/MS).

Tolls, J., 2001. Sorption of veterinary pharmaceuticals in soils: a review. Environ. Sci. Technol. 35, 3397–3406.

Turel, I., 2002. The interactions of metal ions with quinolone antibacterial agents. Coord. Chem. Rev. 232, 27–47.

Underwood, J.C., Harvey, R.W., Metge, D.W., Repert, D.A., Baumgartner, L.K., Smith, R.L., Roane, T.M., Barber, L.B., 2011. Effects of the antimicrobial sulfamethoxazole on groundwater bacterial enrichment. Environ. Sci. Technol. 45, 3096–3101. doi:10.1021/es103605e

Vajda, A.M., Barber, L.B., Gray, J.L., Lopez, E.M., Woodling, J.D., Norris, D.O., 2008. Reproductive Disruption in Fish Downstream from an Estrogenic Wastewater Effluent. Environ. Sci. Technol. 42, 3407–3414. doi:10.1021/es0720661

Williams, A.T., Zitomer, D.H., Mayer, B.K., 2015. Ion exchange-precipitation for nutrient recovery from dilute wastewater. Environ. Sci. Water Res. Technol. 1, 832–838. doi:10.1039/C5EW00142K

Wisconsin DNR, 2010. Effluent Standards And Limitations For Phosphorus. US.

Zhao, D., Sengupta, A.K., 1998. Ultimate removal of phosphate from wastewater using a new class of polymeric ion exchangers. Water Res. 32, 1613–1625. doi:10.1016/S0043-1354(97)00371-0

4 ADSORPTION OF TRICLOSAN VIA BIOCHAR DERIVED FROM PYROLYSIS OF WASTEWATER BIOSOLIDS

This chapter was originally published as:

4.1   Introduction

Organic micropollutants including hormones, pharmaceuticals and personal care products, flame-retardants, artificial sweeteners, and antimicrobials, are widely used in consumer products. As population increases, so does use of these consumer products, which inevitably end up in wastewater treatment systems (Ridder, 2012). Water resource reclamation facilities (WRRFs) are major sources of organic micropollutant discharges into the environment (Servos et al., 2005). Many micropollutants are not degraded, or are slowly degraded, in conventional WRRFs (Rossi et al., 2013). Consequently, micropollutants are ubiquitous in natural waters and are increasingly detected in industrialized and remote environments (Schwarzenbach et al., 2006). Although they are found in waters at low concentrations (ng/L), micropollutants cause adverse ecological impacts such as feminization of fish (Kidd et al., 2007; Vajda et al., 2008).

Triclosan (TCS, structure shown in Appendix 4A) is an antimicrobial that is widely used for personal hygiene and disinfection products including oral care products, and lotion (Carey and Mcnamara, 2015), and is widely found in human urine and WRRF effluents (Pycke et al., 2014). While the FDA banned the use of TCS in handsoaps, it is still a key ingredient in one of the top-selling toothpastes (McNamara and Levy, 2016). Exposure to triclosan might also select for spread of antibiotic resistance, which is an emerging public health issue (Carey and McNamara, 2015; McNamara et al., 2014).

Conventional activated sludge processes are not designed to remove micropollutants, although a large fraction is removed in settling tanks due to adsorption to biosolids. The removal rate of triclosan via adsorption to biosolids can vary

substantially, ranging from 15% to 100% (Blair et al., 2013; Lozano et al., 2013; McAvoy et al., 2002; Singer et al., 2002). Even though a substantial fraction of triclosan may be removed with the solids, triclosan is still discharged into receiving waters. For example, Blair et al. (2013) detected 54 ng/L triclosan in WRRF effluent discharged to Lake Michigan. Advanced tertiary treatment techniques have been investigated for increased removal of micropollutants in WRRFs. Advanced oxidation, UV treatment, and membrane filtration can be effective techniques for micropollutant removal (Kimura et al., 2003). These methods can have high infrastructure and operational costs (Carballa et al., 2007; Manda et al., 2014). Activated carbon can also achieve substantial removal of a broad spectrum of micropollutants from water by adsorption (Margot et al., 2013), but activated carbon production and feedstock supply can give rise to high environmental impacts (Manda et al., 2014).

Alternative sorbents capable of effectively removing micropollutants are of interest to WRRFs. Biochar, which is the carbonaceous residual solid product produced by pyrolysis (a process that involves heating biomass in the absence of oxygen), may have potential as an effective, low-cost sorbent for the capture of micropollutants. Biochar can be produced using a wide range of biomass feedstock sources, including wood wastes, plant residuals and animal wastes (Cao and Harris, 2010; Ghani et al., 2013; Keiluweit et al., 2010). Biochar products have attracted increased attention in agronomy as a stable soil amendment to enhance soil fertility and plant growth (Carey et al., 2013; Gaunt and Lehmann, 2008). In addition to agronomy applications, biochar has been evaluated as a low-cost sorbent to capture inorganic and organic contaminants.

Biochar derived from pyrolysis of wood wastes has been applied for removal of inorganic contaminants from water. The maximum adsorption capacity was 4.25 mg/g and 7.51 mg/g for lead and chromium, respectively, which exceeds performance for some activated carbon (Liu and Zhang, 2009; Mohan et al., 2011). Biochar can also be utilized to retain nutrients. Yao et al. (2011) used biochar produced from sugar beet tailings to remove 73% phosphate from water. Carey et al. (2013) used biosolids-derived biochar to remove ammonium from water. The ammonium-saturated biochar subsequently improved growth of Kentucky Bluegrass.

In addition to removal of inorganic compounds, biochar produced from a wide range of feedstocks has also been found to adsorb organic contaminants such as catechol, humic acid, and endocrine disrupting chemicals (Jung et al., 2013; Kasozi et al., 2010). No research yet exists describing the use of wastewater biosolids-derived biochar to capture micropollutants. This waste-to-resource process would be implemented by pyrolyzing wastewater-derived biosolids to produce a readily renewable sorbent onsite. Furthermore, pyrolysis removes organic micropollutants such as triclosan from biochar (Ross et al., 2016), indicating that the biochar could be re-pyrolyzed to remove any sorbed micropollutants.

The objective of this research was to determine if biosolids-derived biochar could be used to adsorb triclosan, a pervasive micropollutant, in water and wastewater. Bench-scale batch tests were conducted to determine adsorption capacities under a range of physical conditions (pre-conditioning of biochar, solution pH, and pyrolysis temperature). Isotherm modeling and characterization of the biochar surface were performed to better understand the mechanism of interaction between triclosan and the biochar surface. It

was hypothesized that biosolids-derived biochar could remove triclosan via adsorption, and the surface properties of biochar changed with the increasing of pyrolysis temperature, therefore improving triclosan adsorption.

4.2   Materials and Methods

4.2.1   Biochar production and pre-conditioning for adsorption

Milorganite®, a heat-dried blend of anaerobically digested primary solids and waste activated sludge biosolids produced by the Milwaukee Metropolitan Sewage District (MMSD), was used as feedstock. The feedstock was pyrolyzed to produce biochar by placing 30 g of heat-dried biosolids in a 250 ml flask and purging with argon gas for 15 minutes. The flask opening was wrapped with aluminum foil and the flask was heated in a muffle furnace at 300°C, 500°C, 600°C, 700°C or 800°C for 60 minutes and cooled in a desiccator before conditioning.

All biochar was washed with Milli-Q® (Billerica, MA) water to remove residual surface impurities. To produce acid-treated biochar, 1N HCl was used to pretreat the biochar, while base-treated biochar was conditioned with 1N NaOH, both at dosages of 1 g biochar per 10 ml solution. The mixtures were agitated on a shaker table at 200 rpm for 12 hours. The biochar slurry was filtered with Whatman® (Ann Arbor, MI) 0.7 μm glass fiber filters via vacuum filtration, and the recovered biochar was rinsed with deionized water. The Milli-Q, acid, or base-conditioned biochar was dried at 90°C and stored in a desiccator prior to use in adsorption experiments.

4.2.2   Characterization of biochar properties

Scanning electron microscope (SEM) imaging - Granular biochar was dried and adhered on an SEM specimen mount with carbon tape. The surface morphology was observed via JEOL (JEOL USA, Inc. MA, USA) JSM-6510LV SEM at an accelerating voltage of 15 kV and ×1000 magnification.

Elemental, proximate, and surface area analysis - Biochar specific area was measured via a Brunauer-Emmett-Teller (BET) surface analysis instrument (NOVA 4200e, Quantachrome instruments, Boynton Beach, FL). Ash content is the inorganic residue left after dry oxidation (Sluiter et al., 2004). The carbon, nitrogen, hydrogen, and sulfur contents were analyzed via an ultimate analysis instrument (Vario Micro Cube, Elementar, Hanau, Germany). The oxygen content was calculated as the difference (Carey et al., 2013).

FT-IR analysis - A Nicolet™ 380 FTIR (Thermo Scientific, MA, USA) was used to investigate biochar surface functional groups. Method details are provided in Appendix 4D.

Zeta potential and point of zero charge (PZC) analysis - To determine the biochar's surface charge, which is potentially associated with the adsorption mechanism, zeta potentials were measured using a Malvern Zetasizer Nano ZS (Malvern Instruments Ltd, MA, USA). Method details are provided in Appendix 4E. Through interpolation, the PZC was determined as the pH where the zeta potential was equal to zero.

4.2.3   Adsorption tests

Batch adsorption tests were conducted to determine the adsorption capacity of triclosan on biochar. Glass serum bottles (60 mL) were silanized using 5% by volume dichlorodimethylsilane (99.5%, Sigma Aldrich, St. Louis, MO, USA) and 95% by volume heptane (99%, Sigma-Aldrich, St. Louis, MO, USA) solution to prevent chemicals from adsorbing onto the glass. Triclosan (97%, Sigma Aldrich, St. Louis, MO) was pre-dissolved in HPLC-grade methanol (99%, Sigma-Aldrich, St. Louis, MO, USA) for use as stock solution. The volumetric ratio of methanol stock to water was below 0.5% for all tests, which negates co-solvent effects (Schwarzenbach et al., 2005). All adsorption tests were conducted in triplicate in 50 mL of solution.

To determine the effect of pre-conditioning, triclosan stock solution was spiked to produce a final concentration of approximately 200 µg/L TCS in Milli-Q water. Acid (HCl), base (NaOH), or Milli-Q water-treated biochar (prepared at 600°C) was dosed at 0.4 g/L.

The impact of bulk solution pH on triclosan adsorption was tested using 0.4 g/L of 600°C HCl-treated biochar (selected based on previous pre-conditioning experiments). The pH of the Milli-Q water was adjusted to 3, 5, 7, 9, or 11 using HCl and NaOH. Triclosan was added at a concentration of approximately 300 µg/L for all pH experiments.

Adsorption isotherm experiments were conducted in serum bottles by spiking approximately 300 µg/L of TCS in Milli-Q water (initial pH approximately 6.5). Biochar pyrolyzed at different temperatures (300°C, 500°C, 600°C, 700°C and 800°C) was dosed at 0.2 g/L, 0.4 g/L, 0.6 g/L, 0.8 g/L, or 1g/L. Filtrasorb® 400 granular activated carbon

(GAC, Calgon Carbon, IL, USA) was used as a comparison to biochar adsorption performance.

A municipal secondary-treated wastewater effluent sample from Jones Island Water Reclamation Facility, Milwaukee, WI, was used to test triclosan adsorption to biochar in complex matrices. Water quality parameters including pH, chemical oxygen demand (COD), total organic carbon (TOC), turbidity, and total suspended solids (TSS) were measured according to standard methods (APHA et al., 1998), results of which are provided in Table 4G of Appendix 4G. Triclosan stock solution was injected into wastewater effluent at approximately 300 µg/L. Each bottle was dosed with 0.4 g/L of 600°C HCl biochar. To investigate the adhesion of triclosan to suspended solids, solutions injected with TCS without adding biochar were used as a control. The background triclosan concentration in the wastewater was below detection.

The serum bottle reactors were mixed end-over-end using a Cole-Parmer (IL, USA) Roto-Torque Variable Speed Rotator for 24 hours (which provided sufficient time to reach equilibrium, as determined by the kinetic tests described in Appendix 4B). Water samples were collected from the serum bottles and filtered with 0.45µm PTFE syringe filters (Agela Technologies, Wilmington, DE) prior to subsequent analysis.

4.2.4 Analysis of triclosan with liquid chromatography-mass spectrometry (LC-MS)

Aqueous-phase triclosan concentrations were measured with liquid chromatography-mass spectrometry (LCMS-2020, Shimadzu Corporation, MD, USA). Method details are provided in Appendix 4C. The triclosan quantification limit (based on a signal-to-noise ratio of 10:1) was 5 µg/L.

4.2.5   Adsorption calculations and statistical analysis

The adsorption capacity of triclosan on biochar (Q_e, µg TCS/g biochar) was

calculated using eq. 4.1:

$$Q_e = \frac{(C_0 - C_e) \times V}{M} \quad \text{eq. 4.1}$$

where C_0 is the initial concentration of triclosan (µg/L), C_e is the concentration at

equilibrium (µg/L), V is the volume of solution (mL), and M is the mass of the sorbent

(g).

Isotherm modeling (linear, Langmuir and Freundlich) and statistical analyses (t-

test and ANOVA, α level=5%) were performed using GraphPad Prism 6 (La Jolla. CA,

USA) software.

4.3   Results and Discussion

4.3.1   The impact of biochar preconditioning on adsorption performance

Preconditioning the biochar with HCl significantly enhanced triclosan adsorption

onto biochar relative to biochar preconditioned with NaOH or Milli-Q water (Figure 4.1;

ANOVA, $p = 0.0094$). The initial bulk solution pH was approximately 6.5, and it

decreased approximately 1 pH unit over the course of testing, likely due to the intrinsic

HCl-biochar surface acidity (Hossain et al., 2011; Singh et al., 2010). Based on these

data, acid pre-conditioning is necessary for biosolids-derived biochar to be effectively

used as a triclosan adsorbent.
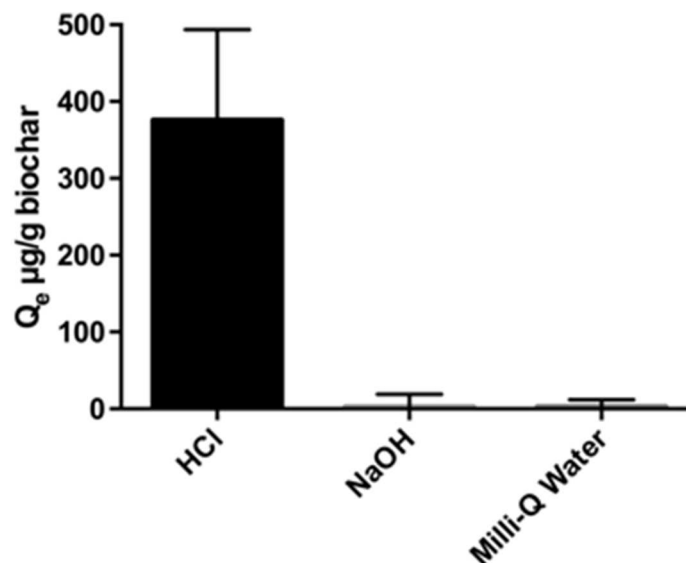
Figure 4.1 The effect of biochar pre-conditioning with 1 N HCl, 1 N NaOH or Milli-Q water on triclosan adsorption capacity, Q_e. Biochar was pyrolyzed at 600 °C, and added to water at a dose of 0.4 g/L. The water was spiked with 200 μg/L triclosan. The data represent average results and error bars show ±1 standard deviation of triplicate experiments.

There are several possible reasons why HCl pre-conditioning might enhance adsorption. As shown in the SEM images presented in Figure 4.2, HCl appeared to more effectively clean the biochar surface than the Milli-Q water or NaOH. Acid-treated biochar also appeared to have fewer granular impurities and be more porous than both base- and Milli-Q-conditioned biochar. These visual differences suggest that HCl-biochar may offer more surface area for adsorption reactions. Surface area analysis by BET verified that HCl substantially increased the specific surface area of the biochar, as shown in Table 4.1. The HCl-biochar specific surface area was an order of magnitude greater than Milli-Q-biochar. As shown in Figure 4.2B, the NaOH-treated biochar surface was smoother and had fewer pores than acid-treated biochar. Other researchers have observed that NaOH conditioning of activated carbon can decrease the specific surface area

because pores and cracks swell in the presence of aqueous base (Park and Jang, 2002;

Shim et al., 2001). For carbon-based adsorbents such as activated carbon and biochar, the

functionality as a sorbent is partially due to the highly porous surface of the solid and the

extremely high surface area to volume ratio (Wang et al., 2005).
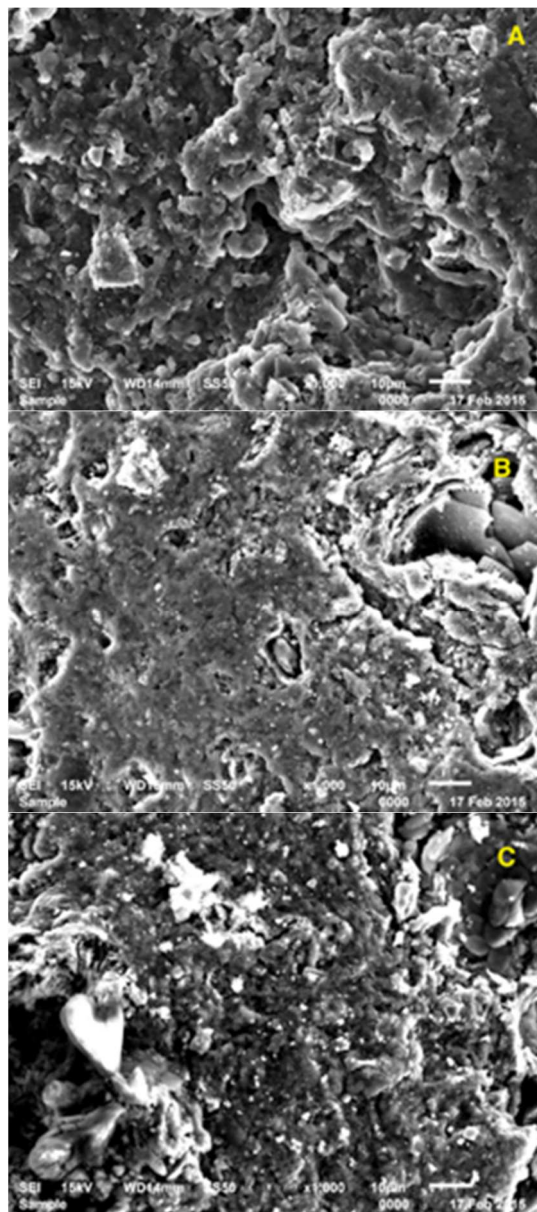
Figure 4.2 SEM images of biochar produced at 600ºC conditioned with A) 1N HCl, B) 1N NaOH, and C) Milli-Q water. Surface porosity and impurities vary with pre-conditioning.

Table 4.1 Proximate analysis and BET surface area data for biochar, activated carbon and heat-dried biosolids.

Sample name	C [%]	H [%]	N [%]	S [%]	O [%]	Fixed Carbon [%]	Volatiles [%]	Ash [%]	BET surface area [m^3/g]
600°C Milli-Q	30	1	4	0.8	4.2	16	24	60	21
600°C HCl	35	2	5	0.9	16.1	37	22	41	141
Activated Carbon	82	0.9	0.5	0.8	5.8	87	3	10	755
Heat-dried biosolids	37	5	7	1	24	8	67	26	1

In addition to specific surface area, the fraction of fixed carbon and ash content can influence adsorption. The ash content was lower in HCl-biochar than in Milli-Q-biochar (Table 4.1). The removal of ash during acid conditioning likely increased the porous carbon structure available for adsorption and increased the specific surface area. Thus, the cleaning and eroding effect of HCl conditioning makes it a suitable pre-conditioning step for enhancing the adsorption capacity of biochar.

Previous research has shown that the surface chemistry of carbon-based adsorbents can be altered using inorganic acid modification. On carbon-based adsorbents, HCl conditioning increased weak or strong acidic oxygen functional groups and single-bonded oxygen functional groups such as phenols, ethers and lactones (Chen and Wu, 2004; Dandekar et al., 1998). For Calgon Carbon® Filtrasorb® 400 activated carbon, conditioning with 2N HCl significantly affected functional group composition, as shown by FT-IR spectrum data indicating that the hydroxyl functional groups on the carbon were transformed into carboxylic, carbonyl, or ether groups after acid washing (Cañizares et al., 2006). These changes in surface chemistry enhanced phenol adsorption. Since the backbone structure and surface chemistry of HCl-biochar is similar to activated carbon, it

is likely that similar chemical behavior occurs on the surface of biochar following acid conditioning (Lehmann and Joseph, 2009; Sohi et al., 2010). Indeed, the FT-IR spectra (Appendix 4D, Figure 4D) shows differences among the three types of preconditioned biochar in this study. For HCl-treated biochar, the presence of broad bands at 1200 cm^{-1} and 600 cm^{-1} indicates that acid treatment increased carboxylic C-O bonds, such as phenol, and aromatic C-H bonds on the biochar surface. These shifts in chemical composition can alter H-bonding and π-interaction between the sorbent and solutes in water (Chen and Wu, 2004). The phenyl groups on triclosan molecules likely interact with phenol groups on HCl-biochar via hydrogen bonding, and aromatic groups on both adsorbate and adsorbent are able to form non-covalent π-π stacking (McGaughey et al., 1998), which supports the finding of increased adsorption on the HCl-biochar.

4.3.2   The impact of bulk solution pH on adsorption performance

Changes in adsorption as a function of bulk solution pH are important not only from a practical standpoint, i.e., near-neutral pH is preferable in water/wastewater applications to avoid drastic pH adjustments, but also from a mechanistic perspective. Exploring the relationship between pH and adsorption helps to understand which mechanisms of adsorption play major roles in removal, e.g., coulombic or non-coulombic interactions, which enable science-based process design and operation.

The bulk solution pH (tested from pH 3 to pH 11) significantly impacted the adsorption capacity of triclosan on biochar, as shown in Figure 4.3 (ANOVA, $p<0.0001$). While there was no statistical difference in adsorption capacity at pH 5, 7, and 9, the overall trend from pH 3 to 11 suggests that triclosan adsorption increased as pH dropped. Protonated triclosan molecules dominate as pH drops below 7.9 (pKa of triclosan), and

because they are more hydrophobic than the deprotonated anions, increased adsorption is likely to occur on the biochar at lower water pH. The triclosan adsorption capacity at pH 3 was greater than all other pH values ($p < 0.05$).
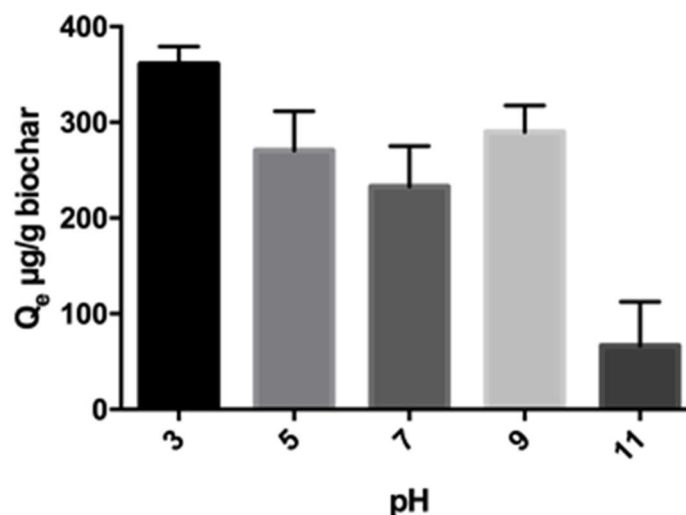
Figure 4.3 The impact of initial bulk solution pH on triclosan adsorption (Q_e) to biochar. The biochar was produced at 600°C and conditioned with 1N HCl. For all experiments, the initial nominal triclosan concentrations were approximately 300 µg/L and the biochar concentrations were 0.4 g/L. Error bars represent ±1 standard deviation of triplicate experiments.

The bulk solution pH also affects the surface charge of the biochar. The point of zero charge (PZC) is the pH at which the number of negative charges are exactly offset by the number of positive charges on the surface, i.e., the net surface charge is zero (Silber et al., 2010). When solution pH is above the PZC, the biochar surface will carry a net negative charge, thus repulsing anions. Zeta potential measurements of the biochar in this study indicate a PZC below 4, where the PZC was approximately 3.28 - 3.5, 3 - 3.28, and < 3 for 600°C HCl, NaOH, and Milli-Q-treated biochar, respectively (data shown in Appendix 4E). When the biochar surface is positively charged (pH < PZC), essentially no deprotonated triclosan is present. Thus, direct coulombic attraction cannot account for

increased adsorption at pH 3, and is unlikely to contribute to triclosan adsorption on biosolids-derived biochar.

Non-coulombic bonding may lend itself to triclosan adsorption as triclosan has both hydrogen donor and acceptor moieties, facilitating hydrogen bonding. As pH drops below the PZC, additional protonated functional groups may be present on the biochar surface, offering greater potential for hydrogen bonding, and perhaps contributing to the increase in triclosan adsorption at pH 3.

Enhanced triclosan adsorption at pH 3 may also be attributed to the increased ionic strength when adjusting the solution pH with HCl. When driven by coulombic attractions, the adsorption of organic compounds has been shown to increase with bulk solution ionic strength, potentially due to shrinkage or aggregation of sorbates (Aldegs et al., 2008; Campinas and Rosa, 2006; Delle Site, 2001). Although ionic strength impacts could also be relevant at high pHs due to NaOH addition, the strong electrostatic repulsion between the negatively charged biochar surface and the deprotonated triclosan and the relative increase in hydrophilicity of the protonated triclosan are likely to dominate, leading to decreased adsorption, as observed in Figure 4.3. The impact of ionic strength on triclosan adsorption should be investigated in future research.

When used for wastewater treatment applications, biosolids-derived biochar would most likely be used in near-neutral pH solutions. For practical usage, wastewater effluent pH is unlikely to be adjusted to acidic levels in order to achieve higher adsorption capacity, and it is possible that extreme acidic conditions might not be favorable for adsorption of other micropollutants. Accordingly, neutral pH is sufficient for practical use.

4.3.3   Isotherm modeling and the impact of pyrolysis temperature

The adsorption capacity as a function of equilibrium concentration was modeled using linear, Langmuir, and Freundlich isotherms, the complete results of which are shown in Table 4F in Appendix 4F. Overall, the Freundlich model provided the best fit, which suggests that many layers of triclosan may adsorb to the biochar surface (Schwarzenbach et al., 2005). With the exception of 300°C biochar, the K_f (adsorption affinity factor) generally increased while n (n is an indicator of distribution of binding energy on adsorbent surface—the more drastically the binding affinity changes across the adsorbent surface, the smaller the n value) decreased as pyrolysis temperature increased (Figure 4.4 and Table 4.2). These results suggest that triclosan adhesion to the biochar surface increases with pyrolysis temperature. Generally, for the same feedstock, as pyrolysis temperature increases, biochar will have higher residual carbon content and higher aromaticity, which strengthens the bonding between organic compounds and char surface (McGaughey et al., 1998; Newalkar et al., 2014). Biochar surface properties also varied with pyrolysis temperature, which was discussed in Appendix 4H. Changes in these biochar surface properties with pyrolysis temperature suggest that 800˚C biochar will experience stronger interaction and higher adsorption capacity, thus supporting the observed increase in triclosan adsorption.
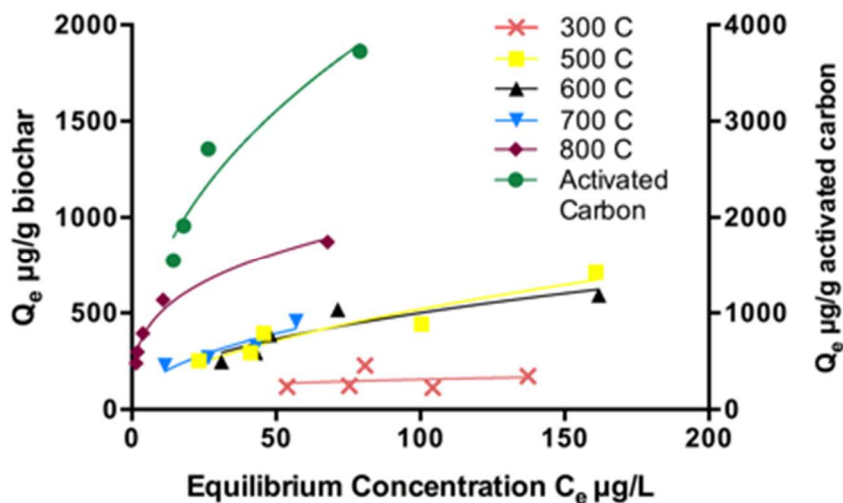
Figure 4.4 Comparison of triclosan adsorption isotherms using HCl-biochar pyrolyzed at varying temperatures and activated carbon. Isotherms are fit to the Freundlich model. Experiments are performed in triplicates and averages are shown. For readability, error bars are not shown

Table 4.2 Isotherms of HCl-biochar produced at multiple temperatures and activated carbon fitted with the Freundlich model.

Isotherm model	Equation	Parameter	Sorbent					
			300˚C	500˚C	600˚C	700˚C	800˚C	Activated carbon
Freundlich	$Q_e = K_f C_e^n$	K_f	56.5	43.2	62.0	62.9	254	554
		n	0.22	0.54	0.45	0.46	0.30	0.44
		R^2	0.06	0.91	0.84	0.85	0.98	0.93

Biochar acidity is also affected by pyrolysis temperature. Biochar produced at low temperature is usually acidic (Hossain et al., 2011; Singh et al., 2010). This can greatly affect biochar's ability to remove acidic organic molecules in the deprotonated form. While surface acidity is relevant in some scenarios, it is important to note that at neutral pH, the majority of triclosan molecules are protonated. Therefore, adsorption

mechanisms may rely more on hydrophobic interactions and partitioning, whereas biochar surface acidity could have less relative impact.

The adsorption behavior of activated carbon was similar to the 800˚C HCl-biochar (Figure 4.4). The Freundlich n value indicated that the bonding between the activated carbon and triclosan was weaker than the bonding between 800˚C biochar and triclosan, which could be attributed to the intrinsic difference between the different feedstocks. However, activated carbon offers greater triclosan adsorption capacity compared to all types of biochar tested. According to Table 4.1, activated carbon has a much lower ash content, higher carbon content, and higher BET surface area than biochar, which explains why commercialized activated carbon is a more effective adsorbent than the wastewater-derived biochar.

None of the isotherm models provided a good fit for the 300˚C biochar. Pyrolysis temperature can affect physical and chemical properties related to adsorption, resulting in differences in the biochar's triclosan adsorption capacity. The poor isotherm fits for the 300˚C biochar may be due to the lack of sorption caused by heterogeneity or low specific surface area (3.87 m^2/g). Volatiles, such as py-oil, might be present at higher levels in biochar pyrolyzed at lower temperatures and may clog pores, thereby limiting available sorption sites. For 300˚C HCl-biochar, there was no change in capacity as equilibrium concentration increased. Thus, the adsorption sites on the 300˚C HCl-biochar were likely initially saturated with residual organic matter, thereby severely limiting the triclosan adsorption capacity. This suggests that pyrolysis temperatures above 300˚C are needed to produce biochar for use as a micropollutant adsorbent.

4.3.4   Adsorption performance using low chemical concentrations

While activated carbon has higher adsorption capacity compared to biochars at high equilibrium concentrations, it does not differ significantly from the biochars at low equilibrium concentrations (ANOVA, p=0.0748). Figure 4.4 shows that at lower equilibrium concentrations, the isotherms appear to converge, which indicates that similar capacities may be observed for all of the biochars as well as activated carbon. Although testing with high triclosan concentrations in Milli-Q water gives an idea of the influence of solution pH and pyrolysis temperature on adsorption mechanisms, concentrations in actual WRRF effluents would likely be in the range of 0.02 µg/L to 20 µg/L (Foran et al., 2000; Ying and Kookana, 2007). As shown in Figure 4.5, when an initial concentration of approximately 20 µg/L triclosan was used, there was no significant difference between adsorption capacity of the HCl-biochars produced at 300-800˚C or activated carbon (ANOVA, p=0.07). This result is significant in that for practical use at environmental levels of triclosan, biochar produced on-site at lower temperatures could perform as well as activated carbon.
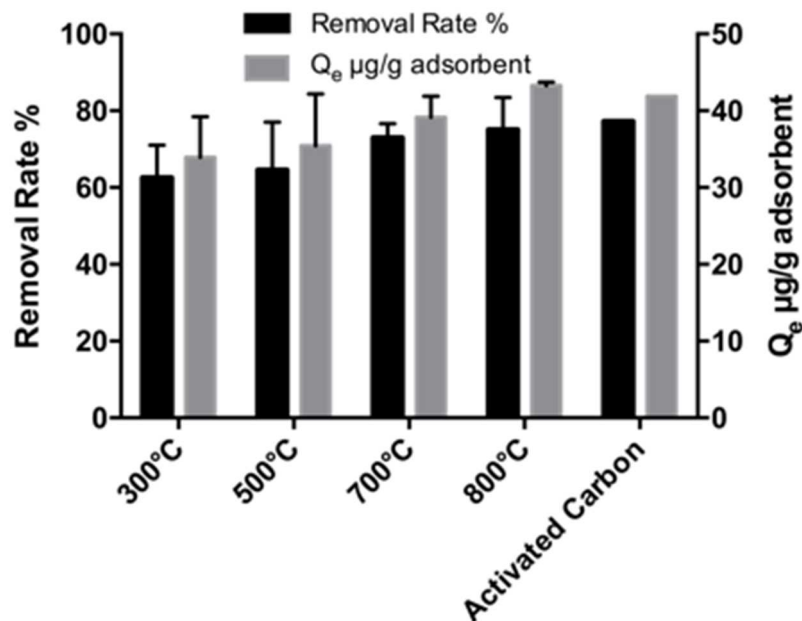
Figure 4.5 Comparison of adsorption capacities of HCl-biochar pyrolyzed at 300°C, 500°C, 700°C, and 800°C, and activated carbon. Triclosan was spiked at 20 µg/L, and the solution pH was 7. Error bars represent standard deviation of triplicate experiments.

4.3.5   Triclosan adsorption on biochar in treated secondary effluent

Acid-treated biochar was tested in secondary treated municipal wastewater effluent to investigate the feasibility of triclosan adsorption in a complex matrix. For the same amounts of sorbent and triclosan, the triclosan removal rate decreased from $70\pm10\%$ in Milli-Q water to $32\pm5.0\%$ in wastewater effluent. The triclosan adsorption capacity in wastewater effluent was 239 ± 42 µg/g biochar, as compared to 518 ± 49 µg/g biochar in Milli-Q water (Figure 4.4). The suppression effect of the wastewater matrix was expected due to the co-existence of TSS and organic constituents, which were present in higher concentrations relative to the triclosan (Appendix 4G, Table 4G). In control experiments where no biochar was added, triclosan concentrations were similar before and after the experiment, indicating minimal adsorption to the wastewater solids.

It is likely that the organic matter in the wastewater sorbed to the biochar and reduced available sites for triclosan to sorb on the biochar. Future work should focus on developing a mechanistic understanding of adsorption competition due to complex wastewater matrices, thereby providing a means to improve the selectivity of biochar for target micropollutants.

4.4   Conclusions

This work demonstrated that acid-conditioned (HCl) biosolids-derived biochar could be a suitable alternative to activated carbon for removing triclosan, a pervasive micropollutant, from water at near-neutral pH. Preconditioning of the biochar using acid was essential for triclosan adsorption. One practical limitation of using HCl to condition the biochar as a sorbent may be the cost of chemical inputs. Pyrolysis temperature of biosolids has an influence on the biochar's physical properties, such as pore radius, pore volume and surface area. The hypothesis of increasing pyrolysis temperature improving triclosan adsorption matches the result. While acid preconditioning was necessary for triclosan adsorption, high pyrolysis temperatures do not appear to be necessary for production considering the low triclosan concentrations commonly encountered in environmental applications.

Biochar characterization indicated that adsorption may occur mainly due to high surface area, hydrophobicity, and potential interaction between biochar and triclosan functional groups including hydrogen bonding and π-stacking. This research indicated that biosolids-derived biochar is a suitable sorbent for hydrophobic, neutral organic micropollutants. Additional research should be conducted to evaluate biosolids-derived

biochar as a sorbent for other compounds with varied hydrophobicity and cationic

compounds.

4.5   References

Aldegs, Y., Elbarghouthi, M., Elsheikh, A., Walker, G., 2008. Effect of solution pH, ionic strength, and temperature on adsorption behavior of reactive dyes on activated carbon. Dye. Pigment. 77, 16–23. doi:10.1016/j.dyepig.2007.03.001

APHA, AWWA, WEF, 1998. Standard methods for the examination of water and wastewater, Standard Methods for the Examination of Water and Wastewater.

Blair, B.D., Crago, J.P., Hedman, C.J., Treguer, R.J.F., Magruder, C., Royer, L.S., Klaper, R.D., 2013. Evaluation of a model for the removal of pharmaceuticals, personal care products, and hormones from wastewater. Sci. Total Environ. 444, 515–21. doi:10.1016/j.scitotenv.2012.11.103

Campinas, M., Rosa, M.J., 2006. The ionic strength effect on microcystin and natural organic matter surrogate adsorption onto PAC. J. Colloid Interface Sci. 299, 520–9. doi:10.1016/j.jcis.2006.02.042

Cañizares, P., Carmona, M., Baraza, O., Delgado, A., Rodrigo, M.A., 2006. Adsorption equilibrium of phenol onto chemically modified activated carbon F400. J. Hazard. Mater. 131, 243–8. doi:10.1016/j.jhazmat.2005.09.037

Cao, X., Harris, W., 2010. Properties of dairy-manure-derived biochar pertinent to its potential use in remediation. Bioresour. Technol. 101, 5222–8. doi:10.1016/j.biortech.2010.02.052

Carballa, M., Omil, F., Ternes, T., Lema, J.M., 2007. Fate of pharmaceutical and personal care products (PPCPs) during anaerobic digestion of sewage sludge. Water Res. 41, 2139–2150. doi:10.1016/j.watres.2007.02.012

Carey, D.E., Mcnamara, P.J., 2015. The impact of triclosan on the spread of antibiotic resistance in the environment   . Front. Microbiol.   .

Carey, D.E., McNamara, P.J., Zitomer, D.H., 2013. Biosolid Derived Biochar to Immobilize and Recycle Ammonium from Wastewater for Agronomy, in: Proceeding of the Water Environment Federation. Water Environment Federation, pp. 107–120.

Chen, J.P., Wu, 2004. Acid/Base-Treated Activated Carbons: Characterization of Functional Groups and Metal Adsorptive Properties. Langmuir 20, 2233–2242. doi:10.1021/la0348463

Dandekar, A., Baker, R.T.K., Vannice, M.A., 1998. Characterization of activated carbon, graphitized carbon fibers and synthetic diamond powder using TPD and DRIFTS. Carbon N. Y. 36, 1821–1831. doi:10.1016/S0008-6223(98)00154-7

Delle Site, A., 2001. Factors affecting sorption of organic compounds in natural sorbent/water systems and sorption coefficients for selected pollutants. A review. J. Phys. Chem. Ref. Data 30, 187–439. doi:10.1063/1.1347984

Foran, C.M., Bennett, E.R., Benson, W.H., 2000. Developmental evaluation of a potential non-steroidal estrogen: Triclosan. Mar. Environ. Res. 50, 153–156. doi:10.1016/S0141-1136(00)00080-5

Gaunt, J.L., Lehmann, J., 2008. Energy Balance and Emissions Associated with Biochar Sequestration and Pyrolysis Bioenergy Production. Environ. Sci. Technol. 42, 4152–4158. doi:10.1021/es071361i

Ghani, W.A.W.A.K., Mohd, A., da Silva, G., Bachmann, R.T., Taufiq-Yap, Y.H., Rashid, U., Al-Muhtaseb, A.H., 2013. Biochar production from waste rubber-wood-sawdust and its potential use in C sequestration: Chemical and physical characterization. Ind. Crops Prod. 44, 18–24. doi:10.1016/j.indcrop.2012.10.017

Heidler, J., Halden, R.U., 2007. Mass balance assessment of triclosan removal during conventional sewage treatment. Chemosphere 66, 362–369.

Hossain, M.K., Strezov, V., Chan, K.Y., Ziolkowski, A., Nelson, P.F., 2011. Influence of pyrolysis temperature on production and nutrient properties of wastewater sludge biochar. J. Environ. Manage. 92, 223–228. doi:10.1016/j.jenvman.2010.09.008

Jung, C., Park, J., Lim, K.H., Park, S., Heo, J., Her, N., Oh, J., Yun, S., Yoon, Y., 2013. Adsorption of selected endocrine disrupting compounds and pharmaceuticals on activated biochars. J. Hazard. Mater. 263 Pt 2, 702–10. doi:10.1016/j.jhazmat.2013.10.033

Kasozi, G.N., Zimmerman, A.R., Nkedi-Kizza, P., Gao, B., 2010. Catechol and humic acid sorption onto a range of laboratory-produced black carbons (biochars). Environ. Sci. Technol. 44, 6189–6195. doi:10.1021/es1014423

Keiluweit, M., Nico, P.S., Johnson, M.G., Kleber, M., 2010. Dynamic Molecular Structure of Plant Biomass-Derived Black Carbon (Biochar). Environ. Sci. Technol. 44, 1247–1253. doi:10.1021/es9031419

Kidd, K.A., Blanchfield, P.J., Mills, K.H., Palace, V.P., Evans, R.E., Lazorchak, J.M., Flick, R.W., 2007. Collapse of a fish population after exposure to a synthetic estrogen. Proc. Natl. Acad. Sci. U. S. A. 104, 8897–8901. doi:10.1073/pnas.0609568104

Kimura, K., Amy, G., Drewes, J.E., Heberer, T., Kim, T.-U., Watanabe, Y., 2003. Rejection of organic micropollutants (disinfection by-products, endocrine disrupting

compounds, and pharmaceutically active compounds) by NF/RO membranes. J. Memb. Sci. 227, 113–121. doi:10.1016/j.memsci.2003.09.005

Lehmann, J., Joseph, S., 2009. Biochar for Environmental Management, Science And Technology. Earthcan.

Liu, Z., Zhang, F.-S., 2009. Removal of lead from water using biochars prepared from hydrothermal liquefaction of biomass. J. Hazard. Mater. 167, 933–9. doi:10.1016/j.jhazmat.2009.01.085

Lozano, N., Rice, C.P., Ramirez, M., Torrents, A., 2013. Fate of Triclocarban, Triclosan and Methyltriclosan during wastewater and biosolids treatment processes. Water Res. 47, 4519–27. doi:10.1016/j.watres.2013.05.015

Lu, G.Q., Low, J.C.F., Liu, C.Y., Lua, A.C., 1995. Surface area development of sewage sludge during pyrolysis. Fuel 74, 344–348. doi:10.1016/0016-2361(95)93465-P

Manda, B.M.K., Worrell, E., Patel, M.K., 2014. Innovative membrane filtration system for micropollutant removal from drinking water – prospective environmental LCA and its integration in business decisions. J. Clean. Prod. 72, 153–166. doi:10.1016/j.jclepro.2014.02.045

Margot, J., Kienle, C., Magnet, A., Weil, M., Rossi, L., de Alencastro, L.F., Abegglen, C., Thonney, D., Chèvre, N., Schärer, M., Barry, D.A., 2013. Treatment of micropollutants in municipal wastewater: ozone or powdered activated carbon? Sci. Total Environ. 461–462, 480–98. doi:10.1016/j.scitotenv.2013.05.034

McAvoy, D.C., Schatowitz, B., Jacob, M., Hauk, A., Eckhoff, W.S., 2002. Measurement of triclosan in wastewater treatment systems. Environ. Toxicol. Chem. 21, 1323–1329. doi:10.1002/etc.5620210701

McGaughey, G.B., Gagné, M., Rappé, A.K., 1998. π-Stacking interactions. Alive and well in proteins. J. Biol. Chem. 273, 15458–15463. doi:10.1074/jbc.273.25.15458

McNamara, P.J., Lapara, T.M., Novak, P.J., 2014. The impacts of triclosan on anaerobic community structures, function, and antimicrobial resistance. Environ. Sci. Technol. 48, 7393–7400. doi:10.1021/es501388v

McNamara, P.J., Levy, S.B., 2016. Triclosan: an instructive tale. Antimicrob. Agents. Chemother. 60, 7015-7016. oid: 10.1128/AAC.02105-16

Mohan, D., Rajput, S., Singh, V.K., Steele, P.H., Pittman, C.U., 2011. Modeling and evaluation of chromium remediation from water using low cost bio-char, a green adsorbent. J. Hazard. Mater. 188, 319–33. doi:10.1016/j.jhazmat.2011.01.127

Newalkar, G., Iisa, K., D'Amico, A.D., Sievers, C., Agrawal, P., 2014. Effect of Temperature, Pressure, and Residence Time on Pyrolysis of Pine in an Entrained Flow Reactor. Energy & Fuels 28, 5144–5157. doi:10.1021/ef5009715

Park, S.-J., Jang, Y.-S., 2002. Pore structure and surface properties of chemically modified activated carbons for adsorption mechanism and rate of Cr(VI). J. Colloid Interface Sci. 249, 458–63. doi:10.1006/jcis.2002.8269

Pycke, B.F.G., Geer, L.A., Dalloul, M., Abulafia, O., Jenck, A.M., Halden, R.U., 2014. Human fetal exposure to triclosan and triclocarban in an urban population from Brooklyn, New York. Environ. Sci. Technol. 48, 8831–8838.

Ridder, D.J. De, 2012. Adsorption of organic micropollutants onto activated carbon and zeolites.

Ross, J.J., Zitomer, D.H., Miller, T.R., Weirich, C.A., McNamara, P.J., 2016. Emerging investigators series: pyrolysis removes common microconstituents triclocarban, triclosan, and nonylphenol from biosolids. Environ. Sci. Water Res. Technol. doi:10.1039/C5EW00229J

Rossi, L., Queloz, P., Brovelli, A., Margot, J., Barry, D.A., 2013. Enhancement of Micropollutant Degradation at the Outlet of Small Wastewater Treatment Plants. PLoS One 8. doi:10.1371/journal.pone.0058864

Schwarzenbach, R.P., Escher, B.I., Fenner, K., Hofstetter, T.B., Johnson, C.A., von Gunten, U., Wehrli, B., 2006. The challenge of micropollutants in aquatic systems. Science 313, 1072–1077. doi:10.1126/science.1127291

Schwarzenbach, R.P., Gschwend, P.M., Imboden, D.M., 2005. Environmental organic chemistry. John Wiley & Sons.

Servos, M.R., Bennie, D.T., Burnison, B.K., Jurkovic, A., McInnis, R., Neheli, T., Schnell, A., Seto, P., Smyth, S.A., Ternes, T.A., 2005. Distribution of estrogens, 17β-estradiol and estrone, in Canadian municipal wastewater treatment plants. Sci. Total Environ. 336, 155–170. doi:10.1016/j.scitotenv.2004.05.025

Shim, J.-W., Park, S.-J., Ryu, S.-K., 2001. Effect of modification with HNO3 and NaOH on metal adsorption by pitch-based activated carbon fibers. Carbon N. Y. 39, 1635–1642. doi:10.1016/S0008-6223(00)00290-6

Silber, A., Levkovitch, I., Graber, E.R., 2010. pH-Dependent Mineral Release and Surface Properties of Cornstraw Biochar: Agronomic Implications. Environ. Sci. Technol. 44, 9318–9323. doi:10.1021/es101283d

Singer, H., Müller, S., Tixier, C., Pillonel, L., 2002. Triclosan: Occurrence and Fate of a Widely Used Biocide in the Aquatic Environment: Field Measurements in Wastewater Treatment Plants, Surface Waters, and Lake Sediments. Environ. Sci. Technol. 36, 4998–5004. doi:10.1021/es025750i

Singh, B., Singh, B.P., Cowie, A.L., 2010. Characterisation and evaluation of biochars for their application as a soil amendment. Soil Res.

Sluiter, A., Hames, B., Ruiz, R.O., Scarlata, C., Sluiter, J., Templeton, D., Energy, D. of, 2004. Determination of Ash in Biomass. Biomass Anal. Technol. Team Lab. Anal. Proced. 1–6. doi:TP-510-42622

Sohi, S.P., Krull, E., Lopez-Capel, E., Bol, R., 2010. A review of biochar and its use and function in soil, Advances in Agronomy. doi:10.1016/S0065-2113(10)05002-9

Vajda, A.M., Barber, L.B., Gray, J.L., Lopez, E.M., Woodling, J.D., Norris, D.O., 2008. Reproductive Disruption in Fish Downstream from an Estrogenic Wastewater Effluent. Environ. Sci. Technol. 42, 3407–3414. doi:10.1021/es0720661

Wang, S., Zhu, Z.H., Coomes, A., Haghseresht, F., Lu, G.Q., 2005. The physical and surface chemical characteristics of activated carbons and the adsorption of methylene blue from wastewater. J. Colloid Interface Sci. 284, 440–6. doi:10.1016/j.jcis.2004.10.050

Yao, Y., Gao, B., Inyang, M., Zimmerman, A.R., Cao, X., Pullammanappallil, P., Yang, L., 2011. Biochar derived from anaerobically digested sugar beet tailings: characterization and phosphate removal potential. Bioresour. Technol. 102, 6273–8. doi:10.1016/j.biortech.2011.03.006

Ying, G.-G., Kookana, R.S., 2007. Triclosan in wastewaters and biosolids from Australian wastewater treatment plants. Environ. Int. 33, 199–205. doi:10.1016/j.envint.2006.09.008

5 ESTIMATION OF THERMODYNAMIC PROFILES FOR ADSORPTION OF ORGANIC MICROPOLLUTANTS TO BIOSOLIDS-DERIVED BIOCHAR

5.1   Introduction

Increasing world population and anthropogenic activities generate more severe water utilization problems, including scarcity of freshwater resources and the threat of emerging contaminants to water quality. Organic micropollutants, including pharmaceuticals, hormones, antimicrobials, etc. that are discharged into natural and engineered systems are among those emerging contaminants. Low concentrations (ng/L to μg/L) of organic micropollutants in the environment do not pose acute toxicity, but the long-term impact can disturb aquatic ecological balance (Vajda et al., 2011). They may also induce antibiotic resistance in bacteria in natural and engineered environments (Carey et al., 2016; Schwarzenbach et al., 2006), which may potentially pose human health risks. One of the major sources of organic micropollutants is municipal WRRF discharge (Blair et al., 2013; Phillips et al., 2012; Servos et al., 2005) due to the lack of complete removal in conventional biological wastewater treatment processes.

The adsorptive behavior of organic micropollutants on solid materials can facilitate their removal from wastewater. One such practice is the use of solid adsorbents as a tertiary polishing step to remove organic micropollutants. Compared to advanced oxidation, UV treatment, and reverse osmosis, removal of micropollutants via adsorption through a packed filter bed can have lower capital and operating costs (Carballa et al., 2007; Manda et al., 2014). Biochar (pyrolyzed carbonaceous material) has demonstrated an ability to retain organic micropollutants via adsorption, giving it the potential to serve as an alternative adsorbent to commercial activated carbon for wastewater treatment (Ahmad et al., 2013; Jung et al., 2013; Wang et al., 2015). Using the biosolids produced during wastewater treatment as the feedstock to produce biochar for use as an adsorbent

has inherent advantages for WRRF due to on-site accessibility and the necessity of waste disposal.

To better understand the effectiveness of adsorption, quantitative methods to characterize adsorption equilibrium, including isotherms and thermodynamic profiles, are needed. Isotherm equations predict adsorption capacities on solid phases at different equilibrium aqueous-phase concentrations at a constant temperature. The distribution constant, K, in isotherm expressions (such as K_L for the Langmuir isotherm model and K_f for the Freundlich isotherm model) is susceptible to change when the temperature changes, as described by the thermodynamic equilibrium constant (K_c=exp (-ΔG^0/RT)). This underlying thermodynamic basis for isotherm modeling enables experimental derivation of critical thermodynamic parameters of adsorption, including isosteric heat, standard enthalpy, entropy and free energy change of adsorption.

Isosteric heat of adsorption is the differential heat of adsorption at a fixed surface loading (or adsorption capacity) at equilibrium. Variation in isosteric heat with surface loading indicates surface energy heterogeneity. Changes in enthalpy (ΔH) provide information regarding the adsorption mechanism. For weak intermolecular forces (e.g., H-bonding or π-interactions), the change in enthalpy is much less than that for stronger chemical adsorption (which is usually on the order of hundreds of kJ/mol) (Chowdhury et al., 2011; Thomas, 1961), wherein covalent bonds are formed. The thermodynamic parameters were estimated in some research that used plant-derived biochars (Lian et al., 2014; Mahmoud et al., 2012; Vithanage et al., 2016). For example, Vithanage et al (2016) reported that for carbofuran's adsorption on tea waste-biochar, the negative total free energy change reflected that adsorption did not need external energy input. The enthalpy

change was -46 kJ/mol, indicating the exothermic nature of the adsorption and weak physical interaction. However, little is known about the thermodynamic profile for micropollutant adsorption to biosolids-derived biochar. Knowledge of adsorption thermodynamic parameters briefly provide insight into the spontaneity of adsorption, the adsorption mechanisms, and the adsorbent surface properties.

The objective of this research was to generate thermodynamic adsorption profiles for a suite of micropollutants onto biosolids-derived biochar to assist in characterizing the spontaneity of adsorption, the adsorption mechanisms, and the adsorbent binding affinity for the target micropollutants. Bench-scale batch experiments were conducted to address the following specific research objectives: 1) assess the impact of reaction temperature on biochar adsorption, 2) ascertain the thermodynamic profile of biochar adsorbing a suite of micropollutants through experimental approaches, and 3) evaluate the impact of competitive adsorption on micropollutant adsorption. The micropollutants selected for this study were carbamazepine (CBZ), 17β-estradiol (E2), 17α-ethinylestradiol (EE2) and triclosan (TCS), all of which are frequently detected in treated wastewater effluents (Blair et al., 2013; Monsalvo et al., 2014). In circumneutral pH wastewater, these contaminants are neutral molecules with varied hydrophobicity. Benzyldimethylammonium chloride (BAC-C10), which is an organic quaternary ammonium salt, was also studied as a representative cationic micropollutant. It was hypothesized that 1) biosolids-derived biochar could adsorb neutral and cationic micropollutants; 2) increasing temperature positively impacts biosolids-derived biochar adsorption capacity; 3) the adsorption capacity, binding affinity and entropy change have positive correlations with micropollutant polarity and hydrophobicity; and 4) competitive

adsorption will decrease adsorption of each individual micropollutant, but the competition will not alter binding affinity and entropy change.

5.2   Materials and Methods

5.2.1   Biosolids-derived biochar production and pre-conditioning

A heat-dried blend of anaerobically digested primary solids and waste activated sludge produced by the Milwaukee Metropolitan Sewage District (MMSD) in Milwaukee, WI, was used as pyrolysis feedstock. The feedstock was pyrolyzed to produce biochar in accordance with the method specified in **Chapter 3**: heating to 600 °C, followed by HCl acid conditioning to reduce ash and increase surface area, as shown in **Chapter 4**. The dried biochar particles were sieved (No. 16 in mesh) to approximately 1.36 mm in diameter for use in subsequent adsorption experiments.

5.2.2   Adsorption batch experiments

Benzyldimethyldecylammonium chloride (BAC-C10, 97%, Sigma Aldrich, St. Louis, MO), carbamazepine (CBZ, 97%, Sigma Aldrich, St. Louis, MO), 17β-estradiol (E2, 97%, Sigma Aldrich, St. Louis, MO), 17α-ethynylestradiol (EE2, 97%, Sigma Aldrich, St. Louis, MO) and triclosan (TCS, 97%, Sigma Aldrich, St. Louis, MO) were pre-dissolved in HPLC-grade methanol for use as feedstock solutions. Feedstock solutions were prepared by adding each micropollutant individually (or as a mixture of all micropollutants for multi-solute experiments) into Milli-Q water to achieve an approximate concentration of 1000±100 µg/L of each micropollutant. The volumetric

ratio of methanol stock to water was below 0.5% to negate co-solvent effects
(Schwarzenbach et al., 2005). Water pH was adjusted to 7 using HCl and NaOH.

Triplicate batch adsorption tests were conducted in silanized 50 mL serum bottles
to develop isotherms for the target micropollutants at a range of temperatures. The
experimental temperature was maintained at 4, 25, 35 or 50˚C (277, 298, 308 or 323 K).
Biosolids-derived biochar was dosed at 0.12 g/L, 0.2 g/L, 0.8 g/L, 2 g/L, or 2.4 g/L to
produce each set of isotherms. The serum bottle reactors were mixed end-over-end using
a Cole-Parmer (IL, USA) Roto-Torque Variable Speed Rotator. The bottles were mixed
for 48 hours to provide sufficient time to reach equilibrium, in accordance with **Chapter
4**. Water samples were collected from the serum bottles and filtered using 0.45 µm PTFE
syringe filters (Agela Technologies, Wilmington, DE) prior to subsequent micropollutant
analysis using a Shimadzu LC-MS-2020 (method details are provided in Appendix 5A).

5.2.3   Data analysis

The adsorption capacity of each micropollutant on biochar (Q_e, µg/g biochar or
mol/g biochar) was calculated using eq. 5.1:

$$Q_e = \frac{(C_0 - C_e) \times V}{M} \quad \text{eq. 5.1}$$

where C_0 is the initial concentration of micropollutant (µg/L), C_e is the
concentration at equilibrium (µg/L or mol/L), V is the volume of solution (L), and M is
the mass of the adsorbent (g). The Q_e and C_e values were used to fit isotherm curves.

Isotherms were developed to estimate thermodynamic parameters of
micropollutant adsorption on the biochar. The isosteric heat of adsorption (ΔH_{st}) for a

given surface loading, Q_e, was derived from the Clausius-Clapeyron equation (eq. 5.2) using a plot of $\ln(C_e)$ versus $1/T$ to obtain the slope:

$$\Delta H_{st} = R \left.\frac{d(lnC_e)}{d(1/T)}\right|_{Q_e} \text{ eq. 5.2}$$

where ΔH_{st} is the isosteric heat of adsorption (kJ/mol), R is the ideal gas constant (J/mol·K), C_e is the aqueous-phase concentration at equilibrium (mol/L) and T is temperature (K). One linear curve is also denoted as an isostere.

The enthalpy (ΔH^0) and entropy change (ΔS^0) of adsorption were estimated using the van't Hoff equation, as shown in eq. 5.3:

$$lnK_c = -\frac{\Delta H^0}{RT} + \frac{\Delta S^0}{R} \text{ eq. 5.3}$$

where K_c is the thermodynamic equilibrium constant, which is related to, but not exactly the same as, the isotherm constant, K (Tran et al., 2017). eq. 5.4 can be used to derive K_c from the Freundlich constant, K_f:

$$K_c = \frac{K_f\rho}{1000}\left(\frac{10^6}{\rho}\right)^{1-n} \text{eq. 5.4}$$

where n is a Freundlich constant, and ρ is the density of pure water (1 g/mL) (Ghosal and Gupta, 2015). The thermodynamic constant K_c can be obtained from linear isotherm constant K (L/g) by a factor of 1,000 g/L (Milonjić, 2007). A linear curve can be obtained by plotting $\ln(K_c)$ versus $1/T$. The enthalpy change can be estimated from the slope, and the entropy change can be estimated from the y-axis intercept (eq. 5.3).

The free energy change of adsorption (ΔG^0) was estimated using eq. 5.5:

$$\Delta G^0 = -RTlnK_C \text{ eq. 5.5}$$

Linear regression, correlation, non-linear fitting and significance of difference analysis were performed using GraphPad Prism 6 (La Jolla, CA, USA).

5.3   Results and Discussion

5.3.1   Single-solute adsorption equilibrium and the impact of temperature

The adsorption capacity (or surface loading, Q_e) versus equilibrium concentration in a single-solute aqueous phase for the target compounds was fit to the commonly used Freundlich, Langmuir and linear isotherms for trace amount micropollutant adsorption. The BAC-C10, CBZ, and EE2 isotherms showed strong linearity (low n values) (Figure 5.1, Appendix 5B, Table 5B). The E2 and TCS isotherms demonstrated non-linear adsorption; therefore, only the Freundlich and Langmuir isotherms were compared for adsorption equilibrium of these two compounds. In general, the Freundlich isotherm has higher R^2 values, therefore, it provides a better fit than the Langmuir isotherm.
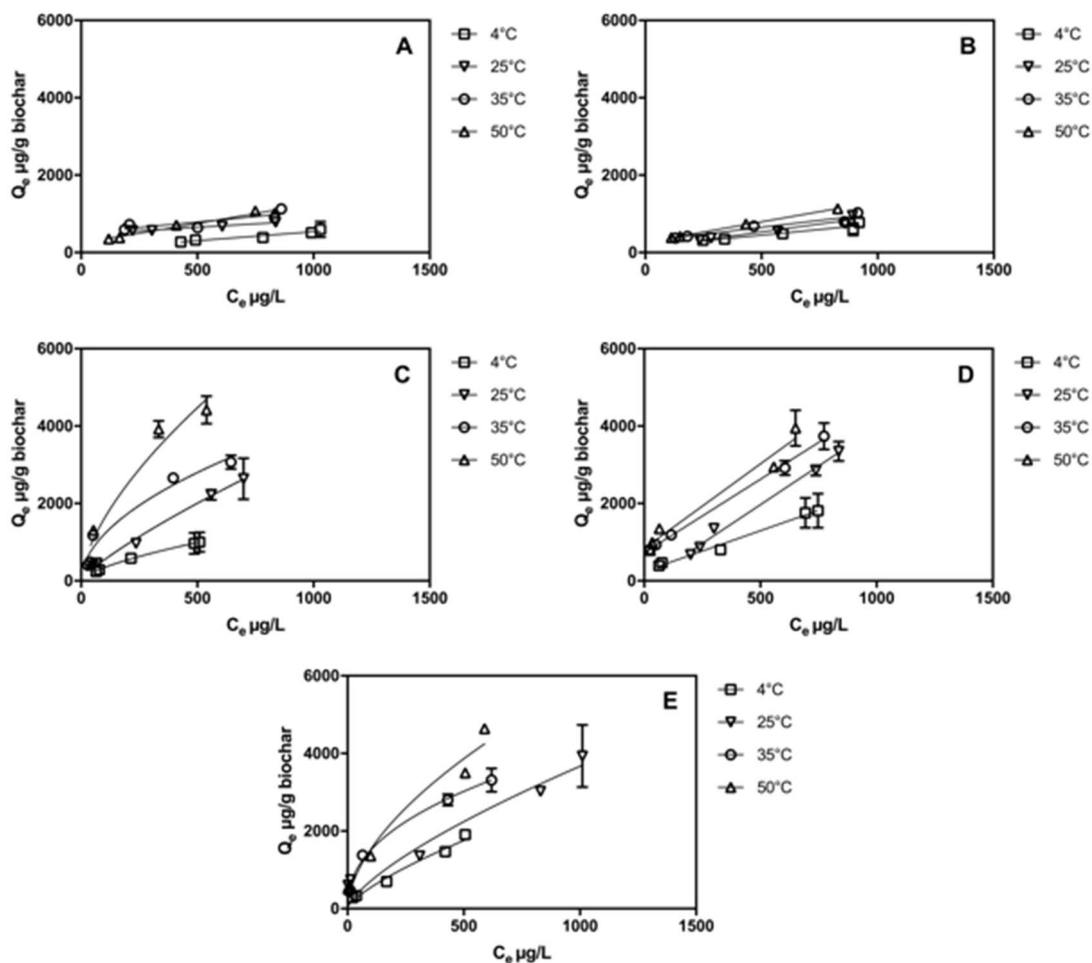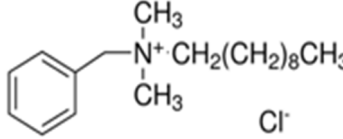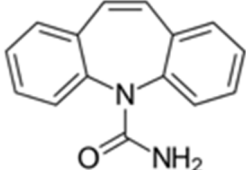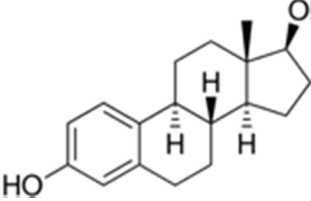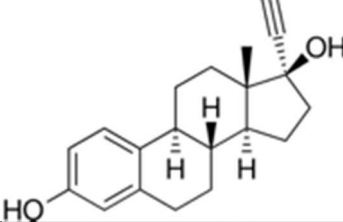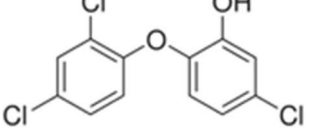
Figure 5.1 Adsorption isotherms for A) BAC-C10, B) CBZ, C) E2, D) EE2, and E) TCS at 4, 25, 35, and 50˚C (277, 298, 308 and 323 K, respectively). The adsorption equilibrium of each compound was obtained in a single-solute batch-mode adsorption system. The data represent average results and error bars show ±1 standard deviation of triplicate experiments. Some error bars are small and not visible.

For the aqueous-phase concentration range tested, BAC-C10 and CBZ had much lower equilibrium Q_e values than E2, EE2 and TCS, indicating poorer adsorption under these conditions. The BAC-C10 molecule has a hydrophobic hydrocarbon chain linked to a positively charged nitrogen atom that is also bonded to a benzyl group (Table 5.1) (Martínez-Carballo et al., 2007). The existence of both hydrophobic (benzene) and

hydrophilic (N-benzyl group) moieties defines the amphiphilic nature of BAC-C10 as a

surfactant. The molecules in bulk aqueous phase tend to form aggregates, i.e., micelles,

with hydrocarbon chains pointing towards the center and the hydrophilic heads in contact

with the surrounding water. Since biosolids-derived biochar has a slightly negative

charge (as shown in **Chapter 4**), the low adsorption capacities of BAC-C10 could be

attributed to the combined effect of both the hydrophilic and cationic nature of the

micelles. Among the tested neutral compounds, CBZ has the lowest $logK_{ow}$ and the

highest solubility in water (Table 5.1), which could explain its low adsorption capacities.

Table 5.1 Physical and chemical properties of the micropollutants in this study. Property data were adapted from PubChem and ChemSpider

Compound	Molecular Structure	pK$_a$	log K$_{ow}$	Aqueous solubility mg/L	Polarity
BAC-C10		N/A	N/A	≥10000	polar
CBZ		13.9	2.45	112	polar
E2		10.8	3.94	3.6	non-polar
EE2		10.3	3.67	11.3	moderately polar
TCS		7.9	4.76	10	non-polar

Interestingly, the degree of linearity of the adsorption isotherm was related to the compound polarity. TCS and E2, with non-linear adsorption, are nearly non-polar (Petersen, 2015; The Human Metabolome Database). The compounds with linear adsorption isotherms, BAC-C10, CBZ and EE2, are more polar molecules. One explanation for this trend is that when organic compounds are present at low concentrations (< mg/L), biochar exhibits linear adsorption on its more polar amorphous organic matter fraction and non-linear uptake on the non-polar charred fractions (Chen et

al., 2008, 2012; Lehmann and Stephen, 2009). Linear adsorption on the amorphous fraction of biochar is relatively weaker (lower affinity) than non-linear adsorption on the char fraction (Lehmann and Stephen, 2009), which should be reflected in the enthalpy change of adsorption.

In general, increasing temperature increased the distribution constant, K, of both the Freundlich and linear isotherms (Appendix 5B, Table 5B). For the same equilibrium aqueous-phase concentration, higher temperature favors greater adsorption and stronger affinity of the target compounds on the biochar, indicating more energy input required for these reactions. This indicates that adsorption of organic micropollutants from water onto biosolids-derived biochar is endothermic. Estimation of enthalpy change can quantitatively establish the endothermic nature of this adsorption process.

5.3.2   Estimation of thermodynamic parameters for single-solute adsorption

The estimated isosteric heat of adsorption for each compound in a single-solute system at different surface loadings, Q_e (mmol/g biochar), is shown in Figure 5.2. The linear curves of $\ln(C_e)$ over $1/T$ (isosteres) at varied surface loadings are shown in Appendix 5C, Figure 5C. The calculated isostere parameters are shown in Table 5C. As all isosteric heat values were positive, adsorption of organic micropollutants from the aqueous phase onto biosolids-derived biochar was an endothermic process. Endothermic adsorption is rare for gas/carbonaceous solid adsorption systems (Thomas, 1961), but is often observed for aqueous/carbonaceous solid adsorption systems (Chen et al., 2012; Fontecha-Cámara et al., 2006; Srivastava et al., 2007).

The endothermic nature of adsorption may be due to 1) overcoming interactions with water molecules, in the case of weak physical adsorption, or 2) the formation of

covalent bonds during chemical adsorption. In the case of aqueous-phase adsorption, heat-consuming endothermic physical adsorption can occur if water molecules interact with the adsorbate or adsorbent, and these interactions must be overcome before the adsorbate can adhere on the adsorbent. The heat-consuming steps that must be overcome can include adsorbate diffusion in the water matrix, which has to break hydrogen bonds formed among water molecules (Fontecha-Cámara et al., 2006); adsorbate diffusion in adsorbent pores (Anirudhan and Radhakrishnan, 2008; García-Araya et al., 2003); and the adsorbate replacing pre-adsorbed water molecules, which also needs heat input to break hydrogen bonds between water molecules and the adsorbent. Alternatively, if the formation of covalent bonds is the dominant mechanism, the absolute value of the change of enthalpy should be on the order of 10^2 kJ/mol (Chowdhury, 2003; Thomas, 1961).
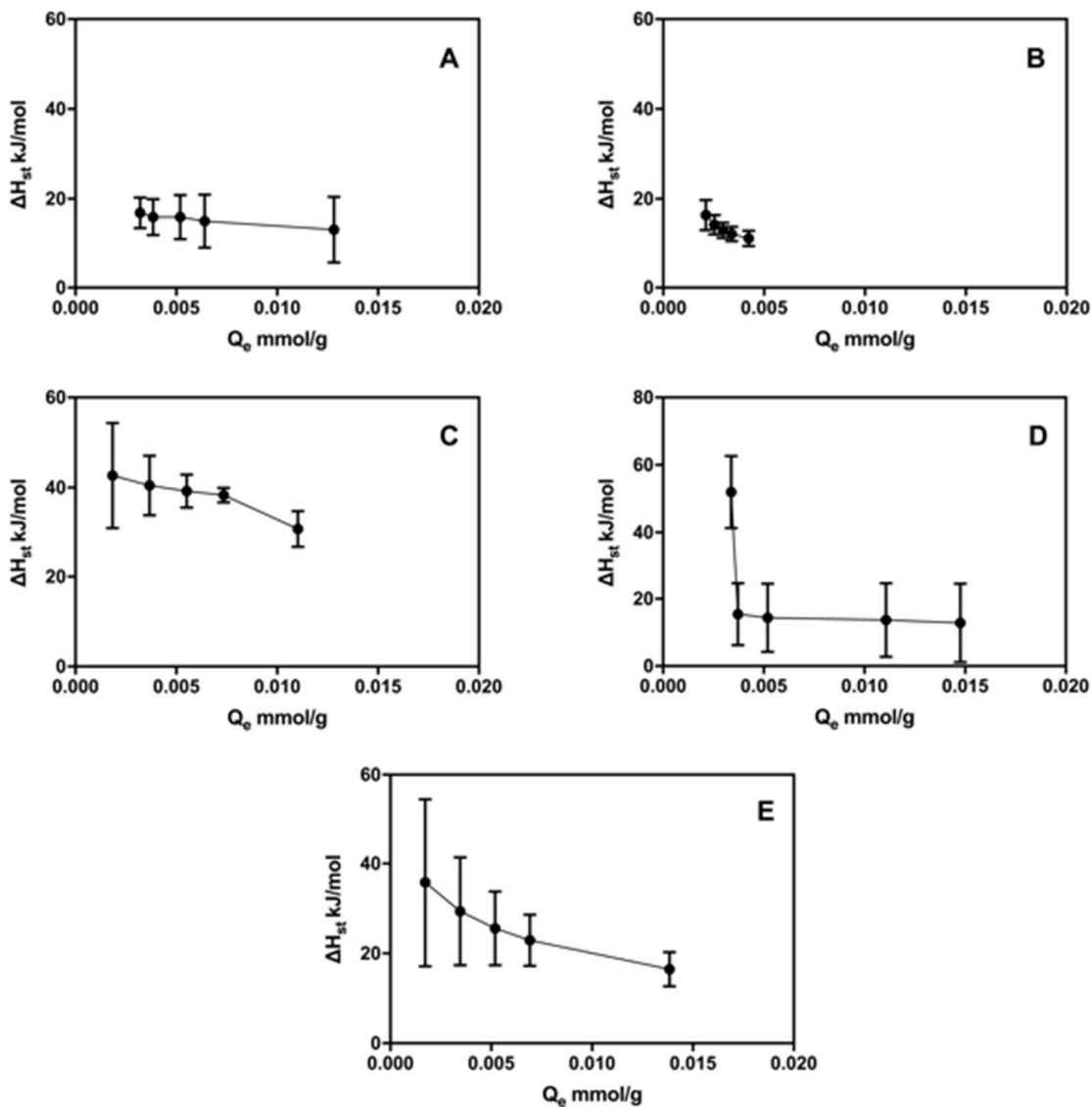
Figure 5.2 Isosteric heat change (ΔH_{st}) as a function of surface loading (Q_e) for A) BAC-C10, B) CBZ, C) E2, D) EE2 and E) TCS in a single-solute adsorption system. The data represent average results and error bars show ±1 standard deviation of triplicate experiments.

The average values of isosteric heat decreased as the adsorbate surface loading increased. Isosteric heat is associated with adsorption site binding affinity for a given surface loading. Thus, the decreasing trend of isosteric heat suggests that, at low surface loading, high-affinity adsorption sites were initially occupied, absorbing more heat. Low-

affinity adsorption sites that required less heat input bound the adsorbate as the surface coverage gradually increased. Biosolids-derived biochar therefore features heterogeneous binding sites capable of adsorbing the study compounds (Srivastava et al., 2007).

More drastic changes in isosteric heat distribution across the surface loading range were observed for E2 and TCS, which agrees with the non-linearity of their adsorption isotherms. The Freundlich parameter n is an indicator of binding affinity distribution on an adsorbent surface. When n is less than 1, the binding affinity changes more drastically across the adsorbent surface (Benjamin and Lawler, 2013). As previously mentioned, linear adsorption of polar compounds on the amorphous fraction of biochar is usually characterized by weaker affinity. The linear adsorption explains the lower isosteric heats of BAC-C10 and CBZ than those of E2 and TCS. The isosteric heat of EE2 decreased sharply for low surface loading, but the rate of change slowed as surface loading increased. The isosteric heat change could stem from EE2 being less polar compared to BAC-C10 and CBZ, which allowed a fraction of the molecules to adsorb on biochar's heterogeneous fraction, while the majority of the EE2 molecules exhibited less heterogeneous linear adsorption.

The Gibbs free energy, enthalpy and entropy change of single-solute adsorption are related to the thermodynamic equilibrium constant K_c via the van't Hoff equation (Appendix 5D, Figure 5D). The experimentally-derived values are shown in Table 5.2. The estimated total enthalpy changes (which signify the total binding energy per unit of adsorption) for the micropollutants were all positive, demonstrating the endothermic nature of their adsorption from the aqueous phase onto biosolids-derived biochar. Adsorption enthalpy changes were one order of magnitude less than the realm of

chemisorption, indicating the dominant role of non-covalent binding for physical adsorption. Among the tested compounds, those characterized by linear adsorption, BAC-C10, CBZ and EE2, experienced less change in enthalpy (12.2, 8.3 and 11.7 kJ/mol, respectively) in comparison to E2 and TCS (48.9 and 81.4 kJ/mol), which were better characterized by non-linear adsorption.

The entire process for solutes diffusing and adsorbing onto sites was spontaneous, as demonstrated by the negative change in Gibbs free energy. The compounds in the adsorbed state had more entropy than compounds in the dissolved state, as demonstrated by the positive ΔS^0 value. The positive ΔS^0 value denotes the existence of non-specific hydrophobic interactions between the organic molecules or micelles and the biochar surface; these non-specific interactions are often associated with a gain in entropy (Chen et al., 2012; Meyer et al., 2006). For the neutral compounds CBZ, E2, EE2 and TCS, the increase in entropy (ΔS^0) positively correlated with the hydrophobicity parameter, $logK_{ow}$ (correlation coefficient=0.8)

Table 5.2 Experimentally derived changes in Gibbs free energy (ΔG^0), enthalpy (ΔH^0) and entropy (ΔS^0) for adsorption of micropollutants under single-solute conditions

Compound	Temperature K	ΔG^0 kJ/mol	ΔH^0 kJ/mol	$T\Delta S^0$ kJ/mol	ΔS^0 J/mol/K
BAC-C10	277	-14.2	12.2	25.6	93.0
	298	-14.6		27.7	
	308	-16.3		28.6	
	323	-18.6		30.0	
CBZ	277	-14.7	8.3	22.9	82.8
	298	-16.6		24.4	
	308	-16.8		25.3	
	323	-18.7		26.5	
E2	277	-17.4	48.9	64.3	232.3
	298	-12.8		69.1	
	308	-28.9		71.5	
	323	-25.6		75.0	
EE2	277	-17.6	11.7	29.4	106.7
	298	-20.6		31.6	
	308	-21.1		32.6	
	323	-22.5		34.2	
TCS	277	-15.6	81.4	96.7	349.3
	298	-18.1		104.0	
	308	-33.8		107.5	
	323	-28.3		112.7	

5.3.3   Multi-solute adsorption equilibrium and thermodynamic profile

As was the case for single-solute conditions, the Freundlich isotherm provided a better fit for E2 and TCS (Figures 5.2C and 5.2E, respectively), while the linear isotherm provided a better fit for BAC-C10, CBZ and EE2 (Figures 5.2A, 5.2B and 5.2D, respectively) adsorption in multi-solute conditions. In general, for multi-solute conditions, temperature increased adsorption of the micropollutants, except for BAC-C10 at low temperatures. Also, BAC-C10 had low Q_e values and poor fit for linear isotherms at 4°C and 25°C. The poor isotherm fits and negligible impact of low temperatures on BAC-C10 adsorption could result from decreased adsorption stemming from competition

from other compounds. For the temperatures tested, EE2 adsorption in multi-solute conditions was inhibited, as shown by the significant decrease in the linear distribution coefficient ($p<0.05$). The E2 multi-solute isotherm parameters also differed from the single-solute isotherms, with a significantly lower Freundlich constant K_f ($p>0.05$). TCS was a stronger competitor for adsorption sites than EE2 and E2. Past research attributed the different competitive behaviors to the hydrophobicity of the competitor compounds (Wang et al., 2006; Yu and Huang, 2005). The higher the hydrophobicity of the competitor, the stronger the competition (Pan and Xing, 2010; Yu and Huang, 2005).

Not all compounds experienced suppressed adsorption due to competition in the multi-solute conditions (Appendix 5F, Table 5F). For CBZ and TCS, adsorption was not significantly altered by multi-solute competition at the tested temperatures (ANOVA, $p>0.05$). The competitive behavior of CBZ could be attributed to their higher polarity based on Chiou and Kile's study that showed that a polar solute (atrazine) strongly suppressed nonlinear sorption of a non-polar solute (trichloroethylene).
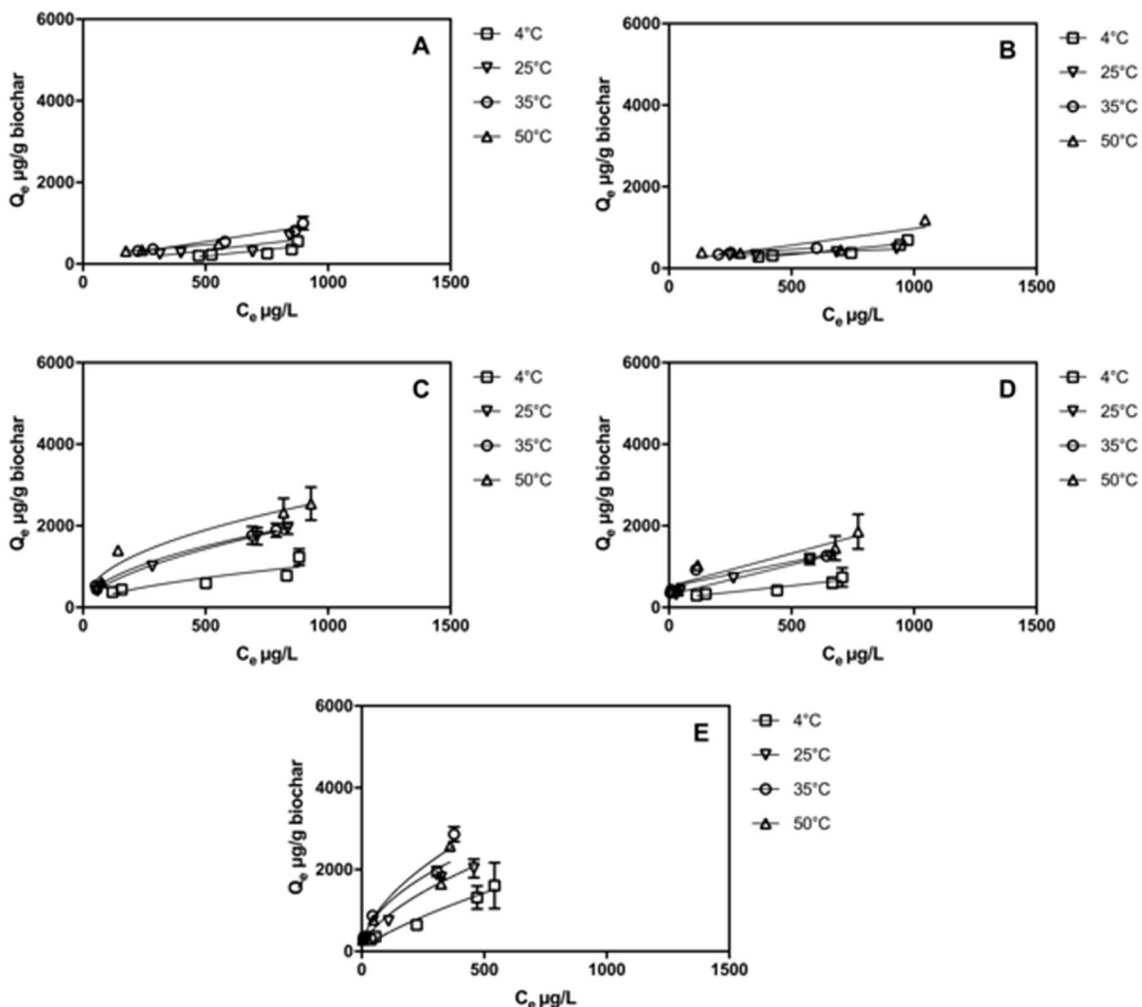
Figure 5.3 Multi-solute system adsorption isotherms of A) BAC-C10, B) CBZ, C) E2, D) EE2, and E) TCS at 4, 25, 35, and 50 °C (277, 298, 308 and 323 K, respectively). The data represent average results and error bars show ±1 standard deviation of triplicate experiments. Some error bars are small and not visible.

Competitive adsorption did not change the endothermic nature of adsorption and the heterogeneous distribution of binding sites on the biochar's surface according to the change in isosteric heat with surface loading plots (Figure 5.4). Negative Gibbs free energy changes still indicate the spontaneity of competitive adsorption for the temperatures tested (Table 5.3).

Comparison of the van't Hoff curves (Appendix 5H, Figure 5H) showed that the

total enthalpy and entropy changes for all compounds were not significantly altered by competitive adsorption in multi-solute conditions (Appendix 5I, Table 5I, $p>0.05$), even though multi-solute competition decreased some adsorption capacities, to differing extents. The binding energy (enthalpy change) and extent of disorder (entropy change) are inherent thermodynamic properties of a reaction and are closely related to the thermodynamic equilibrium constant. Accordingly, only changes in reaction activation energy or physical states of the adsorbent and adsorbate can impact thermodynamic properties of adsorption (Michaelides et al., 2003).
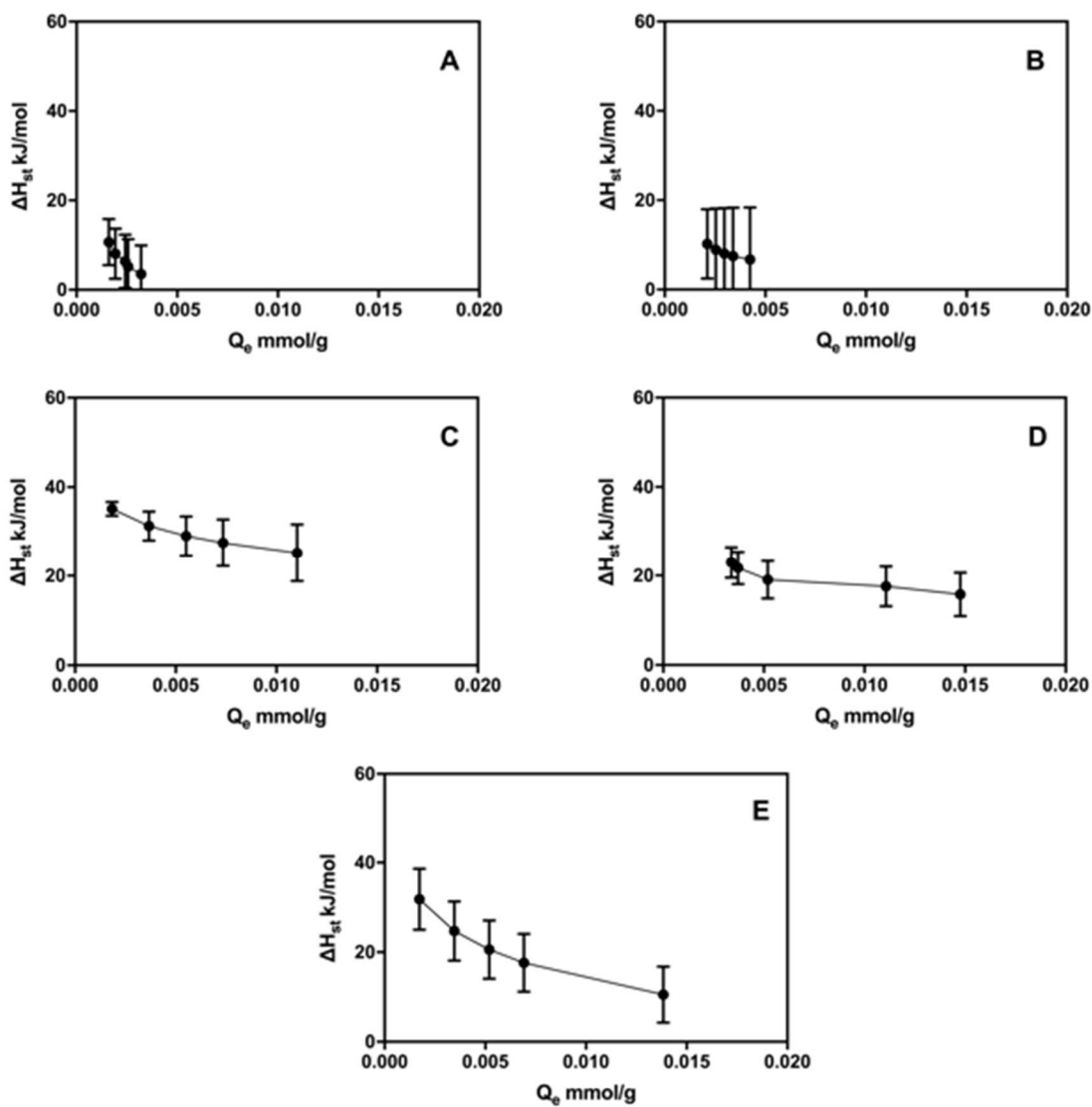
Figure 5.4 Isosteric heat change (ΔH_{st}) with surface loading (Q_e)for A) BAC-C10, B) CBZ, C) E2, D) EE2 and E) TCS, in multi-solute conditions. The data represent average results and error bars show ± 1standard deviation of triplicate experiments.

Table 5.3 Experimentally derived changes in Gibbs free energy (ΔG^0), enthalpy (ΔH^0) and entropy (ΔS^0) for micropollutant adsorption under multi-solute conditions.

Compound	Temperature K	ΔG^0 kJ/mol	ΔH^0 kJ/mol	$T\Delta S^0$ kJ/mol	ΔS^0 J/mol/K
BAC-C10	277	-14.8	7.7	22.5	81.1
	298	-16.2		24.2	
	308	-17.5		25.0	
	323	-16.6		26.2	
CBZ	277	-14.6	4.2	17.9	64.7
	298	-13.5		19.3	
	308	-15.1		19.9	
	323	-18.0		20.9	
E2	277	-20.7	52.0	71.4	257.7
	298	-21.0		76.8	
	308	-29.4		79.4	
	323	-31.9		83.2	
EE2	277	-14.9	14.3	29.42	106.2
	298	-18.1		31.6	
	308	-18.2		32.7	
	323	-19.8		34.3	
TCS	277	-14.0	89.9	104.5	377.5
	298	-23.8		112.5	
	308	-27.4		116.2	
	323	-30.8		121.9	

5.4   Conclusion

This research demonstrated that biosolids-derived biochar adsorbed neutral micropollutants and the cationic compound BAC-C10, albeit to differing extents. More polar compounds such as BAC-C10 and CBZ exhibited more linear adsorption with higher Freundlich isotherm n values, indicating weak interactions with the more polar amorphous moieties of biochar. The neutral micropollutants' hydrophobicity positively affected their extent of adsorption. Accordingly, the most hydrophobic compound tested, TCS, had the highest adsorption capacity under the experimental conditions. The estimation of the thermodynamic parameters of adsorption indicated that all of the

adsorption reactions were endothermic. Therefore, heat input had a positive impact on the adsorption, implying that biochar will work better as wastewater temperature increases. Moreover, the thermodynamic parameters indicated heterogeneity in adsorption site distribution on the biochar surface, which is expected for biochar derived from a heterogeneous feedstock (wastewater biosolids). The underlying binding mechanism for neutral compounds could potentially be dominated by non-specific hydrophobic interactions based on the positive correlation between change in entropy and log K_{ow}. Under multi-solute conditions, E2 and EE2 adsorption was suppressed, while TCS adsorption was unaffected, indicating biosolids-derived biochar's preference for adsorption of more hydrophobic compounds. The adsorption of CBZ was essentially unaffected under multi-solute condition due to the competitive effect of more polar molecules. Parameters reflecting thermodynamic properties, such as binding energy and entropy change of adsorption, were not affected by the presence or absence of other solutes in the matrix.

Studying the impact of temperature and the thermodynamic profile of adsorption is beneficial for understanding the binding mechanism and limiting factors, such as diffusion and temperature, for adsorption on biosolids-derived biochar. For future research, quantitative correlations between biochar's surface properties and the binding energy are needed, which would be beneficial in guiding engineering process design to most effectively remove micropollutants from contaminated water matrices.

5.5   References

Ahmad, M., Lee, S.S., Oh, S.E., Mohan, D., Moon, D.H., Lee, Y.H., Ok, Y.S., 2013. Modeling adsorption kinetics of trichloroethylene onto biochars derived from soybean stover and peanut shell wastes. Environ. Sci. Pollut. Res. 20, 8364–8373.

doi:10.1007/s11356-013-1676-z

Anirudhan, T.S., Radhakrishnan, P.G., 2008. Thermodynamics and kinetics of adsorption of Cu(II) from aqueous solutions onto a new cation exchanger derived from tamarind fruit shell. J. Chem. Thermodyn. 40, 702–709. doi:10.1016/j.jct.2007.10.005

Benjamin, M.M., Lawler, D.F., 2013. Water Quality Engineering: Physical / Chemical Treatment Processes. Wiley.

Blair, B.D., Crago, J.P., Hedman, C.J., Klaper, R.D., 2013. Pharmaceuticals and personal care products found in the Great Lakes above concentrations of environmental concern. Chemosphere 93, 2116–2123. doi:10.1016/j.chemosphere.2013.07.057

Blair, B.D., Crago, J.P., Hedman, C.J., Treguer, R.J.F., Magruder, C., Royer, L.S., Klaper, R.D., 2013. Evaluation of a model for the removal of pharmaceuticals, personal care products, and hormones from wastewater. Sci. Total Environ. 444, 515–21. doi:10.1016/j.scitotenv.2012.11.103

Carballa, M., Omil, F., Ternes, T., Lema, J.M., 2007. Fate of pharmaceutical and personal care products (PPCPs) during anaerobic digestion of sewage sludge. Water Res. 41, 2139–2150. doi:10.1016/j.watres.2007.02.012

Carey, D.E., Zitomer, D.H., Hristova, K.R., Kappell, A.D., McNamara, P.J., 2016. Triclocarban Influences Antibiotic Resistance and Alters Anaerobic Digester Microbial Community Structure. Environ. Sci. Technol. 50, 126–134. doi:10.1021/acs.est.5b03080

Chen, B., Zhou, D., Zhu, L., 2008. Transitional adsorption and partition of nonpolar and polar aromatic contaminants by biochars of pine needles with different pyrolytic temperatures. Environ. Sci. Technol. 42, 5137–5143. doi:10.1021/es8002684

Chen, Z., Chen, B., Zhou, D., Chen, W., 2012. Bisolute sorption and thermodynamic behavior of organic pollutants to biomass-derived biochars at two pyrolytic temperatures. Environ. Sci. Technol. 46, 12476–12483. doi:10.1021/es303351e

Chiou, C.T., Kile, D.E., 1998. Deviations from sorption linearity on soils of polar and nonpolar organic compounds at low relative concentrations. Environ. Sci. Technol. 32, 338–343. doi:10.1021/es970608g

Chowdhury, P.S. and S., 2003. Insight Into Adsorption Thermodynamics. J. Hazard. Mater. 162, 440. doi:10.1007/978-3-642-30391-3

Chowdhury, S., Mishra, R., Saha, P., Kushwaha, P., 2011. Adsorption thermodynamics, kinetics and isosteric heat of adsorption of malachite green onto chemically modified rice husk. Desalination 265, 159–168. doi:10.1016/j.desal.2010.07.047

Dubinin, M.M., Radushkevich, L.V., 1947. Equation of the characteristic curve of

activated charcoal. Proc. Acad. Sci. Phys. Chem. Sec. USSR 55, 331–333. doi:10.1016/j.clay.2009.07.022

Ebadi, A., Soltan Mohammadzadeh, J.S., Khudiev, A., 2009. What is the correct form of BET isotherm for modeling liquid phase adsorption? Adsorption 15, 65–73. doi:10.1007/s10450-009-9151-3

Fontecha-Cámara, M.A., López-Ramón, M. V., Álvarez-Merino, M.A., Moreno-Castilla, C., 2006. About the endothermic nature of the adsorption of the herbicide diuron from aqueous solutions on activated carbon fiber. Carbon N. Y. doi:10.1016/j.carbon.2006.05.031

García-Araya, J.F., Beltrán, F.J., Álvarez, P., Masa, F.J., 2003. Activated carbon adsorption of some phenolic compounds present in agroindustrial wastewater. Adsorption 9, 107–115. doi:10.1023/A:1024228708675

Ghosal, P.S., Gupta, A.K., 2015. An insight into thermodynamics of adsorptive removal of fluoride by calcined Ca–Al–(NO$_3$) layered double hydroxide. RSC Adv. 5, 105889–105900. doi:10.1039/C5RA20538G

Jung, C., Park, J., Lim, K.H., Park, S., Heo, J., Her, N., Oh, J., Yun, S., Yoon, Y., 2013. Adsorption of selected endocrine disrupting compounds and pharmaceuticals on activated biochars. J. Hazard. Mater. 263 Pt 2, 702–10. doi:10.1016/j.jhazmat.2013.10.033

Lehmann, J., Stephen, J., 2009. Biochar for Environmental Management:Science And Technology. doi:10.4324/9781849770552

Limousin, G., Gaudet, J.-P., Charlet, L., Szenknect, S., Barthès, V., Krimissa, M., 2007. Sorption isotherms: A review on physical bases, modeling and measurement. Appl. Geochemistry 22, 249–275. doi:10.1016/j.apgeochem.2006.09.010

Manda, B.M.K., Worrell, E., Patel, M.K., 2014. Innovative membrane filtration system for micropollutant removal from drinking water – prospective environmental LCA and its integration in business decisions. J. Clean. Prod. 72, 153–166. doi:10.1016/j.jclepro.2014.02.045

Martínez-Carballo, E., Sitka, A., González-Barreiro, C., Kreuzinger, N., Fürhacker, M., Scharf, S., Gans, O., 2007. Determination of selected quaternary ammonium compounds by liquid chromatography with mass spectrometry. Part I. Application to surface, waste and indirect discharge water samples in Austria. Environ. Pollut. 145, 489–496. doi:10.1016/j.envpol.2006.04.033

Meyer, E.E., Rosenberg, K.J., Israelachvili, J., 2006. Recent progress in understanding hydrophobic interactions. Proc. Natl. Acad. Sci. U. S. A. 103, 15739–46. doi:10.1073/pnas.0606422103

Michaelides, A., Liu, Z.P., Zhang, C.J., Alavi, A., King, D.A., Hu, P., 2003. Identification of general linear relationships between activation energies and enthalpy changes for dissociation reactions at surfaces. J. Am. Chem. Soc. 125, 3704–3705. doi:10.1021/ja027366r

Milonjić, S.K., 2007. A consideration of the correct calculation of thermodynamic parameters of adsorption. J. Serbian Chem. Soc. 72, 1363–1367. doi:10.2298/JSC0712363M

Monsalvo, V.M., McDonald, J.A., Khan, S.J., Le-Clech, P., 2014. Removal of trace organics by anaerobic membrane bioreactors. Water Res. 49, 103–112. doi:10.1016/j.watres.2013.11.026

Pan, B., Xing, B., 2010. Competitive and complementary adsorption of bisphenol a and 17α-ethinyl estradiol on carbon nanomaterials. J. Agric. Food Chem. 58, 8338–8343. doi:10.1021/jf101346e

Petersen, R.C., 2015. Triclosan Computational Conformational Chemistry Analysis for Antimicrobial Properties in Polymers. J. Nat. Sci. 1, e54.

Phillips, P.J., Chalmers, A.T., Gray, J.L., Kolpin, D.W., Foreman, W.T., Wall, G.R., 2012. Combined sewer overflows: An Environmental source of hormones and wastewater micropollutants. Environ. Sci. Technol. 46, 5336–5343. doi:10.1021/es3001294

Schwarzenbach, R.P., Escher, B.I., Fenner, K., Hofstetter, T.B., Johnson, C.A., von Gunten, U., Wehrli, B., 2006. The challenge of micropollutants in aquatic systems. Science 313, 1072–1077. doi:10.1126/science.1127291

Schwarzenbach, R.P., Gschwend, P.M., Imboden, D.M., 2005. Environmental organic chemistry. John Wiley & Sons.

Servos, M.R., Bennie, D.T., Burnison, B.K., Jurkovic, A., McInnis, R., Neheli, T., Schnell, A., Seto, P., Smyth, S.A., Ternes, T.A., 2005. Distribution of estrogens, 17β-estradiol and estrone, in Canadian municipal wastewater treatment plants. Sci. Total Environ. 336, 155–170. doi:10.1016/j.scitotenv.2004.05.025

The Human Metabolome Database. URL http://www.hmdb.ca/metabolites/HMDB00151

Srivastava, V.C., Mall, I.D., Mishra, I.M., 2007. Adsorption thermodynamics and isosteric heat of adsorption of toxic metal ions onto bagasse fly ash (BFA) and rice husk ash (RHA). Chem. Eng. J. 132, 267–278. doi:10.1016/j.cej.2007.01.007

Thomas, J.M., 1961. The existence of endothermic adsorption. J. Chem. Educ. 38, 138. doi:10.1021/ed038p138

Tran, H.N., You, S.J., Hosseini-Bandegharaei, A., Chao, H.P., 2017. Mistakes and inconsistencies regarding adsorption of contaminants from aqueous solutions: A critical review. Water Res. 120, 88–116. doi:10.1016/j.watres.2017.04.014

Tóth, J., 1971. State Equations of the Solid-Gas Interface Layers. Acta Chim. Acad. Sci. Hungaricae 69, 311–328.

Vajda, A.M., Barber, L.B., Gray, J.L., Lopez, E.M., Bolden, A.M., Schoenfuss, H.L., Norris, D.O., 2011. Demasculinization of male fish by wastewater treatment plant effluent. Aquat. Toxicol. 103, 213–21. doi:10.1016/j.aquatox.2011.02.007

Wang, X., Sato, T., Xing, B., 2006. Competitive sorption of pyrene on wood chars. Environ. Sci. Technol. 40, 3267–3272. doi:10.1021/es0521977

Wang, Y., Lu, J., Wu, J., Liu, Q., Zhang, H., Jin, S., 2015. Adsorptive removal of fluoroquinolone antibiotics using bamboo biochar. Sustain. 7, 12947–12957. doi:10.3390/su70912947

Yu, Z., Huang, W., 2005. Competitive Sorption between 17α-Ethinyl Estradiol and Naphthalene/Phenanthrene by Sediments. Environ. Sci. Technol. 39, 4878–4885. doi:10.1021/es048558k

6 BIOSOLIDS-DERIVED BIOCHAR ADSORPTION TO REMOVE MICROPOLLUTANTS PRIOR TO ION EXCHANGE FOR NUTRIENT RECOVERY COUPLED

6.1   Introduction

The role of water resource recovery facilities (WRRFs) has advanced beyond a sole focus on treating wastewater, and now encompasses recovery of value-added products as well. For instance, anaerobic treatment processes such as anaerobic membrane bioreactors have been investigated for their ability to treat wastewater (i.e., remove biochemical oxygen demand [BOD_5] and suspended solids) while producing energy in the form of biogas (McCarty et al., 2011; Seib et al., 2016) and reducing sludge production (Mota et al., 2013). However, the effluent from anaerobic treatment processes contains high ammonia nitrogen (NH_4-N) and inorganic orthophosphate (PO_4-P) that may necessitate additional treatment to meet stringent discharge regulations (Wisconsin DNR, 2010). The nutrient-rich effluent from anaerobic treatment is a potential resource from which to recover nitrogen and phosphorus. Nutrient recovery from wastewater could help close anthropogenic nutrient loops by supplementing supplies of phosphate mined from depleting natural reserves and nitrogen produced via the energy-intensive Haber-Bosch process (Mayer et al., 2016).

Ion exchange-precipitation is one technique that can be used to remove and concentrate nitrogen and phosphorus from wastewater and recover the nutrients in the form of solid fertilizer products, e.g. struvite ($MgNH_4PO_4$). Clinoptilolite, which is a natural zeolite, can effectively exchange ammonium (Williams et al., 2015). LayneRT (Layne Christensen, The Woodlands, TX) is a commercial hybrid anion exchange resin which provides strong ligand adsorption of orthophosphate (the most common form of phosphorus in nutrient-rich anaerobic effluent (Seib et al., 2016)) via hydrated ferric oxide (HFO) nanoparticles impregnated in a strong base anion exchange polymer

(Sengupta and Pandit, 2011). Regeneration of these ion exchangers is conducted using highly concentrated brines, which results in desorption of ammonium and phosphate into a concentrated brine solution that can subsequently be used for precipitation of nutrient-rich solids suitable for reuse as fertilizer.

In addition to valuable nutrients, anaerobic effluent may also contain a mixture of potentially harmful micropollutants. For instance, the extent of removal for antimicrobials such as triclosan, antibiotics such as sulfamethoxazole, and estrogens is inconsistent through anaerobic treatments, but tends to be low (Alvarino et al., 2014; de Mes et al., 2008; Hruska and Franek, 2012; Malmborg and Magnér, 2015; Monsalvo et al., 2014; Samaras et al., 2013). Recovering nutrients via ion exchange from anaerobic effluents that also contain micropollutants may result in subsequent problems. For instance, a wide range of micropollutants adsorb to polymeric ion exchangers, including estrone, ibuprofen, and sulfadiazine (Jiang et al., 2015; Neale et al., 2010). The tendency of micropollutants to adsorb to ion exchangers may result in elevated concentrations of micropollutants in the regeneration brines (Neale et al., 2010). For the last step of solid fertilizer recovery, i.e., controlled struvite precipitation, studies have revealed that synthetic fragrances, 4-nonylphenols and tetracyclines in the feed water were present in the precipitated struvite crystals. Thus, strategies to mitigate the risks of micropollutants in the recovered nutrient products are needed.

Micropollutant removal prior to nutrient recovery processes would mitigate these risks. Biochar, which has been shown to remove triclosan, bisphenol A, atrazine and sulfamethoxazole (Jung et al., 2013), could offer an effective means of adsorbing micropollutants to provide removal prior to ion exchange nutrient recovery. Among

applicable feedstocks that can be pyrolyzed to produce biochar, wastewater biosolids can provide benefits for WRRF management (Hadi et al., 2015). Specifically, municipal biosolids are centrally treated, which facilitates their use as a feedstock for biosolids-derived biochar production followed by on-site utilization as an adsorbent material at WRRFs. Pyrolysis of dry biosolids can be a self-sustaining process since the by-products, py-gas and py-oil, can be used as energy sources to fuel the process (McNamara et al., 2016).

Use of biosolids-derived biochar as an initial step for separating micropollutants from nutrient-rich water prior to ion exchange for nutrient recovery was evaluated in this study. Two hydrophobic compounds, triclosan (TCS) and 17β-estradiol (E2), and one hydrophilic compound, sulfamethoxazole (SMX) were assessed. The research objectives were to: 1) determine the impact of ammonium and phosphate on micropollutant adsorption to biochar, 2) explore the feasibility for reusing spent biosolids-derived biochar using additional cycles of pyrolysis activation, and 3) conduct a mass distribution calculation on micropollutants and nutrients through a biochar-ion exchanger flow-through column system. It was hypothesized that 1) nutrient ions present in water can promote micropollutant adsorption on biochar; 2) the functionality of spent biochar as an adsorbent can be recovered from pyrolysis; 3) biochar can retain the majority of micropollutants without removing nutrients, in the flow-through column system that incorporate biochar adsorption and ion exchange to recover nutrients.

6.2   Materials and Methods

6.2.1   Biochar preparation/reactivation and batch adsorption experiments

Biochar adsorption experiments were performed to determine the impact of nutrients on micropollutant adsorption to biochar. Additionally, experiments were performed to determine the suitability of reusing spent biochar following activation by pyrolysis.

Biosolids-derived biochar was prepared using methods described in **Chapter 4**. Briefly, heat-dried biosolids from the Jones Island Water Reclamation Facility in Milwaukee, WI was used as the pyrolysis feedstock. The biosolids were heated in the absence of oxygen at 600˚C for 60 minutes in a furnace. The resulting biochar was acid treated using 1 N HCl, which has been shown to improve micropollutant sorption capacity to biochar in **Chapter 4**. To reactivate biochar after one cycle of sorption experiments, spent biochar (biochar used in a previous sorption experiment) was dried in a desiccator for 1 week and pyrolyzed at 600˚C in a furnace for 60 minutes. The reactivated biochar was not acid treated. The reactivated biochar was used to conduct a second cycle of adsorption tests.

The batch adsorption tests were performed in Milli-Q water with 40 mg-N/L as NH_4Cl and 5 mg-P/L as K_2HPO_4 to mimic plausible nutrient levels in mainstream anaerobic effluents (Seib et al., 2016; Williams et al., 2015). The micropollutants TCS (97%, Sigma Aldrich, St. Louis, MO, USA), E2 (98%, Sigma Aldrich, St. Louis, MO, USA) and SMX (Sigma Aldrich, St. Louis, MO, USA) were pre-dissolved in HPLC-grade methanol and stored at 4°C for use as stock solutions. The feed water was injected

with the stock solution to yield approximately 350 µg/L each of TCS, E2 and SMX. The micropollutant concentrations for batch tests were higher than in actual anaerobic effluents (Alvarino et al., 2014; Monsalvo et al., 2014) so that micropollutant adsorption capacities could be determined via liquid chromatography-mass spectrometry (LC-MS; detection limits were in the low µg/L range). The pH of the feed water was adjusted to 7 with NaOH. Biochar was mixed with the solutions at a dosage of 0.4 g/L. Sorption experiments lasted 4 days to ensure equilibrium was reached (Williams et al., 2015). Liquid samples were collected before and after experiments to quantify micropollutants and nutrients, as described in the 6.2.3 *Analytical Methods* section.

6.2.2   Continuous flow-through column experiments

Column adsorption experiments were conducted to determine the removal of micropollutants and nutrients from synthetic water solutions under continuous-flow through conditions, which more closely model real-world applications. All glassware was silanized using a 5% by volume dichlorodimethylsilane (99.5%, Sigma Aldrich, St. Louis., MO, USA) and 95% by volume heptane (99%, Sigma Aldrich, St. Louis, MO, USA) solution to prevent chemicals from adsorbing onto the glass surface.

Downflow fixed-bed column experiments were conducted using 11 mm inner diameter, 60 cm long glass columns (Ace Glass Incorporated, Vineland, NJ, USA). Adsorption columns were operated at room temperature and fed by a peristaltic pump (Syringe Pump NE-9000G, New Era Pump Systems Inc., Farmingdale, NY, USA) programmed at a constant 10 mL/min volumetric flow rate.

The columns were packed with 12.7 cm adsorbents in depth, between two supporting layers of glass wool and glass beads. As shown in Figure 6.1, column

configuration consisted of three adsorption columns operated in series with the first column packed with six grams of biosolids-derived biochar adsorbent targeting removal of the target micropollutants (E2, TCS, and SMX). The effluent from the biochar column was collected in a glass beaker, which was used as the influent for the second column. The second column was packed with six grams of LayneRT resin, an anionic resin, which was used to selectively remove phosphate from solution. The third column was packed with six grams of clinoptilolite, a cationic ion exchanger, which was used to selectively remove ammonium from solution. Influent and effluent water samples were collected in glass amber vials and analyzed for micropollutants, phosphate, and ammonium.
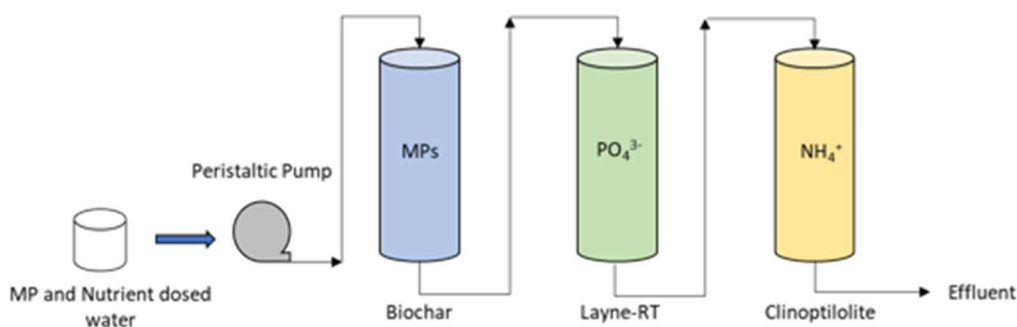
Figure 6.1 Experimental setup for flow-through column studies. Columns were arranged to sequentially remove micropollutants (MPs using biosolids-derived derived biochar), PO_4^{3-} (using LayneRT ion exchange resin), and NH_4^+ (using clinoptilolite ion exchange media).

6.2.3   Analytical methods

Micropollutants were quantified via online solid-phase extraction (SPE) with liquid chromatograph-mass spectrometry (LC-MS). An online SPE cartridge (Phenomenex, Torrance, CA, USA) was incorporated in the LC-MS system (LC-MS 2020, Shimadzu, Columbia, MD, USA) to mitigate interference from the nutrients. All

samples were filtered through 0.45 µm PTFE filters. Prior to SPE, ^{13}C-TCS, estrone (E1) and ^{13}C-SMX were added as internal standards. Details of the analytical methods are similar with that in **Chapter 4**. Quality control parameters such as method detection limit and recovery were similar as described in **Chapter 3**. The standard phenate and ascorbic acid methods were employed to quantify NH$_4$-N and PO$_4$-P (APHA et al., 1998). Samples were measured in triplicate for quality assurance.

6.2.4   Data analysis

For batch experiments, the mass of nutrients or micropollutants adsorbed per mass of ion exchanger (Q$_e$), was calculated using eq. 6.1:

$$Q_e = \frac{(C_0 - C_e) \times V}{M} \text{ (eq. 6.1)}$$

where C$_0$ is the initial concentration of NH$_4$-N (mg/L), PO$_4$-P (mg/L) or micropollutant (µg/L), C$_e$ is the concentration at equilibrium, V is the volume of feed water (L), and M is the mass of biosolids-derived biochar (g).

For column tests, the total input mass of micropollutants or nutrients (M$_{influent}$) was calculated using eq. 6.2:

$$M_{influent} = C_{in,ave.} \times t_{op} \times Q \text{ (eq. 6.2)}$$

where C$_{in, ave}$ is the average influent concentration of NH$_4$-N, PO$_4$-P or micropollutants, t$_{op}$ is the total column operation time, and Q is the flowrate. The total mass in each column's effluent was estimated using eq. 6.3:

$$\sum_{n=1}^{12} Q \times \frac{C_{eff,n+1} + C_{eff,n}}{2} \times (t_{n+1} - t_n) \text{ (eq. 6.3)}$$

where n indicates the nth sampling point during operation (maximum of 12), C$_{eff}$ is the effluent concentration of NH$_4$-N, PO$_4$-P or micropollutants for each column, t$_n$ is the

time when the nth sample was taken, andQ is the flowrate. Total mass removed by each column was calculated as the difference between influent and effluent masses (eq. 6.2-eq. 6.3). The mass of compounds in the effluent from each column was considered to be the influent into the subsequent column, assuming no loss in tubing or columns, as demonstrated in previous column tests (Kimbell, 2017). The carbon usage rate (CUR) of biochar-derived biochar was calculated by dividing the mass of micropollutants removed in the biochar column by the total volume of solution passed through the column.

Statistical analyses (t-test and Tukey's multiple comparison test, α level = 5%) were conducted to test significance of differences using GraphPad Prism 6 (Graphpad Software, Inc., La Jolla, CA).

6.3   Results and discussion

6.3.1   Biochar as an adsorbent for micropollutants in the presence of nutrients

In feed water containing 40 mg/L NH_4-N and 5 mg/L PO_4-P, micropollutants were successfully adsorbed onto biochar (Figure 6.2). Average mass adsorbed was approximately 330±73 µg TCS/g biochar, 572±20 µg E2/g biochar and 145±12 µg SMX/g biochar. For feed water containing micropollutants without nutrients, the average mass adsorbed for TCS, E2 and SMX was 215±42, 233±11 and 64±34 µg/g biochar, respectively. In both cases, less SMX adsorbed in comparison to TCS and E2. In pH 7 solution, TCS and E2 are neutral molecules, while the majority of SMX is in the dissociated anionic form. Biosolids-derived biochar, as characterized in **Chapter 4**, had a slightly negative surface charge in water. Repellence between the biochar's negative surface charge and anionic SMX could lead to lower SMX uptake compared to the

neutral TCS and E2 molecules. Removal of the neutral molecules may be attributed to hydrophobic interactions and intermolecular forces between compounds and biochar functional groups (**Chapter 4** and **5**).

Interestingly, adding nutrient ions to the feed water increased micropollutant uptake, perhaps due to increasing ionic strength. Previous studies revealed similar relationships between ionic strength and adsorption of organic micropollutants to carbonaceous adsorbents. For example, Fontecha-Cámara et al. and Kim et al. observed that adsorption of herbicides and compounds in sunscreen from water onto activated carbon and biochar increased with higher ionic strength (Fontecha-Cámara et al., 2007; Kim et al., 2016). These results were attributed to compression of electrical double layers by adding salt, i.e. ammonium and phosphate salts. The thickness of the double layers surrounding both biochar and micropollutants was compressed by an increase in the ionic strength of the solution (Kim et al., 2016; Rashid et al., 1972). This allows micropollutants to more easily diffuse towards the biochar surface.

Although the adsorption capacities of TCS, E2 and SMX on commercial activated carbon are orders of magnitude higher (> mg/g adsorbent) than biosolids-derived biochar (Behera et al., 2010; Çalışkan and Göktürk, 2010; Fukuhara et al., 2006), at the low micropollutant concentrations encountered in real wastewaters, biosolids-derived biochar could still be adequate for removing micropollutants (**Chapter 4**). An added benefit is the potential for on-site production of biochar at WRRFs.
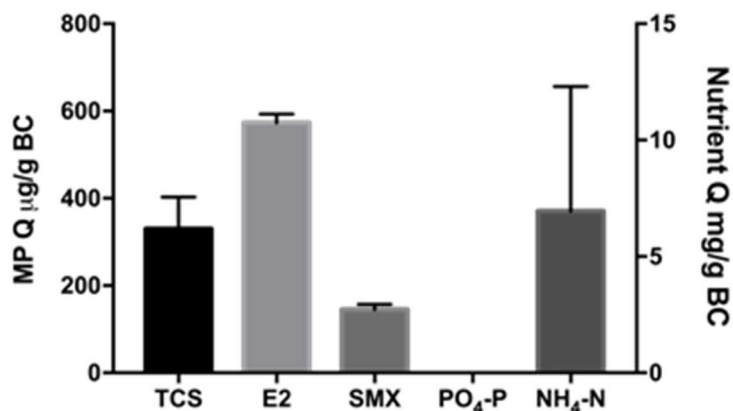
Figure 6.2 Micropollutant (MP) mass adsorption per gram of biochar (BC; primary Y-axis) and nutrient mass adsorption per gram of biochar (secondary Y-axis). The biochar concentration was 0.4 g/L. The bars represent average results and error bars show ±1 standard deviation of triplicate experiments.

The acid-treated biosolids-derived biochar did not efficiently adsorb phosphate or ammonium ions (Figure 6.2), with 0% removal of P and < 7% for N. The surface of this biochar is negatively charged as mentioned in **Chapter 4**; therefore, phosphate ions are likely repulsed. Generally, phosphate adsorption capacities for biochar derived from different feedstocks are low (Hale et al., 2013; Takaya et al., 2016). Certain feedstocks that are modified with, or are intrinsically rich in, cationic metals such as magnesium can achieve phosphate adsorption due to ligand binding (Fang et al., 2014; Yao et al., 2011). The negligible phosphate adsorption observed in this study could be due to lack of this binding mechanism. Unlike phosphate ions that need metals to form ligand bonds, SMX has an aromatic moiety in its molecular structure and is able to form π-stacking on the biochar surface even though SMX was primarily in anionic form under these experimental conditions (**Chapter 3**). However, the repulsive effect of the biochar's surface charge likely interferes with the approach of SMX ions, resulting in relatively low adsorption of SMX. The biochar in this batch test offered no effective adsorption of

ammonium ions, whereas other studies using wastewater biosolids as the pyrolysis feedstock have observed adsorption (Carey et al., 2015; Takaya et al., 2016). Differences in results may stem from different pre-wash strategies (acid wash versus base wash).

6.3.2   Impact of biochar regeneration with pyrolysis

Previous studies suggested that micropollutants were removed from the solid phase through pyrolysis (Hoffman et al., 2016; Ross et al., 2016). Thus, the spent biosolids-derived biochar was regenerated in a furnace at 600°C. After each of two sequential regeneration cycles, the regenerated biochar was still capable of adsorbing micropollutants (Figure 6.3). The first regeneration cycle (denoted as "1-biochar") increased biochar adsorption capacity for TCS, but there was no significant change in TCS adsorption capacities using biochars after the second regeneration (denoted as "2-biochar", Appendix 6A, Table 6A). For E2, the adsorption capacity of the pristine biochar (denoted as "0-biochar") and 2-biochar were essentially the same, whereas the 1-biochar was significantly higher. This indicates that regeneration of biochar did not substantially influence E2 adsorption. However, for SMX, regenerated biochar adsorption capacities were lower than 0-biochar, with no significant decrease in SMX adsorption capacity after multiple regeneration cycles. The results imply that using pyrolysis to regenerate spent biochar is effective for multiple cycles. The wide variation in the relationship between biochar regeneration cycles and micropollutant adsorption capacities could be the result of heterogeneity of the feedstock municipal biosolids (Font et al., 2005). In practice, pyrolysis reactors at WRRFs would be fed a blend of pristine biosolids and spent biochar to produce useable biochar adsorbents while simultaneously removing micropollutants adsorbed in previous adsorption cycles
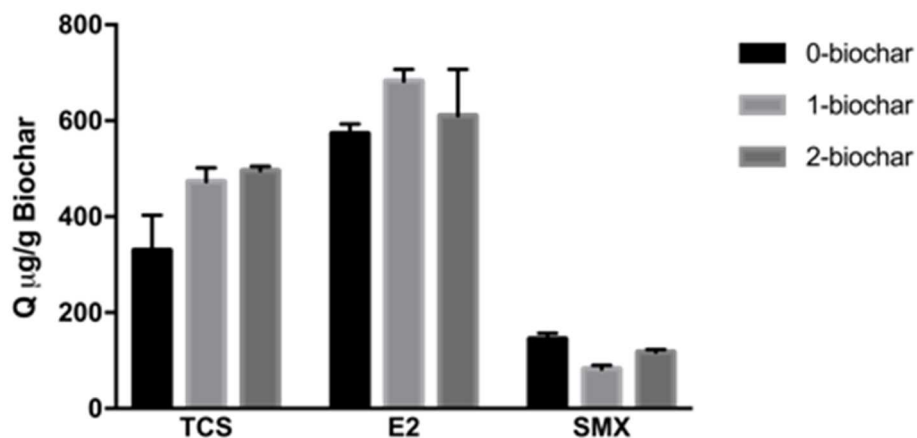
Figure 6.3 Micropollutant mass adsorption per gram of biochar over multiple regeneration cycles. Pristine biochar is denoted as 0-biochar, 1-biochar refers to a single regeneration cycle, and 2-biochar refers to two cycles. The bars represent average results and error bars show ±1 standard deviation of triplicate experiments.

Similar to pristine biochar, regenerated biochar did not effectively adsorb nutrient ions (Appendix 6B, Figure 6B and Table 6B). However, the phosphate in water increased 4% after application of pristine biochar (p=0.004). Due to increasingly strict phosphorous discharging regulation, caution has to be paid when employing biosolids-derived biochar to ensure phosphorous is not released in the treated effluent. There was no significant change in ammonium concentration in water.

Collectively, the batch studies indicated that biosolids-derived biochar could be a reusable adsorbent for selective removal of micropollutants while leaving nutrients in water for subsequent recovery. Unit operations consisting of columns packed with biochar followed by columns packed with nutrient-selective ion exchangers and finally struvite precipitation could be used to recover nitrogen and phosphorus while eliminating potential risks caused by micropollutants in the water or struvite.

6.3.3 Continuous flow columns: Biochar and ion exchangers in series for sequential micropollutant and nutrient removal

Based on biosolids-derived biochar's ability to adsorb micropollutants without co-adsorbing phosphate or ammonium, the biosolids-derived biochar column was operated ahead of the LayneRT and clinoptilolite columns (Figure 6.1). Thus, the biosolids-derived biochar column acted as a pre-polishing step to remove micropollutants ahead of nutrient ion exchange. The columns were denoted as BC-column (biochar), L-column (LayneRT) and C-column (clinoptilolite).

The TCS concentration in the BC-column effluent started at 20% of the influent concentration and gradually increased to approximately 30% after 200 bed volumes (Figure 6.4). For the L-column, effluent, TCS was less than 20% of the treatment train's influent. Approximately 20% of the system influent TCS remained in the C-column effluent. The E2 concentration in the BC-column effluent was 10% of influent within the first 100 bed volumes treated and then increased to 20% of the influent. In the L- and C-columns effluents, E2 concentrations were approximately 10% of the system's influent. SMX in the BC-column effluent rapidly increased and remained above 60% of influent. The SMX concentration in the L- and C- column effluents increased to 40-50% of the influent after 200 bed volumes. Overall, removal of SMX was much poorer than TCS and E2, which may due to the hydrophilicity of SMX. At pH 7, the distribution ratio of ionic compounds, $logD_{ow}$, for TCS, E2 and SMX is 4.70, 3.94 and -0.43, respectively. With higher $logD_{ow}$ values, hydrophobic TCS and E2 are more easily adsorbed to solid biochar. The low $logD_{ow}$ value of SMX is indicative of the compound's tendency to remain in water.
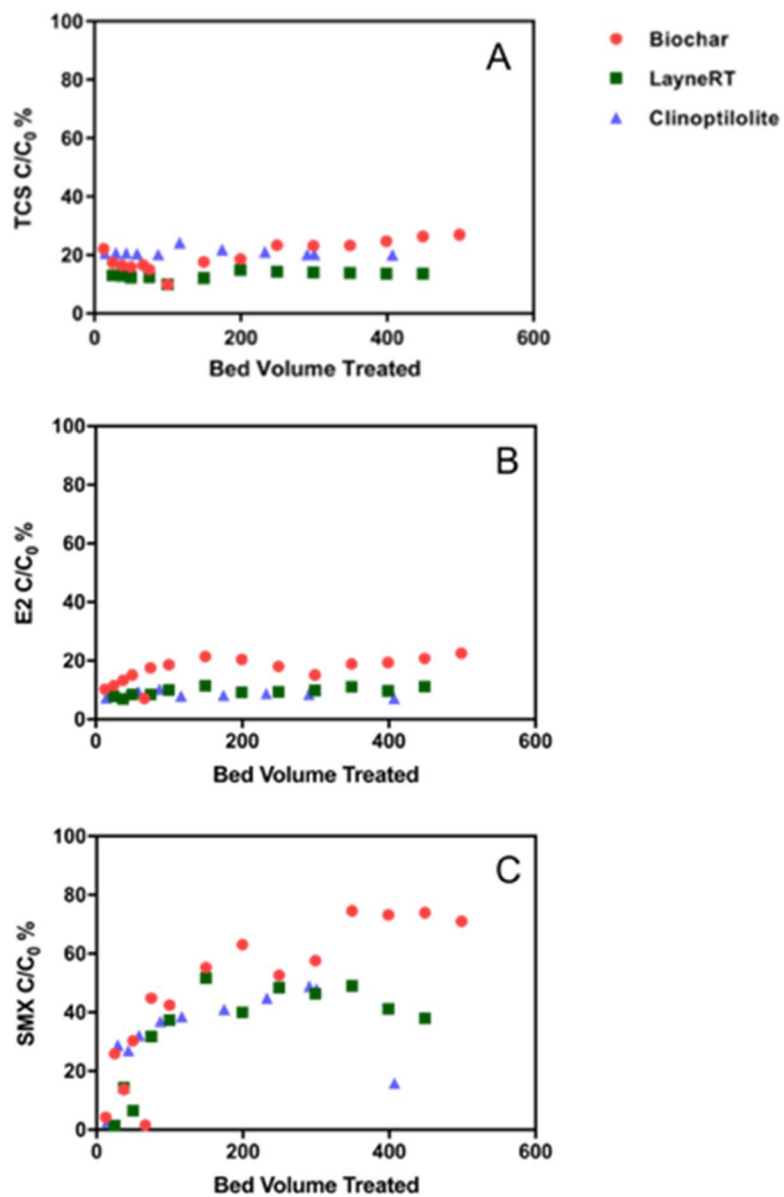
Figure 6.4 A) TCS, B) E2 and C) SMX effluent concentrations relative to influent concentrations (C/C_0) for each column (biochar, LayneRT, and clinoptilolite) as a function of the number of bed volumes treated.

The column system removed 90% of total influent TCS and E2 and 70% of total influent SMX (Figure 6.5). The majority of TCS and E2 was removed by the BC-column. Of the three columns, SMX removal was also greatest in the BC-column. The CUR for

TCS, E2 and SMX was 236 µg/L, 275µg/L and 127µg/L, respectively, the relative order

of which is the same as that observed for biochar adsorption capacities in batch tests. The

L-column retained 9% of influent TCS, 6% of E2, and 20% of SMX, indicating that

LayneRT was able to adsorb micropollutants to a limited extent. Clinoptilolite did not

remove TCS or E2, but removed 2% of influent SMX.
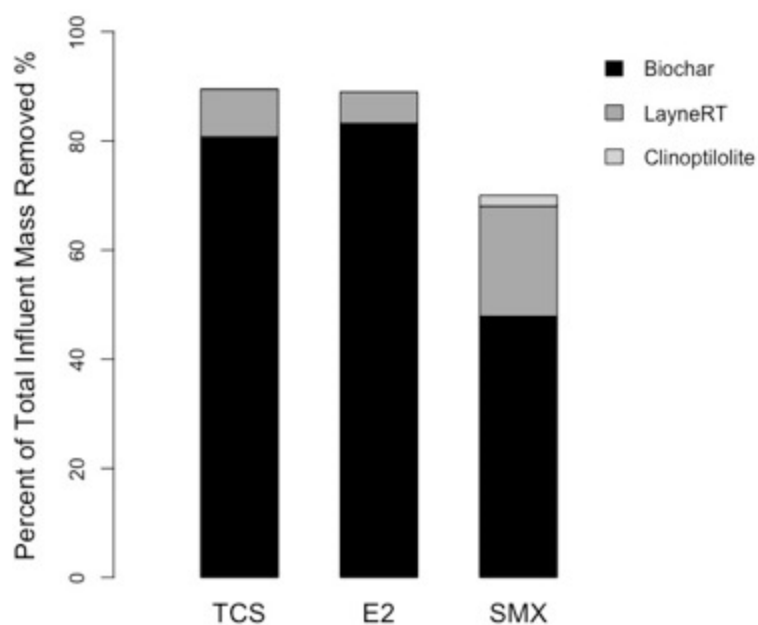
Figure 6.5 Percent of total influent TCS, E2 and SMX mass removed by each media
(bicohar, LayneRT, and clinoptilolite) in the sequential flow-through system in single-
column run.

The use of biochar in the sequential column operation enabled removal of the

majority of TCS, E2 and SMX prior to the nutrient exchange columns. However, since

removal of the more hydrophilic SMX was relatively low, improving removal of

hydrophilic compounds by improving the BC-column performance would be an

important future step.

Nutrient concentrations in the effluent are shown in Figure 6.6. The phosphate concentration increased from an average of 4.85 mg PO_4-P/L to 5.22 mg PO_4-P/L across the BC-column (Figure 6.6), signifying that the biochar media possibly released phosphate. With the more stringent regulation on phosphorous in wastewater treatment discharge, leaching phosphorus from treatment media could be the limitation of the system. However, as shown in this study, putting ion exchange column after can mitigate the phosphorous leaching from biochar column, because almost no phosphorus flowing out from ion exchange columns before breakthrough (Figure 6.7). The C-column had the exact same PO_4-P concentration profile as the L-column because it provided negligible PO_4-P removal, so it reflected the influent PO_4-P profile. The system successfully removed 89.5% of influent PO_4-P (Figure 6.7), all of which was attributed to the L-column.
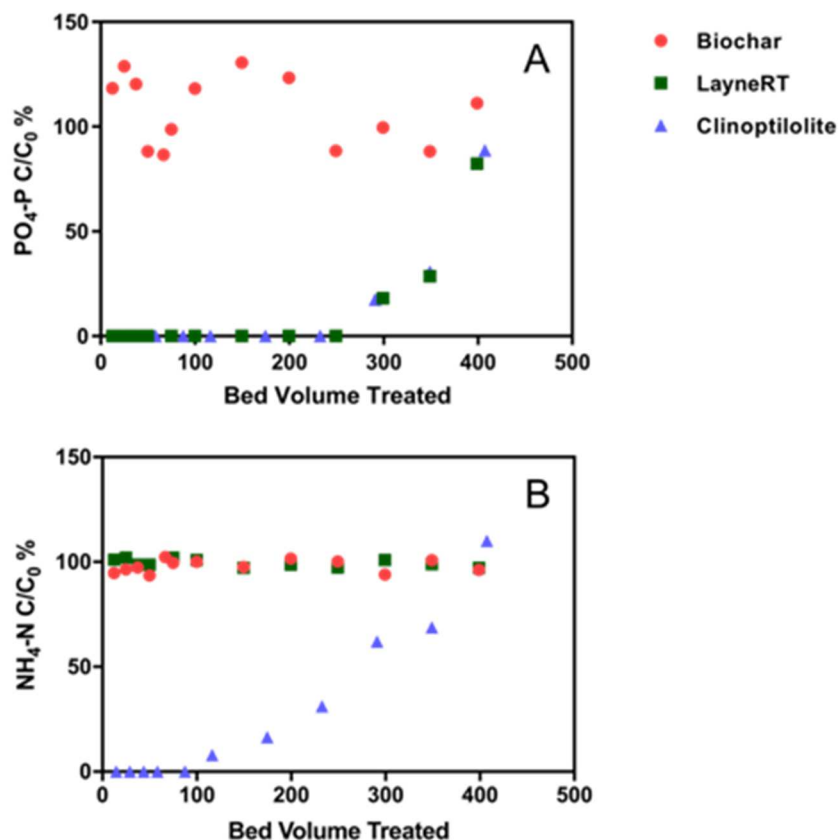
Figure 6.6 A) PO$_4$-P and B) NH$_4$-N effluent concentration relative to influent concentration (C/C$_0$) for each media (biochar, LayneRT, and clinoptilolite) as a function of the number of bed volumes treated in single-column run.

As shown in Figure 6.6, approximately 8% of input NH$_4$-N was removed in the BC-column, and 10% was removed in L-column, but the majority passed through the BC- and L-columns and was mainly removed in the C-column. The C-column achieved an average of 60% of the total influent NH$_4$-N (Figure 6.7), and was exhausted after 40 bed volumes. The removal of NH$_4$-N by BC- and L-columns could be due to a slight inconsistency in NH$_4$-N measurement (standard deviation for multiple measurements was approximately 1.1 mg/L), since the input NH$_4$-N concentration was high (~45 mg/L) compared to the PO$_4$-P concentration in this study.
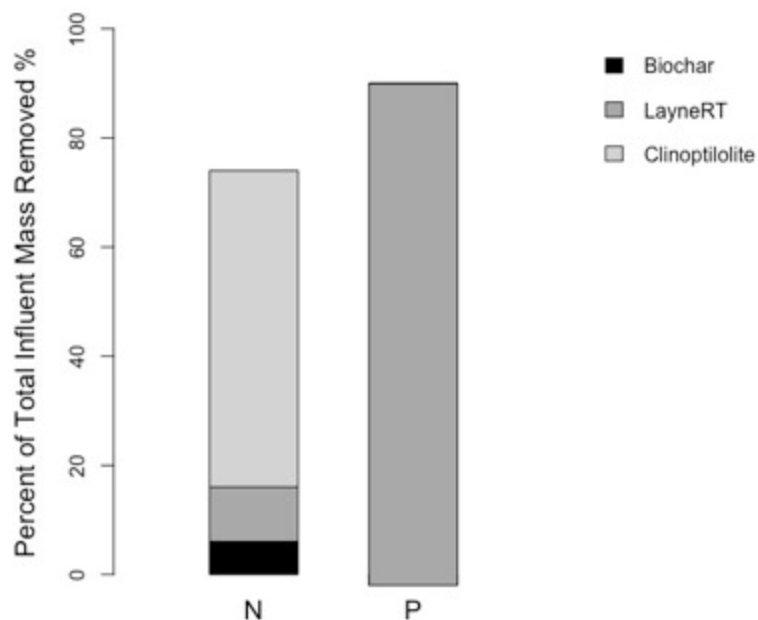
Figure 6.7 Percent of total influent mass of N and P removed by each media (biochar, LayneRT, and clinoptilolite) from the sequential flow-through system in single-column run.

6.4   Conclusions

Biosolids-derived biochar effectively adsorbed TCS and E2, and to a lesser extent, SMX. The presence of nutrient ions in the water significantly increased micropollutant adsorption, which matched the first hypothesis. Nutrient ions were not effectively adsorbed by biochar. Therefore, biosolids-derived biochar has the potential to selectively remove micropollutants from a nutrient-rich stream, such as an anaerobic membrane bioreactor effluent, while leaving the nutrients in the water for subsequent recovery of micropollutant-free nutrient-rich fertilizer products.

To test the second hypothesis, spent biochar was re-pyrolyzed to remove micropollutants. The regenerated biochar was reused for two additional cycles, and the

adsorption capacities for TCS and E2 did not substantially change WRRFs that are equipped with pyrolysis reactors could re-pyrolyze the biochar to remove micropollutants (Ross, et al., 2016) and then reuse the adsorbent biochar without needing an additional acid wash.

The sequential column flow-through system achieved 90% removal of influent TCS and E2, in addition to 70% removal of SMX. The biochar column removed the majority of micropollutants, thereby reducing the chances of micropollutants being adsorbed by ion exchangers. The other benefit of operating the biochar column before ion exchange was that influent nutrients were not efficiently retained by the biochar column, which left a considerable amount of ammonium and phosphate for subsequent recovery. In general, the results matched the third hypothesis. Additionally, biochar leached phosphate which would be a major problem as WRRFs aggressively work to reduce effluent P concentrations. Putting resin columns after biochar mitigates the concern of biochar leaching P. By leveraging micropollutant removal in the biochar column, nutrients can be concentrated in the subsequent ion exchange regenerant for precipitation of recovered struvite with less chance of inclusion of micropollutants in the fertilizer product.

6.5   References

Alvarino, T., Suarez, S., Lema, J.M., Omil, F., 2014. Understanding the removal mechanisms of PPCPs and the influence of main technological parameters in anaerobic UASB and aerobic CAS reactors. J. Hazard. Mater. 278, 506–513. doi:10.1016/j.jhazmat.2014.06.031

APHA, AWWA, WEF, 1998. Standard methods for the examination of water and wastewater, Standard Methods for the Examination of Water and Wastewater.

Behera, S.K., Oh, S.-Y., Park, H.-S., 2010. Sorption of triclosan onto activated carbon, kaolinite and montmorillonite: Effects of pH, ionic strength, and humic acid. J. Hazard. Mater. 179, 684–691. doi:http://dx.doi.org/10.1016/j.jhazmat.2010.03.056

Çalışkan, E., Göktürk, S., 2010. Adsorption characteristics of sulfamethoxazole and metronidazole on activated carbon. Sep. Sci. Technol. 45, 244–255.

Carey, D.E., McNamara, P.J., Zitomer, D.H., 2015. Biochar from Pyrolysis of Biosolids for Nutrient Adsorption and Turfgrass Cultivation. Water Environ. Res. 87, 2098–2106. doi:10.2175/106143015X14362865227391

de Mes, T.Z.D., Kujawa-Roeleveld, K., Zeeman, G., Lettinga, G., 2008. Anaerobic biodegradation of estrogens--hard to digest. Water Sci. Technol. 57, 1177–1182. doi:10.2166/wst.2008.102

Fang, C., Zhang, T., Li, P., Jiang, R., Wang, Y., 2014. Application of magnesium modified corn biochar for phosphorus removal and recovery from swine wastewater. Int. J. Environ. Res. Public Health 11, 9217–37. doi:10.3390/ijerph110909217

Font, R., Fullana, A., Conesa, J., 2005. Kinetic models for the pyrolysis and combustion of two types of sewage sludge. J. Anal. Appl. Pyrolysis 74, 429–438. doi:10.1016/j.jaap.2004.10.009

Fontecha-Cámara, M.A., López-Ramón, M. V, Álvarez-Merino, M.A., Moreno-Castilla, C., 2007. Effect of Surface Chemistry, Solution pH, and Ionic Strength on the Removal of Herbicides Diuron and Amitrole from Water by an Activated Carbon Fiber. Langmuir 23, 1242–1247. doi:10.1021/la062200f

Fukuhara, T., Iwasaki, S., Kawashima, M., Shinohara, O., Abe, I., 2006. Adsorbability of estrone and 17β-estradiol in water onto activated carbon. Water Res. 40, 241–248. doi:http://dx.doi.org/10.1016/j.watres.2005.10.042

Hadi, P., Xu, M., Ning, C., Sze Ki Lin, C., McKay, G., 2015. A critical review on preparation, characterization and utilization of sludge-derived activated carbons for wastewater treatment. Chem. Eng. J. 260, 895–906. doi:10.1016/j.cej.2014.08.088

Hale, S.E., Alling, V., Martinsen, V., Mulder, J., Breedveld, G.D., Cornelissen, G., 2013. The sorption and desorption of phosphate-P, ammonium-N and nitrate-N in cacao shell and corn cob biochars. Chemosphere 91, 1612–1619. doi:10.1016/j.chemosphere.2012.12.057

Hoffman, T.C., Zitomer, D.H., McNamara, P.J., 2016. Pyrolysis of wastewater biosolids significantly reduces estrogenicity. J. Hazard. Mater. 317, 579–584.

Hruska, K., Franek, M., 2012. Sulfonamides in the environment: a review and a case report. Vet Med 57, 1–35.

Jiang, M., Yang, W., Zhang, Z., Yang, Z., Wang, Y., 2015. Adsorption of three pharmaceuticals on two magnetic ion-exchange resins. J. Environ. Sci. 31, 226–234. doi:10.1016/j.jes.2014.09.035

Jung, C., Park, J., Lim, K.H., Park, S., Heo, J., Her, N., Oh, J., Yun, S., Yoon, Y., 2013. Adsorption of selected endocrine disrupting compounds and pharmaceuticals on activated biochars. J. Hazard. Mater. 263 Pt 2, 702–10. doi:10.1016/j.jhazmat.2013.10.033

Kim, E., Jung, C., Han, J., Her, N., Min Park, C., Son, A., Yoon, Y., 2016. Adsorption of selected micropollutants on powdered activated carbon and biochar in the presence of kaolinite. Desalin. Water Treat. 57, 27601–27613.

Kimbell, L., 2017. Biosolids-Derived Biochar for Micropollutant Removal from Wastewater. Marquette University.

Malmborg, J., Magnér, J., 2015. Pharmaceutical residues in sewage sludge: Effect of sanitization and anaerobic digestion. J. Environ. Manage. 153, 1–10. doi:10.1016/j.jenvman.2015.01.041

Mayer, B.K., Baker, L.A., Boyer, T.H., Drechsel, P., Gifford, M., Hanjra, M.A., Parameswaran, P., Stoltzfus, J., Westerhoff, P., Rittmann, B.E., 2016. Total value of phosphorus recovery. Environ. Sci. Technol. 50, 6606–6620.

McCarty, P.L., Bae, J., Kim, J., 2011. Domestic wastewater treatment as a net energy producer - can this be achieved? Environ. Sci. Technol. 45, 7100–6. doi:10.1021/es2014264

McNamara, P.J., Koch, J.D., Liu, Z., Zitomer, D.H., 2016. Pyrolysis of Dried Wastewater Biosolids Can Be Energy Positive. Water Environ. Res. 88, 804–810. doi:10.2175/106143016X14609975747441

Monsalvo, V.M., McDonald, J.A., Khan, S.J., Le-Clech, P., 2014. Removal of trace organics by anaerobic membrane bioreactors. Water Res. 49, 103–112. doi:10.1016/j.watres.2013.11.026

Mota, V.T., Santos, F.S., Amaral, M.C.S., 2013. Two-stage anaerobic membrane bioreactor for the treatment of sugarcane vinasse: Assessment on biological activity and filtration performance. Bioresour. Technol. 146, 494–503. doi:10.1016/j.biortech.2013.07.110

Neale, P.A., Mastrup, M., Borgmann, T., Schäfer, A.I., 2010. Sorption of micropollutant estrone to a water treatment ion exchange resin. J. Environ. Monit. 12, 311–317.

Rashid, M.A., Buckley, D.E., Robertson, K.R., 1972. Interactions of a marine humic acid with clay minerals and a natural sediment. Geoderma 8, 11–27.

Ross, J.J., Zitomer, D.H., Miller, T.R., Weirich, C.A., McNamara, P.J., 2016. Emerging investigators series: pyrolysis removes common microconstituents triclocarban, triclosan, and nonylphenol from biosolids. Environ. Sci. Water Res. Technol. doi:10.1039/C5EW00229J

Samaras, V.G., Stasinakis, A.S., Mamais, D., Thomaidis, N.S., Lekkas, T.D., 2013. Fate of selected pharmaceuticals and synthetic endocrine disrupting compounds during wastewater treatment and sludge anaerobic digestion. J. Hazard. Mater. 244, 259–267. doi:10.1016/j.jhazmat.2012.11.039

Seib, M.D., Berg, K.J., Zitomer, D.H., 2016. Reduced energy demand for municipal wastewater recovery using an anaerobic floating filter membrane bioreactor. Environ. Sci. Water Res. Technol. 2, 290–297. doi:10.1039/C5EW00244C

Sengupta, S., Pandit, A., 2011. Selective removal of phosphorus from wastewater combined with its recovery as a solid-phase fertilizer. Water Res. 45, 3318–3330. doi:10.1016/j.watres.2011.03.044

Takaya, C.A., Fletcher, L.A., Singh, S., Anyikude, K.U., Ross, A.B., 2016. Phosphate and ammonium sorption capacity of biochar and hydrochar from different wastes. Chemosphere 145, 518–527. doi:10.1016/j.chemosphere.2015.11.052

Williams, A.T., Zitomer, D.H., Mayer, B.K., 2015. Ion exchange-precipitation for nutrient recovery from dilute wastewater. Environ. Sci. Water Res. Technol. 1, 832–838. doi:10.1039/C5EW00142K

Wisconsin DNR, 2010. Effluent Standards And Limitations For Phosphorus. US.

Yao, Y., Gao, B., Inyang, M., Zimmerman, A.R., Cao, X., Pullammanappallil, P., Yang, L., 2011. Biochar derived from anaerobically digested sugar beet tailings: characterization and phosphate removal potential. Bioresour. Technol. 102, 6273–8. doi:10.1016/j.biortech.2011.03.006

7   CONCLUSIONS

WRRFs have an essential role in mitigating pollution in environmental waters. They also have potential to produce valuable resources such as fertilizer. In this dissertation, adsorption of nutrients, i.e. orthophosphate and ammonium, and organic micropollutants were studied because these two groups of contaminants are of growing concern in terms of water quality and resource recovery. Specifically, anaerobically treated effluent that contains high nutrient levels can undergo nutrient removal and recovery via ion exchange regeneration followed by struvite precipitation. However, it is important that both the treated water and nutrient-rich fertilizers recovered through this process are free of harmful contaminants such as micropollutants.

While WRRFs are central collection points for micropollutants, they were not designed to remove organic micropollutants. Indeed, biological unit operations are not efficient at removing micropollutants, and anaerobic treatment process in particular are poor at removing micropollutants. Therefore, wide-spread implementation of anaerobic treatment for secondary treatment would likely offer little removal of micropollutants and nutrients.

The overarching goal of this dissertation was to qualitatively and quantitatively assess the adsorptive behavior of neutral and ionic organic micropollutants in terms of their fate and impact during nutrient recovery via ion exchange-regeneration, as well as micropollutant removal using biosolids-derived biochar as a sustainable adsorbent.

7.1 Key findings

The first objective was to assess organic micropollutant's fate and impact on the nutrient removal and recovery process. Ion exchange-regeneration followed with struvite precipitation was employed to remove, concentrate and recover orthophosphate and

ammonium from simulated and real anaerobic treatment effluent. The results demonstrated that ion exchange-regeneration followed by struvite precipitation could effectively remove and recover phosphate and ammonium. The presence of triclosan (TCS), 17β-estradiol (E2), and sulfamethoxazole (SMX) in nutrient-rich waters did not reduce the extent of nutrient exchange and desorption from ion exchangers, but decreased the reaction rate of nutrient exchange. The ammonium-selective clinoptilolite ion exchanger did not adsorb TCS, E2, or SMX, likely due to steric hindrance effect of pores. However, these neutral and anionic micropollutants were able to co-adsorb on phosphate exchangers during exchange of orthophosphate and were desorbed during ion exchanger regeneration. The micropollutants did not precipitate together with struvite, so they do not pose risks in the final solid fertilizer product.

The adsorption/desorption behaviors of the micropollutants indicated that they could accumulate on ion exchangers, which may eventually lead to saturation of the ion exchangers, causing bypass of micropollutants into the ion exchange effluent, which would put additional stress on receiving natural waters. When the micropollutants were present in actual anaerobic wastewater, they did not interfere with nutrient removal and recovery; however, the complex matrix of anaerobic wastewater tended to decrease adsorption of TCS and E2 and increase desorption of TCS and E2 from phosphate-specific exchangers. To avoid co-adsorption as well as release of micropollutants with the ion exchange effluent, other non-selective adsorbents, such as biosolids-derived biochar, could be employed prior to ion exchange to remove micropollutants before recovering nutrients.

The second objective was to evaluate the feasibility and mechanisms of micropollutant adsorption by biosolids-derived biochar. TCS was selected as a representative hydrophobic micropollutant for this work. The influence of pyrolysis temperature, water quality parameters, and biochar properties such as surface charge, functional groups, pore size distribution and surface area on TCS removal and adsorption equilibrium were evaluated. The results demonstrated that acid-conditioned (HCl) biosolids-derived biochar could be a suitable alternative to activated carbon for removing TCS from wastewater at near-neutral pH. Preconditioning of the biochar using acid was essential for TCS adsorption as it increased availability of adsorption sites. Pyrolysis temperature had an influence on the biochar's physical properties, including pore radius, pore volume and surface area. Accordingly, pyrolysis temperature affected TCS adsorption equilibrium at high aqueous-phase concentrations. However, high pyrolysis temperatures do not appear to be necessary considering the low TCS concentrations commonly encountered in environmental applications.

The third objective was to determine the impact of temperature on adsorption equilibrium for a suite of neutral and cationic micropollutants using biosolids-derived biochar as the adsorbent. The thermodynamic parameters were estimated to characterize the spontaneity of adsorption, the adsorption mechanisms, and the adsorbent's binding affinity for the micropollutants. This research demonstrated that biosolids-derived biochar was able to adsorb neutral and cationic compounds, though adsorption of cationic compounds was much less compared to neutral compounds. The extent of adsorption of the neutral micropollutants was positively correlated to micropollutant hydrophobicity as measured by K_{ow}. Increased temperature positively impacted adsorption of the studied

compounds. The estimation of the thermodynamic parameters of adsorption under single-solute conditions indicated that adsorption was endothermic. Moreover, the thermodynamic parameters indicated heterogeneity in the biochar's surface. The binding mechanism for neutral compounds could potentially be dominated by non-specific hydrophobic interactions based on the positive correlation between the change of entropy and log K_{ow}. Under multi-solute conditions, adsorption capacities were suppressed to differing extents, but thermodynamic parameters, such as binding energy and entropy change of adsorption, were not affected by the presence of other solutes.

The fourth objective was to determine the impact of nutrient ions on micropollutant adsorption to biochar, the reusability of biosolids-derived biochar, and its functionality as a pre-polishing step for nutrient ion exchange in a flow-through column system. TCS and E2 were effectively removed by biochar, while SMX was not as readily adsorbed. Nutrient ions increased adsorption of all three micropollutants by biochar. The nutrients were not effectively adsorbed by biochar. Spent biochar was re-pyrolyzed to remove micropollutants, and this regenerated biochar was able to adsorb TCS and E2. The biochar-LayneRT-clinoptilolite flow-through system achieved 90% removal of influent TCS and E2, in addition to 70% removal of SMX. The biochar column removed the majority of micropollutants, thereby reducing the likelihood of micropollutants being adsorbed by ion exchangers. The influent nutrients were not efficiently retained by the biochar column, or even released from biochar, which left ammonium and phosphate for subsequent capturing in their respective selective ion exchanger columns. By leveraging micropollutant removal in the biochar column, nutrients can be concentrated in the

subsequent ion exchange regenerant for precipitation of struvite with less chance of inclusion of micropollutants in the fertilizer product.

7.2   Future work recommendations

This research revealed that neutral and anionic organic micropollutants can potentially have negative impacts on nutrient ion exchange-regeneration process. This finding stems from neutral molecules' interactions with phosphate exchangers via H-bonding and π-interaction, while anionic compounds interact with phosphate exchangers via coulombic attraction. To derive more universal conclusions related to the fate of micropollutants during ion exchange-regeneration, the interactions of cationic or zwitterionic micropollutants with both positively and negatively charged exchangers should be studied. In this dissertation, ion exchange-regeneration experiments were conducted using batch reactors and a single exchange-regeneration cycle. The fate and impact of micropollutants during multi-cycle experiments or long-term operation in continuous flow reactors is recommended to establish the influence of engineering factors, such as flow rates and ion exchanger fouling.

During pyrolysis of the spent biochar adsorbent, micropollutants could be thermochemically degraded or simply volatilized. Methods can be developed to collect emissions from biochar regeneration. Through analyzing the emissions, evaluation of the volatilization potential of the micropollutants and their degradation products should be established to determine if they will have functionality, e.g., estrogenicity. This information is essential to evaluate potential pathways of conversion of waterborne micropollutants to emerging airborne pollutants.

The contribution of each adsorption mechanism to total free energy change for biochar adsorption can be determined through experimental or simulation approaches. Both experimental and simulation methods require thorough characterization of biochar structure to establish quantitative correlations between biochar's surface properties and the binding energy. For example, determination of aromatic carbons via nuclear magnetic resonance can help calculate the contribution of π-interaction to adsorption. With quantitative information on the contribution of mechanisms, improvements in biosolids-derived biochar properties, such as engineering biochar surface functional groups, can be developed to achieve elevated removal efficiency for specific micropollutants.

Appendices

Appendix 3A. Micropollutant structures and physical-chemical properties

TCS, E2 and SMX were selected as representative micropollutants due to their wide range of pK_a and log K_{ow} values. They have been found in anaerobic membrane bioreactor (AnMBR) effluent, with E2 being removed by less than 50% during AnMBR treatment (Monsalvo et al., 2014). The molecular structures, pK_a, and log K_{ow} values for the micropollutants given in Table 3A were obtained from the ChemSpider website. D_{ow} is the octanol-water distribution coefficient, which is pH dependent. The calculation of D_{ow} is shown in eq. 3A.1 (Schwarzenbach et al., 2005):

$$D_{ow} = \alpha_{i,acid} \times K_{ow} \text{ (eq. 3A.1)}$$

where $\alpha_{i,acid}$ is the relative fraction of dissociated anion at a given pH (A^-/HA), which can be calculated using eq. 3A.2 (Sawyer et al., 2003):

$$pH = pK_a + \log[\frac{A^-}{HA}] \text{ (eq. 3A.2)}$$

Table 3A. Molecular structures and physical-chemical properties of the micropollutants tested in this study
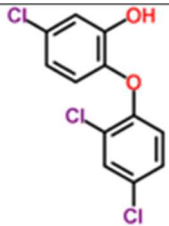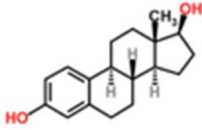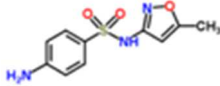
Compound	Molecular Structure	pK_a	log K_{ow}	log D_{ow} at pH 7	log D_{ow} at pH 9
Triclosan (TCS)		7.90	4.76	4.70	3.62
17β-estradiol (E2)		10.79	3.94	3.94	3.93
Sulfamethoxazole (SMX)		5.70	0.89	-0.43	-2.40

Figure 3A illustrates the log concentration of the protonated and deprotonated fractions of TCS, E2, and SMX as a function of solution pH.
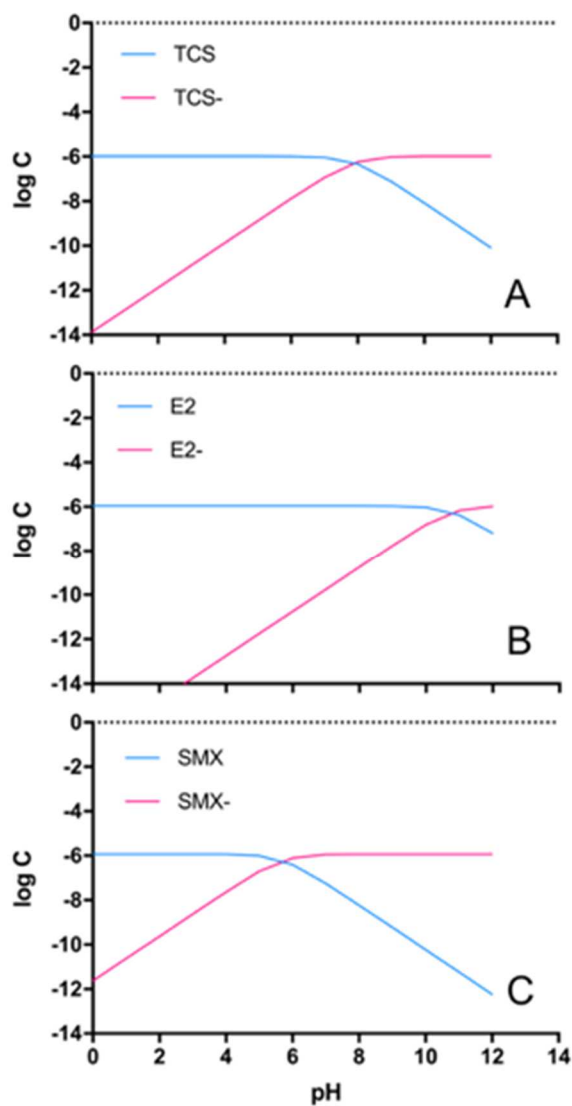
Figure 3A. Log concentration diagrams as a function of pH for A) TCS, B) E2, and C) SMX neutral molecules and dissociated anions.

Appendix 3B. Phosphate and micropollutant mass desorption per gram of ion exchange resin

Resin regeneration was performed using brines containing varied concentrations of NaCl and NaOH, as shown in Tables 3B-1 – 3B-4. The values are the averages for triplicate tests. The regeneration of micropollutants from clinoptilolite was not evaluated as no micropollutants were adsorbed during the ion exchange stage.

Table 3B.1. PO_4-P mass desorption per gram of LayneRT as a function of regenerant brine composition.

% NaOH in brine	% NaCl in brine	P (mg P regenerated/g resin)
2	2	3.27
2	0.5	3.63
2	1	3.79
2	0	3.23
1	2	3.60
1	0.5	3.51
1	1	3.68
0.5	2	3.28
0.5	0.5	3.48
0.5	1	3.47
0	2	0.73

Table 3B.2. Micropollutant mass desorption per gram of LayneRT as a function of regenerant brine composition.

% NaOH	% NaCl	TCS (µg/g resin)	E2 (µg/g resin)	SMX (µg/g resin)
2	2	42.5	50.4	118
2	0.5	12.1	60.3	23.1
2	1	22.5	59.9	78.6
2	0	23.9	5.99	94.8
1	2	13.1	64.0	152
1	0.5	17.0	44.0	141
1	1	22.0	37.6	160
0.5	2	27.4	320	7.77
0.5	0.5	11.9	66.3	11.7
0.5	1	25.1	30.2	155
0	2	13.7	9.81	126

Table 3B.3. PO$_4$-P mass desorption per mass of DOW-HFO-Cu as a function of regenerant brine composition.

% NaOH	% NaCl	P (mg P regenerated/g resin)
2	2.5	3.25
2	0.5	4.05
2	5	3.39
2	0	3.99
1	0.5	3.93
1	5	3.81
1	2.5	3.83
0.1	0.5	3.67
0.1	5	3.27
0.1	2.5	3.69
0	5	0.13

Table 3B.4. Micropollutant mass desorption per gram of DOW-HFO-Cu as a function of regenerant brine composition.

% NaOH	% NaCl	TCS (µg/g resin)	E2 (µg/g resin)	SMX (µg/g resin)
2	2.5	2.25	21.8	150
2	0.5	42.9	5.77	56.4
2	5	46.9	11.9	57.3
2	0	61.1	3.00	71.1
1	0.5	22.9	10.5	61.3
1	5	30.8	31.6	99.1
1	2.5	22.0	1.10	92.0
0.1	0.5	14.5	27.3	3.87
0.1	5	5.63	6.48	76.6
0.1	2.5	23.5	43.2	57.8
0	5	15.2	41.9	7.35

Appendix 3C. LC-MS operation and analysis

Internal standards of 13C-TCS, E1, and 13C-SMX in methanol were added in 2 mL LC-MS vials. The solvent was evaporated before samples were added. The target concentration of the internal standards was 100 µg/L. Filtered water samples were mixed with methanol (50:50) to make 1 mL solutions in the vials. The LC system was plumbed with an online solid phase extraction (SPE) cartridge prior to the chromatography column. A binary gradient of Milli-Q water (Pump A) and 100% HPLC-grade methanol (Pump B) in combination of 99% water + 1% methanol (v/v) (Pump C) was used as the eluent. Pump C began at 1 mL/min for two minutes to load the sample onto the SPE cartridge. Then Pump C eluent was reduced to 0.01 mL/L. Then Pump A and B gradients, which began with 65% methanol at 0.3 mL/min gradient, and increased to 100% methanol within three minutes, were maintained to the 13th minute to unload samples from the SPE cartridge to the chromatography column. Pump C ramped down to 65% methanol and remained to the 14th minute to allow column re-equilibration. The binary eluent flow rate was 0.3 mL/min. The retention time was 8 min for TCS, 7 min for E2, and 5 min for SMX. Sample injections of 10 µL were passed through a Phenomenex[®] (Torrance, CA) Strata™-X reversed phase functionalized polymeric sorbent in an online SPE cartridge and a Luna 3u C18 reverse-phase column. The MS detection methods of TCS, E2, SMX and their internal standards are listed in Table 3C.

Table 3C. Mass spectrometry operation parameters for micropollutants and 13C-labeled internal standards. For all analyses, the acquisition mode was used for ion monitoring (SIM) and the ionization method was electrospray ionization (ESI).

Compound	m/z	Method detection limit (µg/L)
TCS	287	8
13C-TCS	299	NA[a]
E2	271	8
E1	269	NA[a]
SMX	254	9
13C-SMX	260	NA[a]

NA[a] These compounds were used as internal standards, so the method
   detection limit is not applicable

Appendix 3D. Calculations of exchange or adsorption capacity and percent recovery

The mass of nutrients or micropollutants adsorbed per mass of ion exchanger (Q_e) was calculated using eq. 3D.1:

$$Q_e = \frac{(C_0 - C_e) \times V_{feed}}{M} \text{ (eq. 3D.1)}$$

where C_0 is the initial concentration of NH$_4$-N (mg/L), PO$_4$-P (mg/L), or micropollutants (μg/L); C_e is the concentration at equilibrium; V_{feed} is the volume of feed water (L); and M is the mass of ion exchanger (g).

Percent recovery (R) was calculated using eq. 3D.2:

$$R = \frac{C_{reg} \times V_{reg}}{(C_0 - C_e) \times V_{feed}} \times 100\% \text{ (eq. 3D.2)}$$

where C_{reg} is the concentration of NH$_4$-N (mg/L), PO$_4$-P (mg/L), or micropollutants (μg/L) in the regeneration solution; and V_{reg} is the volume of regeneration solution.

Appendix 3E. Modeling of nutrient removal kinetics

Nutrient removal kinetics were modelled as pseudo-second order reactions (which demonstrated the best fit for the data), using eq. 3E.1 (Ho, 2006; Ho and McKay, 1999):

$$\frac{1}{q_t} = \frac{1}{kq_e^2} \times \frac{1}{t} + \frac{1}{q_e} \text{ (eq. 3E.1)}$$

where t is time (min), q_t is the total adsorbed nutrient amount per unit mass of ion exchanger at time t (mg/g), Q_e is the total adsorption at equilibrium, and k is the pseudo-second order reaction rate constant, obtained by plotting $1/Q_e$ versus $1/t$.

Appendix 3F. Response surface methodology (RSM) analysis

The data were fit using first and second order linear regression to explore potential correlations between independent variables, i.e., NaCl and NaOH concentration, versus percent micropollutant desorption. First and second order regression equations are represented in eq. 3F.1 and 3F.2, respectively:

$$R_{MP\ desorption} = \beta_1 x + \beta_0 + \epsilon \text{ (eq. 3F.1)}$$
$$R_{MP\ desorption} = \beta_1 x_1 + \beta_2 x_2 + \beta_{12} x_1 x_2 + \beta_0 + \epsilon \text{ (eq. 3F.2)}$$

where x_i is NaOH or NaCl concentration, β_i is the regression coefficient, which denotes the effect of independent variables to the response variable, and ϵ is the error term.

Appendix 3G. Nutrient removal: time to equilibrium

      To determine the time to equilibrium for nutrient exchange reactions, clinoptilolite was added at a concentration of 10 g/L to the feed water, as described in the main text. LayneRT and DOW-HFO-Cu were added at 1g/L. Samples were collected over time. Phosphate and ammonium were measured using the standard methods (APHA et al., 1998). Nutrient ions concentration remaining in water (mg/L) versus time (min) was plotted, as shown in Figure 3G. The time to equilibrium was determined to be 4 days. The linear fitting parameters using pseudo-second order kinetics are listed in Table 3G.
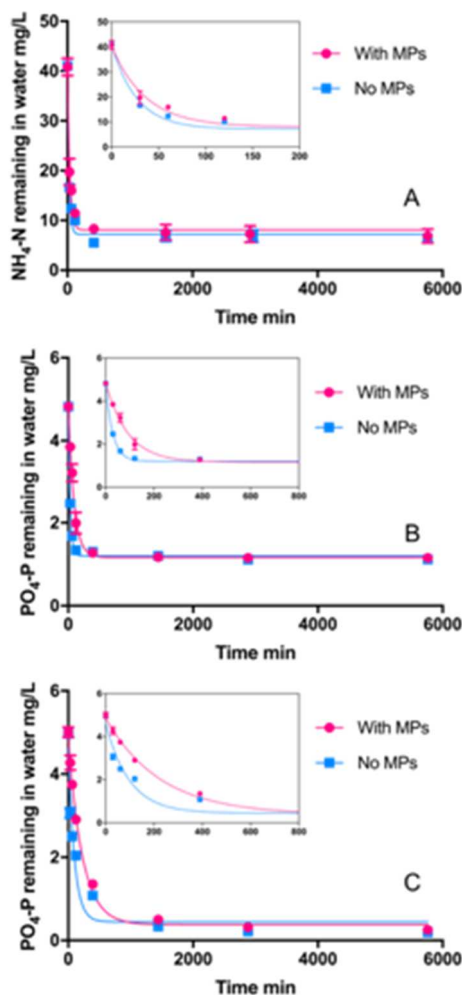
Figure 3G: Nutrient removal for: A) NH_4-N removal by clinoptilolite, B) PO_4-P removal by LayneRT, and C) PO_4-P removal by DOW-HFO-Cu with and without micropollutants (MPs). The insets show the early part of the curve, characterized by more rapid changes in nutrient concentrations as a function of time. The data points represent average results and error bars show ± 1 standard deviation of triplicate experiments.

Table 3G. Averaged fitting parameters of linearized nutrient exchange kinetic curves

Media / Nutrient	With Micropollutants			Without Micropollutants		
	Slope $(1/kQ_e^2)$	Intercept $(1/(Q_e))$	R^2	Slope $(1/kQ_e^2)$	Intercept $(1/(Q_e))$	R^2
Clinoptilolite/NH_4-N	5.558	0.2973	0.9916	3.685	0.2872	0.9789
LayneRT/PO_4-P	24.21	0.2501	0.9833	4.595	0.2761	0.9472
DOW-HFO-Cu/PO_4-P	36.67	0.1951	0.9994	9.469	0.2241	0.9644

Appendix 3H. Ion exchanger surface zeta potential

Ion exchangers were ground to fine powder (<20 μm diameter) in order to make diluted suspensions. The solution pH was then adjusted with HCl or NaOH. The zeta potential was immediately measured, results of which are shown in Figure 3H.
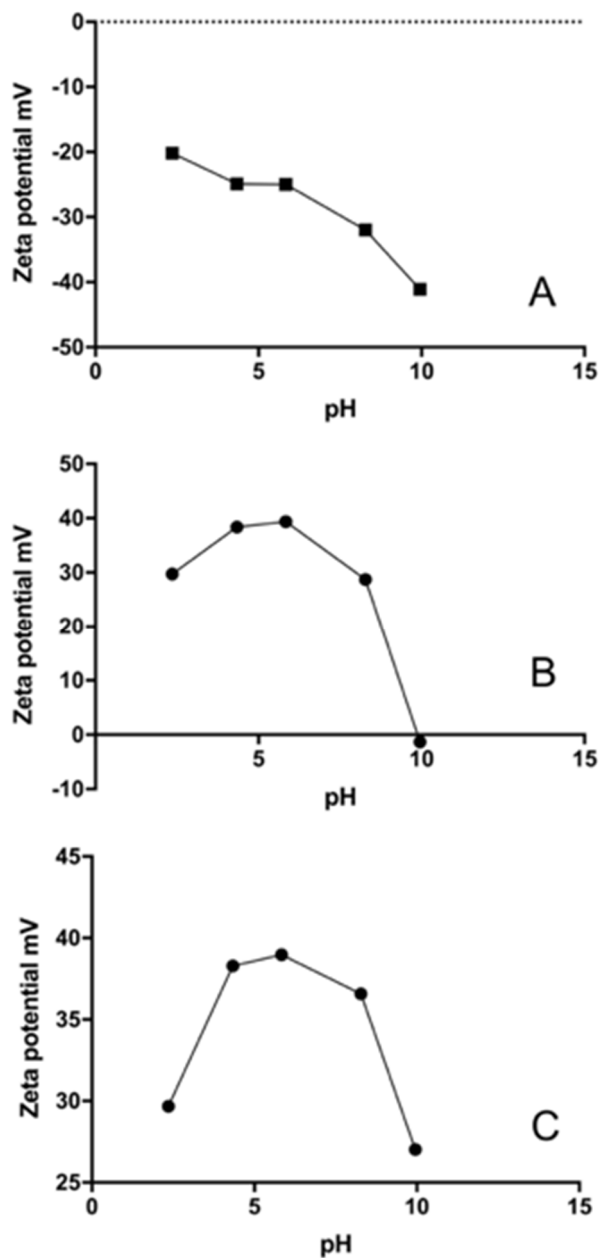
Figure 3H. Zeta potential of the ion exchangers as a function of solution pH, A) clinoptilolite, B) LayneRT, and C) DOW-HFO-Cu.

Appendix 3I. Pore size analysis

Pore size distribution of ion exchangers was calculated from nitrogen/ion exchanger adsorption isotherms by applying the Density Functional Theory (DFT) method using Quantachrome® ASiQwin™ (Quantachrome Instruments, FL) data analysis software (Landers et al., 2013; Quantachrome Instruments, 2010). The change in volume of the spheres dV(r) is a function of the size distribution; therefore, dV(r) is used to represent the frequency of occurrence of a given size (Rathbun et al., 1971). The sharp peak in each figure indicates the mode of half pore width. Gas adsorption measurement was performed using an AutoSorb Gas sorption analyzer from Quantachrome®.
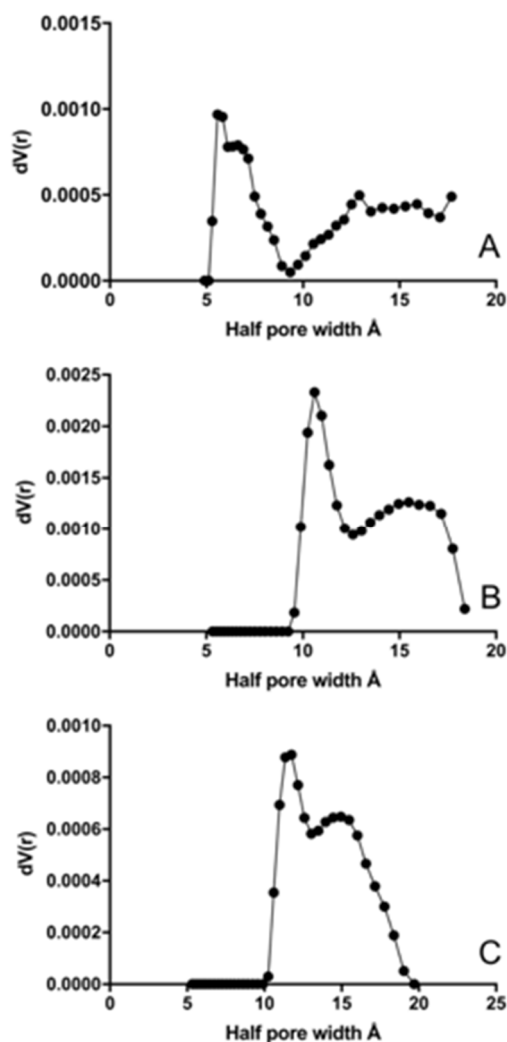
Figure 3I. Pore size distribution of A) clinoptilolite, B) LayneRT, and C) DOW-HFO-Cu, with mode pore size shown as the sharpest pea

Appendix 3J. Nutrient exchange isotherms

Figure 3J shows ion exchange isotherms for NH$_4$ and PO$_4$, with and without micropollutants present in the feed water. The ammonium exchange isotherms are fit with a Langmuir model, while the phosphate exchange data was best fit using an empirical sigmoidal isotherm model (Type D) (Limousin et al., 2007).
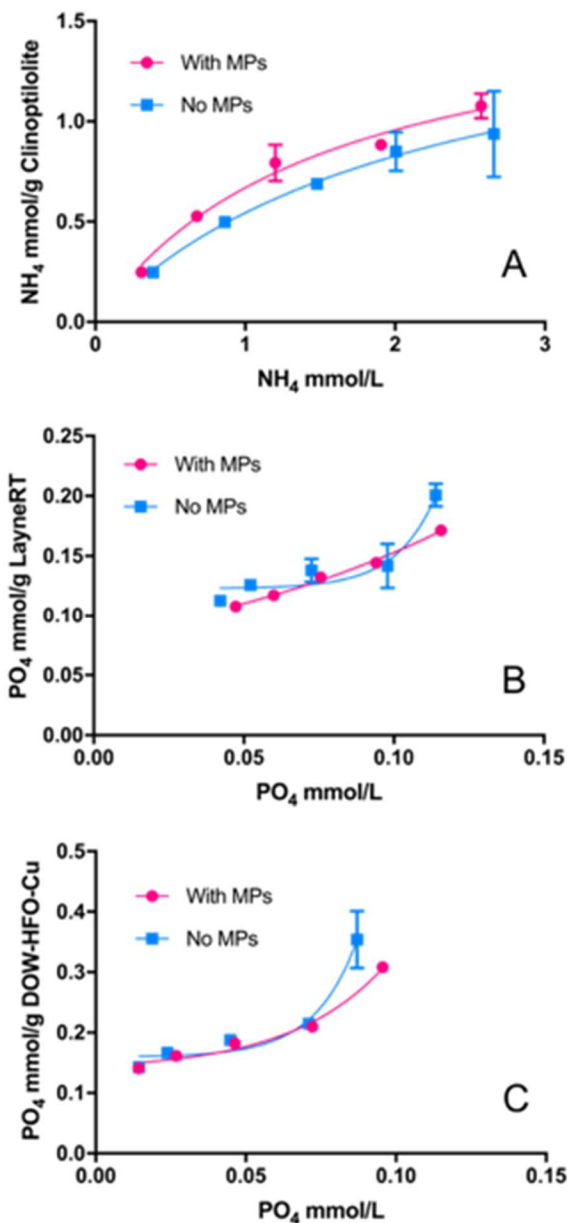
Figure 3J. Nutrient exchange isotherms with and without micropollutants (MPs, ~300 µg/L each TCS, E2, and SMX in the feed water). A) NH$_4$ exchange onto clinoptilolite, B) PO$_4$ exchange onto LayneRT, and C) PO$_4$ exchange onto DOW-HFO-Cu. The data points represent average results and error bars show ± 1 standard deviation of triplicate experiments.

Appendix 3K. Scanning electron microscopy (SEM) imaging

The SEM images of the ion exchangers shown in Figure 3K indicated that phosphate resins have a more homogeneous surface than the natural clinoptilolite. The crack in LayneRT is due to drying of the resin.
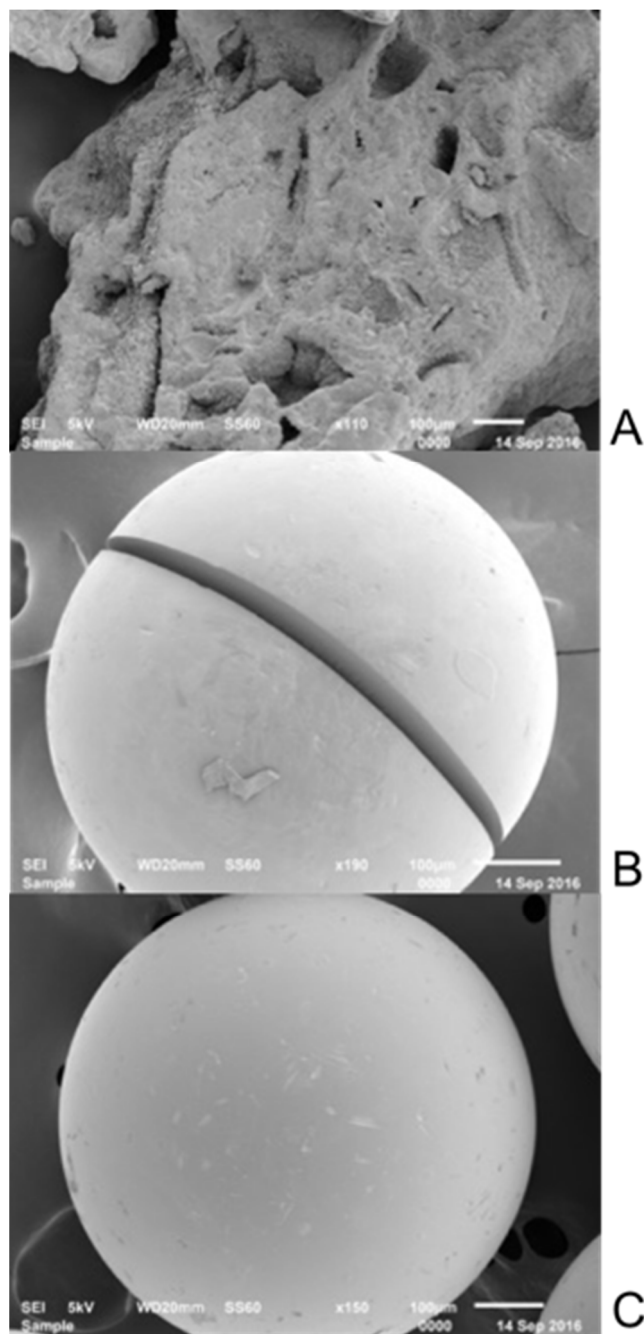
Figure 3K. SEM images of A) clinoptilolite, B) LayneRT, and C) DOW-HFO-Cu.

Appendix 3L. Correlation statistics

Table 3L shows statistics for the second order regression. The independent variables are percent concentrations of NaCl and NaOH in the regeneration brine and the dependent variable is percent desorption of each micropollutant from LayneRT resin or DOW-HFO-Cu resin. The regression was performed in R.

Table 3L. Second order regression statistics (p-values are shown) for the correlation between NaCl and NaOH concentrations in LayneRT or DOW-HFO-Cu regeneration brine and micropollutant percent desorption.

	LayneRT			DOW-HFO-Cu		
	TCS	E2	SMX	TCS	E2	SMX
Intercept	0.08	0.71	0.94	0.19	0.31	0.87
NaCl	0.80	0.79	0.58	0.24	0.30	0.10
NaOH	0.89	0.61	0.42	0.41	0.49	0.19
NaCl*NaOH	0.27	0.91	0.80	0.74	0.93	0.67
$(NaCl)^2$	0.79	0.61	0.73	0.21	0.39	0.14
$(NaOH)^2$	0.87	0.55	0.46	0.76	0.61	0.41
Adjusted R^2	0.02	-0.43	-0.30	0.17	0.1197	0.39

Appendix 3M. Water quality parameters for the belt filter press filtrate sample from anaerobically digested wastewater sludge

Table 3M shows the water quality parameters of the filtrate sample, including pH, chemical oxygen demand (COD), total organic carbon (TOC), and total suspended solids (TSS).

Table 3M. Belt filter press sample for digested sludge filtrate qualities

pH	COD (mg/L)	TOC (mg/L)	TSS (mg/L)
7.49	50	88	12

Appendix 3N. Appendix References

APHA, AWWA, WEF, 1998. Standard methods for the examination of water and wastewater, Standard Methods for the Examination of Water and Wastewater.

Ho, Y.S., 2006. Second-order kinetic model for the sorption of cadmium onto tree fern: A comparison of linear and non-linear methods. Water Res. doi:10.1016/j.watres.2005.10.040

Ho, Y.S., McKay, G., 1999. Pseudo-second order model for sorption processes. Process Biochem. 34, 451–465. doi:10.1016/S0032-9592(98)00112-5

Landers, J., Gor, G.Y., Neimark, A. V, 2013. Density functional theory methods for characterization of porous materials. Colloids Surfaces A Physicochem. Eng. Asp. 437, 3–32.

Limousin, G., Gaudet, J.P., Charlet, L., Szenknect, S., Barthès, V., Krimissa, M., 2007. Sorption isotherms: A review on physical bases, modeling and measurement. Appl. Geochemistry 22, 249–275. doi:10.1016/j.apgeochem.2006.09.010

Monsalvo, V.M., McDonald, J.A., Khan, S.J., Le-Clech, P., 2014. Removal of trace organics by anaerobic membrane bioreactors. Water Res. 49, 103–112. doi:10.1016/j.watres.2013.11.026

Pore size analysis by gas adsorption and the density functional theory – Quantachrome Instruments [WWW Document], 2010.

Rathbun, R.E., Kennedy, V.C., Culbertson, J.K., 1971. Transport and dispersion of fluorescent tracer particles for the flat-bed condition: Rio Grande conveyance channel, near Bernardo, New Mexico. US Government Printing Office.

Sawyer, C.N., McCarty, P.L., Parkin, G.F., 2003. Chemistry for environmental engineering and science.

Schwarzenbach, R.P., Gschwend, P.M., Imboden, D.M., 2005. Environmental organic chemistry. John Wiley & Sons.

Appendix 4A. Triclosan structure and physical-chemical properties

The triclosan molecule, shown in Figure 4A, is a trichlorinated binuclear aromatic that is classified as a pesticide and antimicrobial drug (Halden and Paull, 2005). Triclosan has a pKa value of 7.9. The log K_{ow} value of 4.76 suggests that the compound is hydrophobic. The vapor pressure of 4.65E-06 mm Hg indicates it is characterized by low volatility.
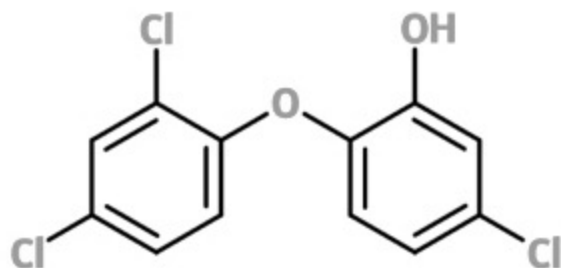
Figure 4A. Triclosan chemical structure

Appendix 4B. Kinetics studies

To determine the adsorption equilibrium capacity, 600°C HCl-biochar was added at a concentration of 0.4 g/L to Milli-Q water spiked with triclosan at an initial concentration of approximately 130 µg/L. Samples were taken over time and were quantified using the LC-MS. The results are shown in Figure 3B. The equilibrium time was determined to be 24 hours, as indicated by less than 5% change in concentration for consecutive samples.
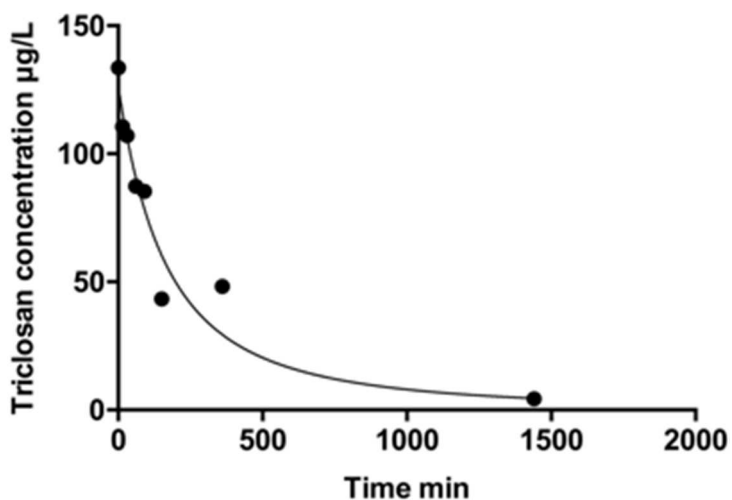
Figure 4B. Triclosan adsorption kinetics curve

Appendix 4C. LC-MS operation

Filtered water samples were mixed with methanol (50/50) in 2 mL amber vials. A binary gradient of Milli-Q water and 100% HPLC-grade methanol was used as the eluent. The method described by Ross et al. (2016) was modified and applied. The gradient began at 80% methanol, raised to 100% methanol at 8 minutes, ramped down to 80% methanol from 8 to 9 minutes and remained at 80% methanol to 13 minutes to allow column re-equilibration. The eluent flow rate was 0.4 mL/min. Sample injections of 20 µL were passed through a Phenomenex® (Torrance, CA, USA) Luna 3u C18 reverse-phase column (150×3 mm, 100Å pore size). Triclosan was detected in mass-spectrometry with negative electrospray ionization (ESI⁻) at a mass-to-charge (*m/z*) ratio of 287.

Appendix 4D. FT-IR spectra of HCl, NaOH, and Milli-Q water treated biochar

Biochar, pyrolyzed at 600°C and pretreated with HCl, NaOH or Milli-Q water, was ground to fine powder (<10 µm). The resulting FT-IR spectra of the different biochars is shown in Figure 4D. Variability observed in the spectra may be due to the amorphous nature of biosolids-derived biochar.
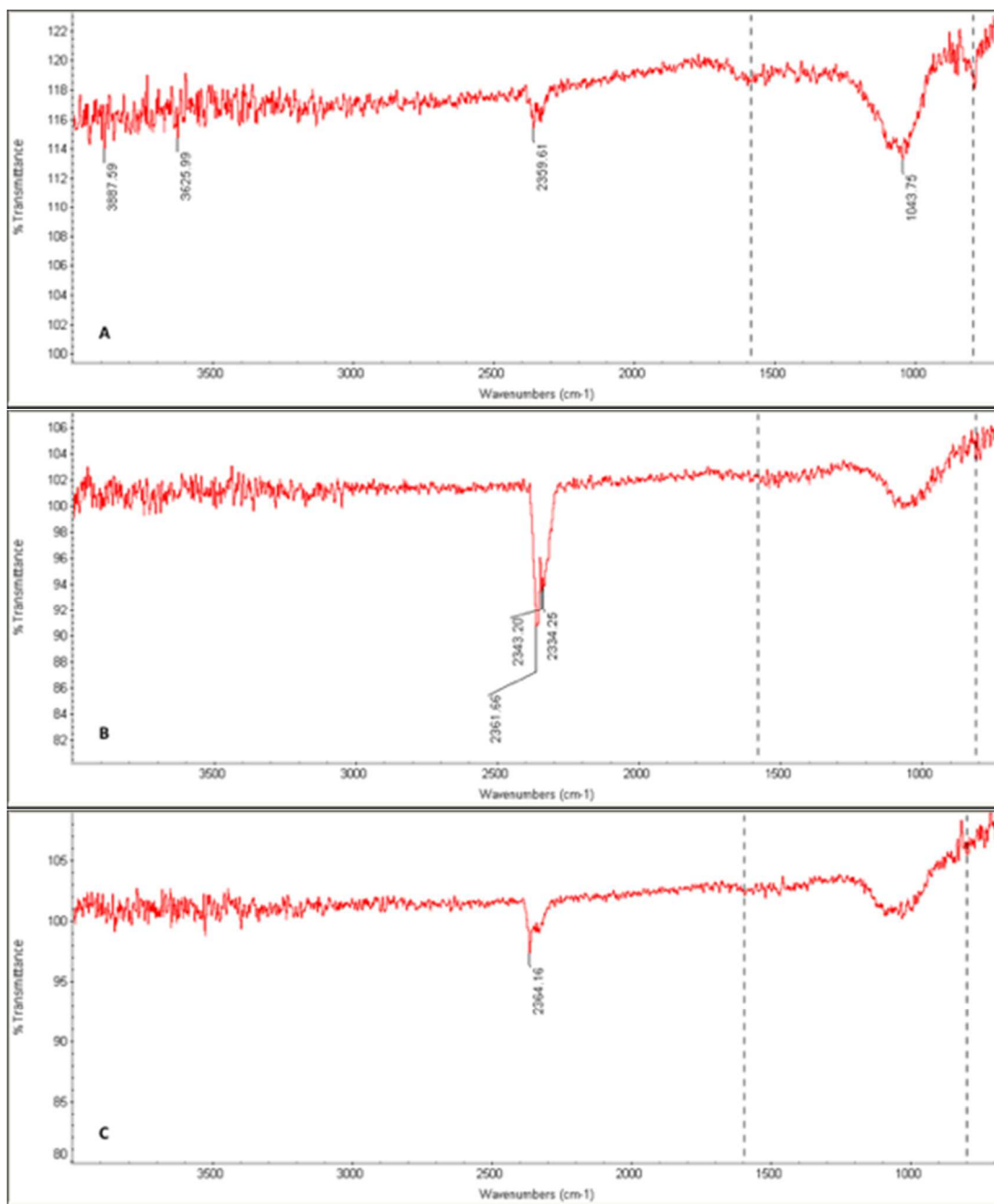
Figure 4D. FT-IR spectra of biochar produced at 600˚C, treated with A) HCl, B) NaOH, and C) Milli-Q water.

Appendix 4E. Biochar zeta potential

Biochar, pyrolyzed at 600°C and pretreated with HCl, NaOH or Milli-Q water, was ground to fine powder (<10 μm). Approximately 0.01 g of biochar powder was suspended in 40 mL of Milli-Q water. The solution pH was then adjusted with HCl or NaOH. The zeta potential was immediately measured using a Malvern Zetasizer Nano ZS (Malvern Instruments Ltd, MA, USA). Results are shown in Figure 4E.
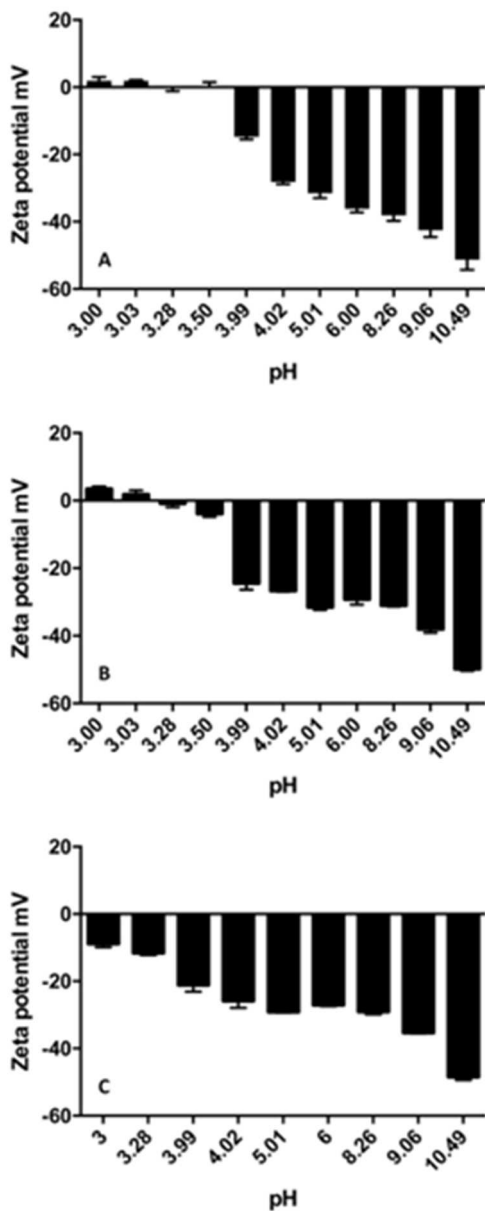
Figure 4E. Zeta potentials of biochar produced at 600°C, pretreated with A) HCl, B) NaOH, and C) Milli-Q water.

Appendix 4F. Isotherm fitting

Table 4F. Isotherms of HCl-biochar produced at multiple temperatures and activated carbon fitted with linear, Langmuir and Freundlich models.

Isotherm model	Equation	Parameter	Sorbent					
			300°C	500°C	600°C	700°C	800°C	Activated carbon
Linear	$Q_e = AC_e + B$	A	0.345	3.09	2.40	4.82	8.29	30.0
		B	120	190	237	153	332	1440
		R^2	0.05	0.94	0.76	0.92	0.86	0.88
Langmuir	$Q_e = \dfrac{Q_{max}K_L C_e}{1 + K_a C_e}$	Q_{max} (x10^4)	0.51	9.02	5.70	1.44	4.42	1.50
		K_L	0.04	0.01	0.02	0.04	0.20	0.03
		R^2	0.07	0.87	0.90	0.76	0.98	0.97
Freundlich	$Q_e = K_f C_e^n$	K_f	56.5	43.2	62.0	62.9	254	554
		n	0.22	0.54	0.45	0.46	0.30	0.44
		R^2	0.06	0.91	0.84	0.85	0.98	0.93

Appendix 4G. Treated wastewater effluent qualities

Table 4G. Treated municipal wastewater effluent qualities

pH	COD (mg/L)	TOC (mg/L)	Turbidity (NTU)	TSS (mg/L)
7.2	BD*	70	2.1	4.6

*: BD: below detection. Detection limit: 125 mg/L

Appendix 4H. Impact of pyrolysis temperature on biochar pore properties

Pyrolysis temperature of biosolids has an influence on the biochar's physical properties, such as pore radius, pore volume and surface area. Pore radius and volume data for biochar were generated via the density functional theory (DFT) method, and surface area was obtained from multi-point BET isotherm through gas sorption analysis.

Figure 4H shows pore size distribution with pore radius (half pore width) for biochar produced from 500 to 800˚C. All of these biochars contained micropores (r<10Å) and mesopores (r between 10-250Å), which is in agreement with previous studies stating that micropores constitute a pore network while mesopores connect pore networks to the biochar surface (Tseng and Tseng, 2006; Xiao and Pignatello, 2015). The minimum critical TCS diameter is 8Å, which can be much less than biochar's pore aperture. Therefore, steric hindrance potentially happens when TCS diffuses deeper into micropore networks, but is less likely to happen when TCS molecules diffuse into pore openings on the biochar surface. Pore radii of biochar produced at 500 and 700˚C (Figure 3HA and 3HB) were no more than 20Å, while 600 and 800˚C biochars had wider spread within the mesopore range.
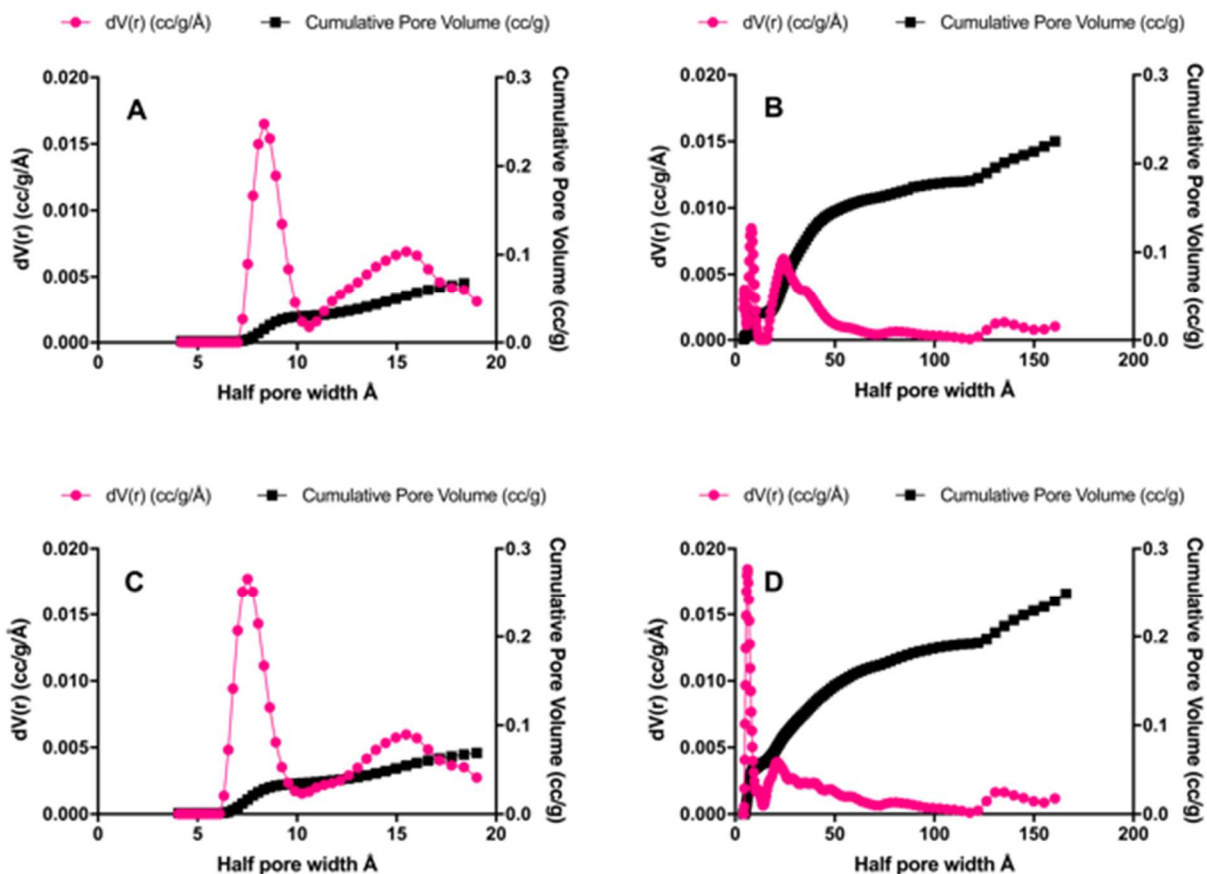
Figure 4H. Pore volume distribution curves for biochar produced at A) 500˚C, B) 600˚C, C) 700˚C and D) 800˚C. The pink circle is the differential volume for pore radius (half pore width) change. The black square is the cumulative pore volume.

The most frequent pore radius value corresponds to the highest peak of differential pore volume distribution (Figure 4H). Table 4H shows the most frequently occurring pore radii of all tested biochars, which generally decreased as pyrolysis temperature increased. The most freequently occuring pore radii of biochar were less than 10 Å for all pyrolysis conditions, indicating that a large portion of biochar pores are micropores (Tseng and Tseng, 2006).

Table 4H shows the values of all parameters from the biochar analysis. The existence of larger mesopores in the 600˚C biochar in comparison to the 500 and 700˚C biochars leads to greater cumulative pore volume of 600˚C biochar than the 500 and 700˚C chars. However, cumulative volume in the 600˚C biochar was smaller than the 800˚C biochar.

The BET surface areas of the biochar are in agreement with the evolution of the cumulative pore volume. For the development of pore properties at temperatures <700˚C, heterogeneity of the feedstock biosolids can possibly be the limiting factor. Even though there is fluctuation at 600-700˚C, 800˚C increased biochar surface area. The fluctuation occurring at 600-700˚C is reflected by the TCS adsorption isotherm parameters. The

difference between the K_f and n values of 600 and 700 ˚C was not as drastic as pore property differences. Accordingly, in addition to pore properties, other factors such as aromaticity of biochar, which evolves with pyrolysis temperature (Wang et al., 2012), affect TCS adsorption at 600-700˚C.

Table 4H. Biochar surface area, pore properties, and TCS adsorption parameters as a function of pyrolysis temperature

	500˚C	**600˚C**	**700˚C**	**800˚C**
Pore radius (mode) Å	8.34	8.05	7.52	6.12
Cumulative pore volume cm³/g	0.07	0.23	0.07	0.25
BET surface area m²/g	141	174	141	221
Freundlich parameter K_f	43.2	62.0	62.9	254
Freundlich parameter n	0.54	0.45	0.46	0.30

Appendix 4I. Appendix references

Halden, R.U., Paull, D.H., 2005. Co-occurrence of triclocarban and triclosan in U.S. water resources. Environ. Sci. Technol. 39, 1420–1426. doi:10.1021/es049071e

Ross, J.J., Zitomer, D.H., Miller, T.R., Weirich, C.A., McNamara, P.J., 2016. Emerging investigators series: pyrolysis removes common microconstituents triclocarban, triclosan, and nonylphenol from biosolids. Environ. Sci. Water Res. Technol. doi:10.1039/C5EW00229J

Tseng, R.-L., Tseng, S.-K., 2006. Characterization and use of high surface area activated carbons prepared from cane pith for liquid-phase adsorption. J. Hazard. Mater. 136, 671–680. doi:10.1016/j.jhazmat.2005.12.048

Wang, T., Camps Arbestain, M., Hedley, M., Bishop, P., 2012. Chemical and bioassay characterisation of nitrogen availability in biochar produced from dairy manure and biosolids. Org. Geochem. 51, 45–54. doi:10.1016/j.orggeochem.2012.07.009

Xiao, F., Pignatello, J.J., 2015. Interactions of triazine herbicides with biochar: Steric and electronic effects. Water Res. 80, 179–188. doi:10.1016/j.watres.2015.04.040

Appendix 5A. LC-MS operation and analysis

Internal standards of benzyldimethyldodecylammonium chloride (BAC-C12), licarbazepine (L-CBZ), estrone (E1), and 13C-TCS methanol stock solutions were added in 2 mL LC-MS vials, separately for single-solute experiments and all together for multi-solute experiments. The solvent was evaporated before samples were added. The target concentration of the internal standards was 100 μg/L. Filtered water samples were mixed with methanol (50:50) to make 1 mL solutions in the vials.

For BAC-C10 and TCS, a binary gradient of Milli-Q water (Pump A) and 100% HPLC-grade methanol (Pump B) was used as the eluent. An isocratic flow of 0.4 mL/min (4% Pump A+96% Pump B) was maintained for 10 min. Sample injection was 5 μL.

For CBZ, a binary gradient of Milli-Q water (Pump A) and HPLC-grade acetonitrile in combination of 0.1% formic acid (v/v) (Pump B) was the eluent. Pump B started at 20% and ramped up to 95% at 9 min. The gradient maintained for 1 min and decreased to 20% at the 12th min. The binary eluent flow rate was 0.3 mL/min. Sample injection volume was 10 μL.

For E2 and EE2, the eluents were Milli-Q water (Pump A) and 100% HPLC-grade methanol (Pump B). Pump B started at 65% and ramped up to 85% at the 8th min. The gradient maintained for 5 min and decreased to 35% at the 15th min. The binary eluent flow rate was 0.4 mL/min. Sample injection volume was 15 μL.

All samples were passed through a Phenomenex$^{®}$ (Torrance, CA) Luna 3u C18 reverse-phase column.

The MS detection limits of BAC-C10, CBZ, E2, EE2, TCS and their internal standards are listed in Table 5A. Recovery of tested compounds was 70 – 130%.

Table 5A. Mass spectrometry operation parameters for micropollutants and internal standards. For all analyses, the acquisition mode was used for ion monitoring (SIM) and the ionization method was electrospray ionization (ESI).

Compound	m/z	Retention time	Internal standard	m/z	Method detection limit (μg/L)
BAC-C10	276	1.4	BAC-C12	304	5
CBZ	237	7.5	L-CBZ	255	4
E2	271	4.2	E1	269	6
EE2	295	4.3			12
TCS	287	2.9	13C-TCS	299	8

Appendix 5B. Isotherm fitting parameters for micropollutants under single-solute conditions

Adsorption equilibrium data was fit with linear, Langmuir and Freundlich isotherms, due to the isotherms' application for low-concentration (< mg/L) adsorption. As Table 4B shows, K, K_L, and K_f values are partitioning coefficients for linear, Langmuir and Freunlich isotherms, respectively. The portioning coefficients are important because of their relationship with thermodynamic equilibrium coefficients.

Table 5B. Isotherm parameters for micropollutants under single-solute conditions

Compound	Isotherm	Parameter	4°C	25°C	35°C	50°C
BAC-C10	Linear	K	0.469	0.359	0.569	1.03
		B	72.63	471.70	503.40	239.70
		R^2	0.923	0.978	0.711	0.972
CBZ	Linear	K	0.59	0.822	0.715	1.05
		B	154.70	120.90	294.20	269.30
		R^2	0.908	0.929	0.925	0.999
E2	Freundlich	K_f	23.35	40.95	63.76	105.70
		n	0.55	0.57	0.51	0.46
		R^2	0.856	0.949	0.954	0.9653
	Langmuir	Q_m	1885	9797	3863	7135
		K_L	0.0022	0.0005	0.0058	0.0033
		R^2	0.856	0.900	0.932	0.936
EE2	Linear	K	2.10	4.00	3.80	4.37
		B	244.40	-31.68	725.20	836.70
		R^2	0.987	0.992	0.997	0.966
TCS	Freundlich	K_f	19.35	26.97	207.30	107.90
		n	0.73	0.71	0.43	0.58
		R^2	0.974	0.866	0.985	0.959
	Langmuir	Q_m	5438	26784	3646	8340
		K_L	0.0009	0.0002	0.0102	0.0018
		R^2	0.955	0.856	0.945	0.840

Appendix 5C. Isostere curves for micropollutants under single-solute conditions
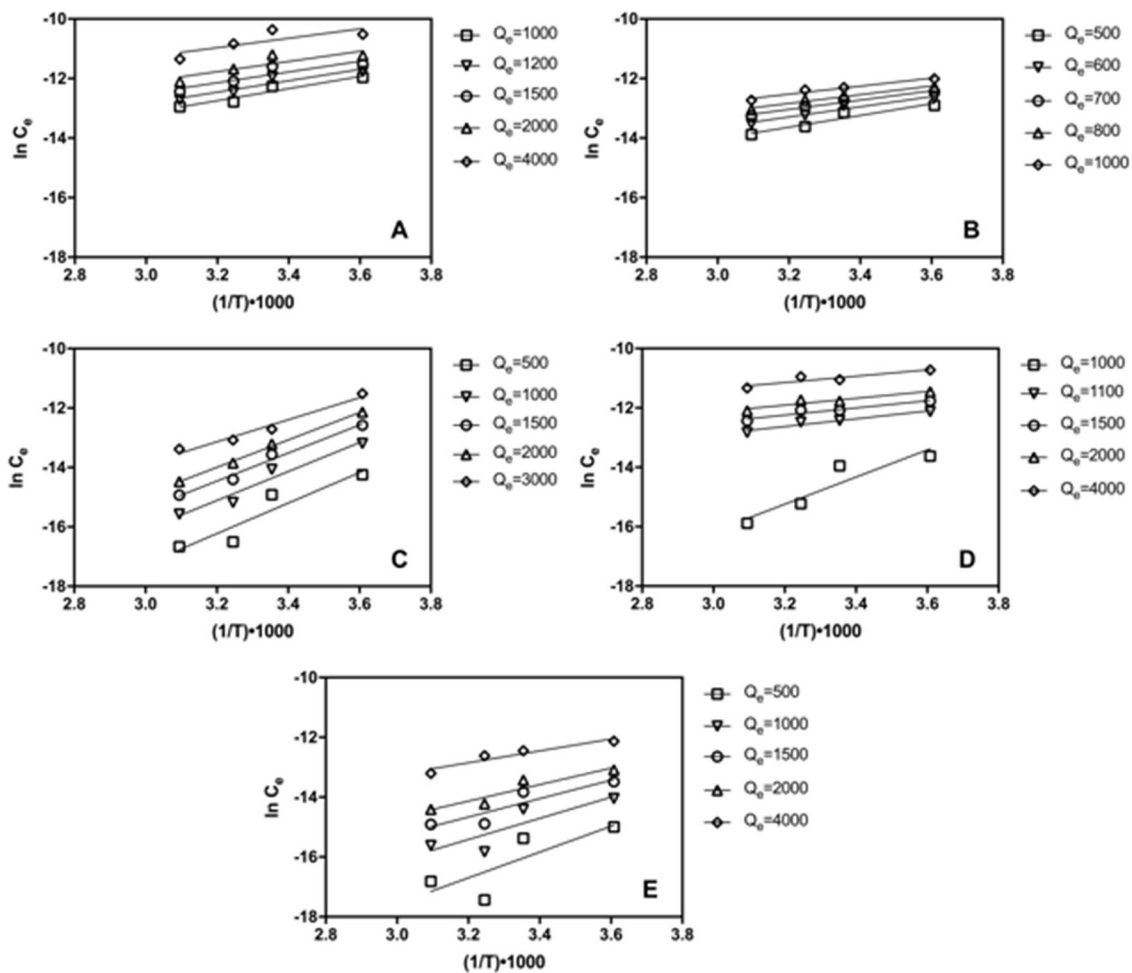
Figure 5C. Isostere curves for A) BAC-C10, B) CBZ, C) E2, D) EE2, and E) TCS at multiple surface loading (Q_e) values, in single-solute tests.

Table 5C. Slopes of isostere curves for micropollutants under single-solute conditions

Compound	Q_e mmol/g biochar	$lnC_e/(1/T)$
BAC-C10-S	0.0032	2.03
	0.0038	1.91
	0.0052	1.91
	0.0064	1.81
	0.0128	1.58
CBZ-S	0.0021	1.97
	0.0025	1.71
	0.0030	1.56
	0.0034	1.47
	0.0042	1.35
E2-S	0.0018	5.13
	0.0037	4.86
	0.0055	4.72
	0.0073	4.61
	0.0110	3.71
EE2-S	0.0034	6.25
	0.0037	1.85
	0.0052	1.72
	0.0111	1.65
	0.0148	1.54
TCS-S	0.0017	4.31
	0.0035	3.53
	0.0052	3.08
	0.0069	2.76
	0.0138	1.98

Appendix 5D. Single-solute van't Hoff curves for calculating change of enthalpy, free energy and entropy

Figure 5D. Single-solute van't Hoff curves for A) BAC-C10, B) CBZ, C) E2, D) EE2, and E) TCS.
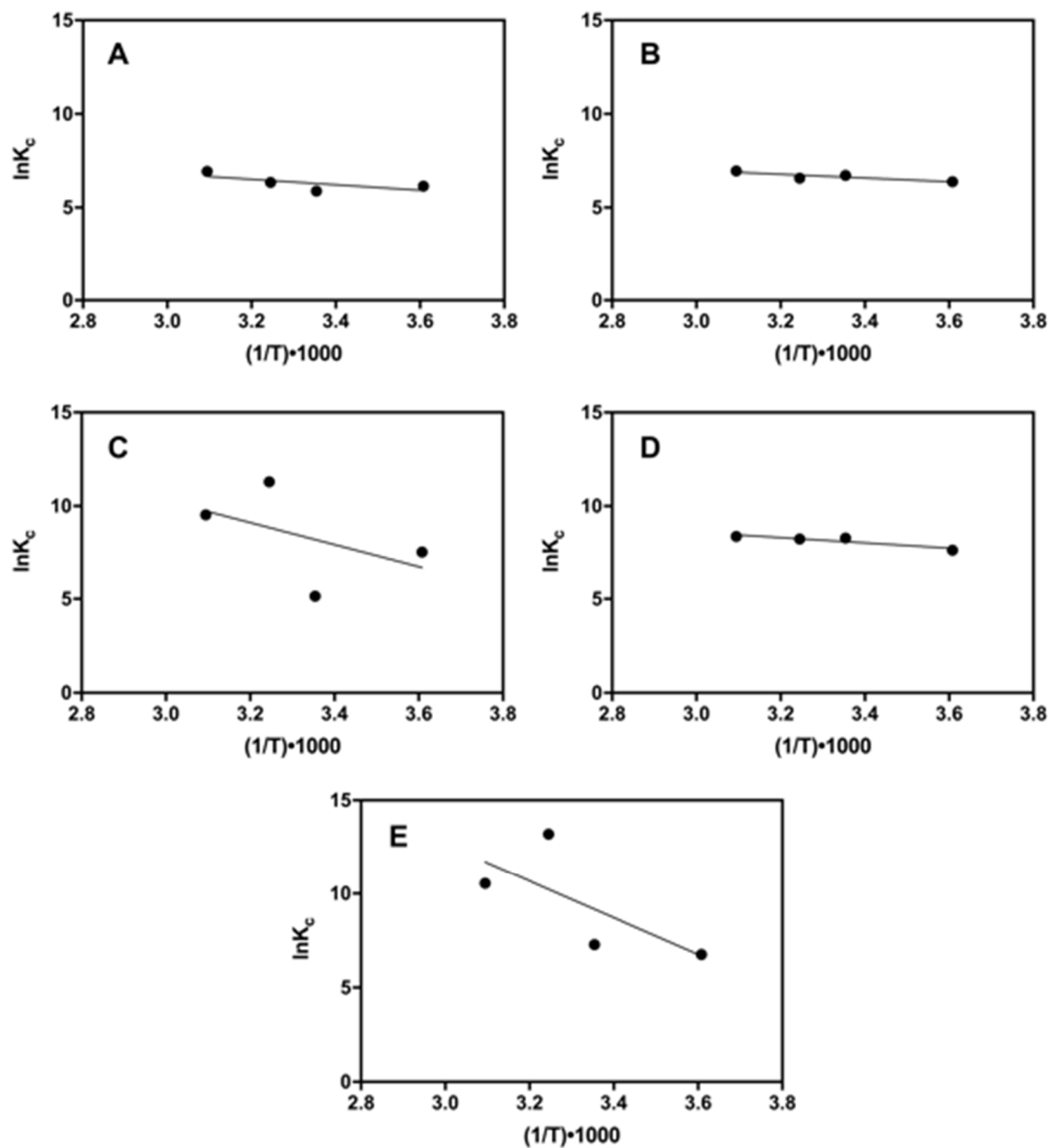
Appendix 5E. Isotherm parameters for micropollutants under multi-solute conditions

Table 5E. Isotherm parameters for micropollutants under multi-solute conditions

Compound	Isotherm	Parameter	4˚C	25˚C	35˚C	50˚C
BAC-C10	Linear	K	0.63	0.70	0.91	0.47
		B	-117.60	-17.31	87.78	232.30
		R^2	0.655	0.672	0.948	0.9999
CBZ	Linear	K	0.57	0.24	0.37	0.81
		B	54.46	252.40	281.20	159.10
		R^2	0.850	0.960	0.981	0.724
E2	Freundlich	K_f	16.67	12.86	108.90	87.22
		n	0.66	0.81	0.52	0.63
		R^2	0.711	0.977	0.971	0.901
	Langmuir	K_L	1518	2871	2354	3089
		B	493.9	440.8	210.6	228
		R^2	0.663	0.961	0.939	0.924
EE2	Linear	K	0.64	1.48	1.23	1.61
		B	211.90	308.10	501.30	518.10
		R^2	0.905	0.996	0.842	0.885
TCS	Freundlich	K_f	13.61	54.21	95.87	109.3
		n	0.75	0.60	0.55	0.51
		R^2	0.812	0.969	0.951	0.910
	Langmuir	K_L	5957	3598	3364	2888
		B	1562	344.7	130.4	123
		R^2	0.767	0.954	0.921	0.815

Appendix 5F. Comparison of significant difference between single-solute and multi solute isotherms

Table 5F. p-values for comparing the difference between single-solute and multi-solute isotherms

Compound	4˚C	25˚C	35˚C	50˚C
BAC-C10	N/A	N/A	0.208	0.062
CBZ	0.926	0.012	0.254	0.589
E2	0.017	<0.0001	<0.0001	<0.0001
EE2	0.0003	<0.0001	0.0002	0.003
TCS	0.035	0.850	0.072	<0.0001

N/A indicates that linear fitting of BAC-C10 in multi-solute condition is not good (<0.7), therefore they cannot be compared with single-solute condition.

Appendix 5G. Isostere curves for micropollutants under multi-solute conditions
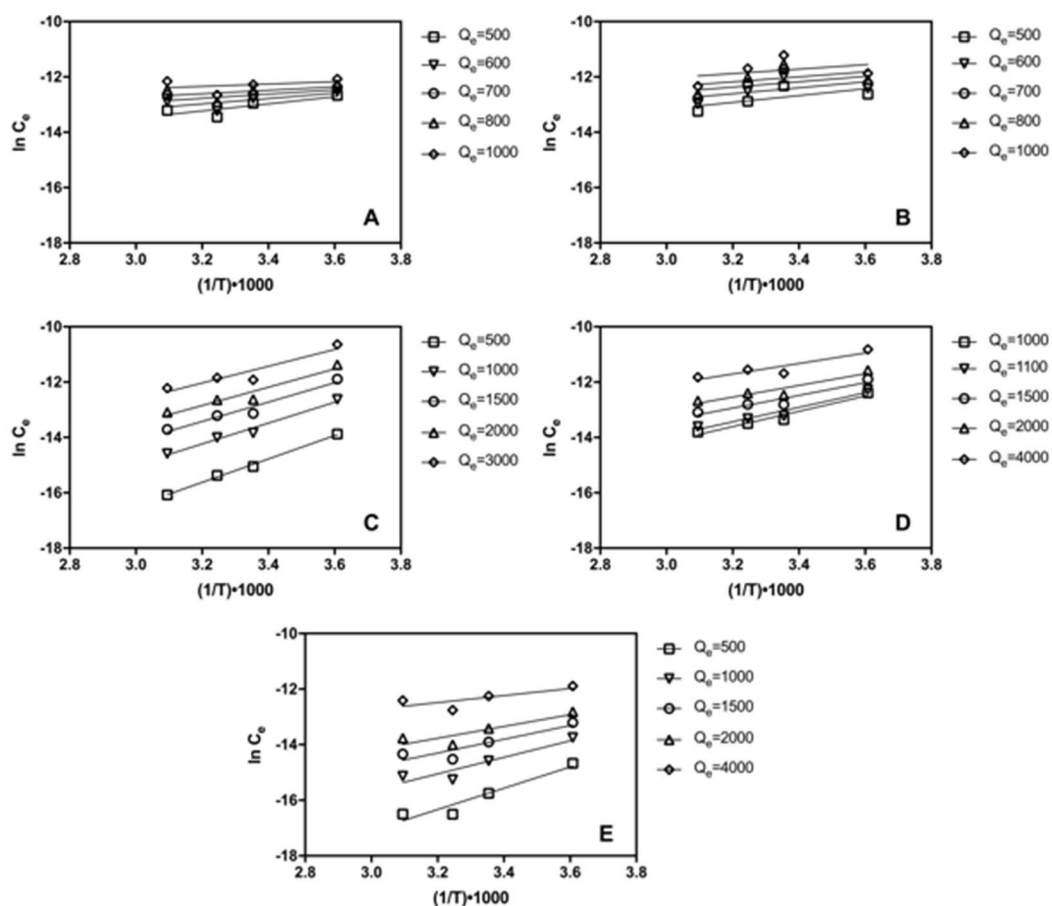

Figure 5G. Isostere curves for A) BAC-C10, B) CBZ, C) E2, D) EE2, and E) TCS at multiple surface loading (Q_e) values in multi-solute tests.

Table 5G. Slopes of isostere curves for micropollutants under multi-solute conditions

Compound	Q_e mmol/g biochar	$lnC_e/(1/T)$
BAC-C10	0.0016	1.28
	0.0019	0.97
	0.0024	0.77
	0.0026	0.62
	0.0032	0.42
CBA	0.0021	1.23
	0.0025	1.07
	0.0030	0.97
	0.0034	0.90
	0.0042	0.81
E2	0.0018	4.23
	0.0037	3.76
	0.0055	3.49
	0.0074	3.30
	0.0110	3.03
EE2	0.0034	2.76
	0.0037	2.62
	0.0052	2.29
	0.0111	2.12
	0.0148	1.90
TCS	0.0017	3.83
	0.0035	2.97
	0.0052	2.47
	0.0069	2.12
	0.0138	1.27

Appendix 5H. Multi-solute van't Hoff curves for calculating change of enthalpy, free energy and entropy
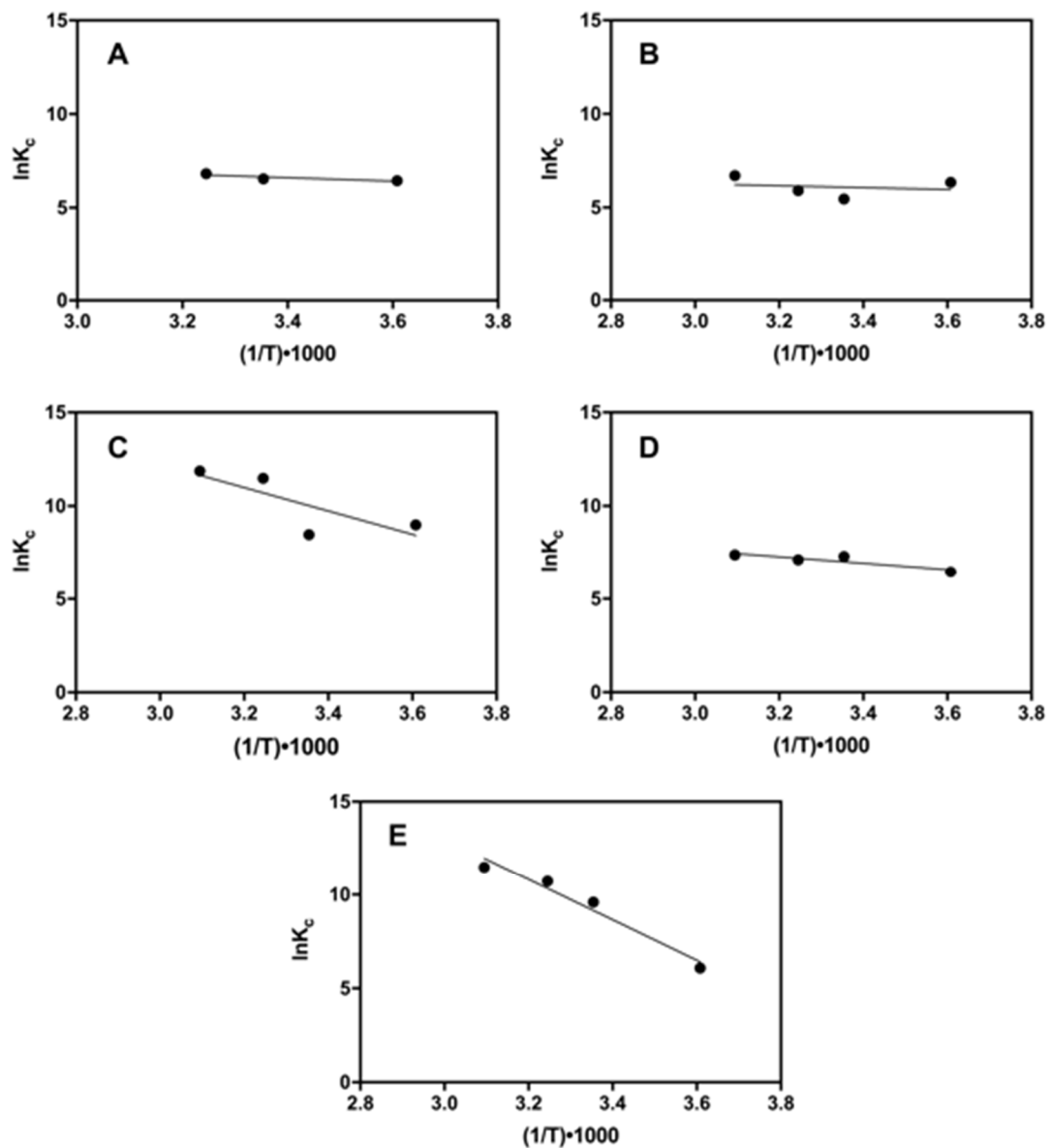

Figure 5H. Multi-solute van't Hoff curves for A) BAC-C10, B) CBZ, C) E2, D) EE2, and E) TCS.

Appendix 5I. Comparison of differences between single-solute and multi-solute adsorption enthalpy and entropy changes

Table 5I. p-values for comparing the difference between single-solute and multi-solute enthalpy and entropy changes

Compound	p for comparing ΔH^0	p for comparing ΔS^0
BAC-C10	0.744	0.166
CBZ	0.795	0.124
E2	0.966	0.248
EE2	0.706	0.0004
TCS	0.894	0.897

Appendix 6A. The impact of biochar regeneration on micropollutant adsorption capacities

       Biochar was regenerated for 2 cycles. Table 6A shows the p-values of Tukey's multiple comparison test on adsorption capacities of micropollutants on pristine biochar (0-biochar) and biochar produced in first and second regeneration cycles (1-biochar and 2-biochar, respectively).

Table 6A. Tukey's multiple comparison test on adsorption capacities of micropollutants on multi-cycle regenerated biochar

Compound	Regeneration cycle comparison (p value)		
	0- VS 1-biochar	0- VS 2-biochar	1- VS 2-biochar
TCS	0.037	0.034	0.890
E2	0.080	0.683	0.307
SMX	0.001	0.053	0.023

Appendix 6B. Changes in nutrient concentration in biochar batch adsorption tests

The concentrations of PO_4-P and NH_4-N in synthetic water solution, before and after biochar adsorption are shown in Figure 6B.
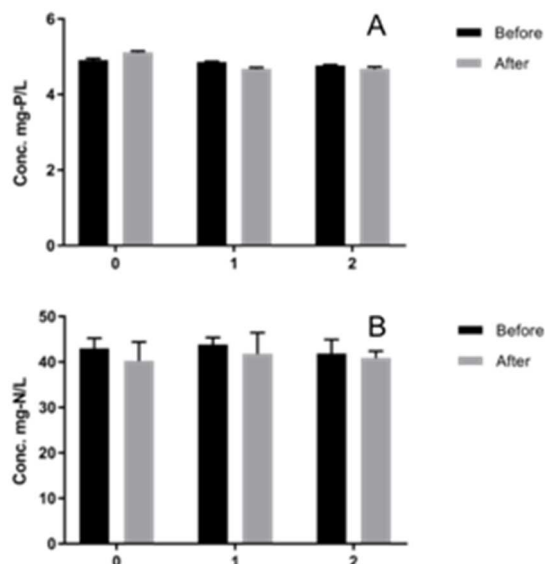

Figure 6B. Nutrient concentrations in water before and after biochar adsorption: A) PO_4-P, and B) NH_4-N. 0 refers to pristine biochar. 1 and 2 refer to the biochar that were regenerated and reused for one and two cycles.

The significance of the concentration difference before and after reaction is tested using a t test. Statistics are shown in Table 6B.

Table 6B. PO_4-P nutrient concentrations before and after biochar adsorption. P value indicates the significance of the concentration difference before and after the reaction.

Biochar type	PO₄-P initial conc. mg/L	PO₄-P end conc. mg/L	p value	NH₄-N initial conc. mg/L	NH₄-N end conc. mg/L	p value
0	4.91±0.04	5.11±0.04	0.004	42.99±2.26	40.22±4.15	0.37
1	4.87±0.01	4.67±0.04	0.002	43.85±1.56	41.78±4.67	0.51
2	4.77±0.02	4.67±0.06	0.063	41.85±3.07	40.88±1.50	0.65